INVESTIGATION OF THE ATMOSPHERIC OZONE FORMATION POTENTIAL OF SELECTED DIBASIC ESTERS

Report to the
Dibasic Esters Group
SOCMA

by
William P. L. Carter[a,b], Dongmin Luo[b], Irina L. Malkina[b],
Sara M. Aschmann[a] and Roger Atkinson[a]

May 15, 1997

[a]Statewide Air Pollution Research Center
University of California
Riverside, California 92521

[b]College of Engineering
Center for Environmental Research and Technology
University of California
Riverside, California 92521

97-AP-RT71-002-FR

ABSTRACT

An experimental and computer modeling study was carried out to estimate the atmospheric ozone formation potentials of the dibasic esters dimethyl succinate [$CH_3OC(O)CH_2CH_2C(O)OCH_3$, DBE-4], dimethyl glutarate [$CH_3OC(O)CH_2CH_2CH_2C(O)OCH_3$, DBE-5], and dimethyl adipate [$CH_3OC(O)CH_2$-$CH_2CH_2CH_2C(O)OCH_3$, DBE-6]. The rate constants for their reactions with OH radicals at 298 K were measured, using a relative rate method, to be (1.5 ± 0.6), (3.5 ± 1.1), and (8.8 ± 2.6) x 10^{-12} cm^3 $molec^{-1}$ s^{-1}, for DBE-4, DBE-5 and DBE-6, respectively. These are relative to an OH + cyclohexane rate constant of 7.49 x 10^{-12} cm^3 $molec^{-1}$ s^{-1}.

A series of environmental chamber experiments were carried out to determine the effects of adding DBE-4 and DBE-5 on NO oxidation, ozone formation, and OH radical levels in simulated model photochemical smog systems. The experiments used two different NO_x levels and used two different surrogate mixtures to represent the reactive organic gases (ROGs) present in the atmosphere. Both DBEs caused reduced OH radical levels in all the experiments, caused reduced rates of NO oxidation and O_3 formation in the experiments using the simpler ROG surrogate, but caused enhanced O_3 formation in experiments using a more complex ROG surrogate which is representative of atmospheric conditions. Similar results are observed in experiments with the higher alkanes, with the radical inhibition in both cases being attributed to alkyl nitrate formation in the reactions of proxy radicals with NO.

Atmospheric reaction mechanisms for the DBEs were estimated by analogy with known atmospheric reactions of other compounds. They had a number of uncertainties, but the estimated DBE-4 and DBE-5 mechanisms were found to be consistent with the results of the chamber experiments if the overall alkyl nitrate yields of ~12% was assumed for DBE-4 and ~25% for DBE-5. These were respectively ~33% lower and about the same as expected based on nitrate yields for alkanes with the same number of carbons. Alternative mechanisms assuming formation of formaldehyde or highly photoreactive α-dicarbonyl products were found not to be consistent with the chamber data.

The estimated and adjusted DBE mechanisms were then used to calculate ozone impacts of these compounds for a variety of atmospheric conditions. The predicted ozone impacts, relative to an equal mass of ethane were: ~0.65 - 0.8 for DBE-4; ~1 - 1.25 for DBE-5; and ~3 - 4.5 for DBE-6. These relative reactivities were only slightly affected by variations in scenario conditions or how ozone was quantified. The chamber data suggests that the model might be slightly overestimating the ozone impacts for DBE-4 and DBE-5 under lower NO_x conditions, with the estimated uncertainty being ~30%. The predictions for DBE-6 are more uncertain because no chamber data were obtained to test the assumed mechanism for this compound.

ACKNOWLEDGEMENTS

The authors acknowledge Mr. Dennis Fitz for assistance in administering this program, and Mr. Kurt Bumiller for assistance in carrying out the environmental chamber experiments. Although this work was funded by the Dibasic Esters Group of the Synthetic Organic Chemicals Manufacturing Association (SOCMA), the opinions and conclusions expressed herein are entirely those of the primary author, William P. L. Carter. Mention of trade names or commercial products do not constitute endorsement or recommendation for use.

TABLE OF CONTENTS

Section Page

LIST OF TABLES

LIST OF FIGURES

INTRODUCTION

Ozone in photochemical smog is formed from the gas-phase reactions of volatile organic compounds (VOCs) and oxides of nitrogen (NO_x) in sunlight. Although Los Angeles has one of the worst ozone problems in the United States, other areas of the country also have episodes where ozone exceeds the federal air quality standard of 0.12 ppm. Ozone control strategies in the past have focused primarily on VOC controls, though the importance of NO_x control has become recognized in recent years. VOC and NO_x controls have differing effects on ozone formation. NO_x is required for ozone formation, and if the levels of NO_x are low compared to the levels of reactive VOCs, then changing VOC emissions will have relatively little effect on ozone. Since NO_x is removed from the atmosphere more rapidly than VOCs, ozone in areas far downwind from the primary sources tend to be more NO_x limited, and thus less responsive to VOC controls. VOC controls tend to reduce the rate that O_3 is formed when NO_x is present, so VOC controls are the most beneficial in reducing O_3 in the urban source areas, where NO_x is relatively plentiful, and where O_3 yields are determined primarily by how rapidly it is being formed. Because of this, any comprehensive ozone control strategy should involve reduction of emissions of both NO_x and VOCs.

Many different types of VOC compounds are emitted into the atmosphere, each reacting at different rates and having different mechanisms for their reactions. Because of this, they can differ significantly in their effects on ozone formation, or their "reactivity". Some compounds, such as CFCs, do not react in the lower atmosphere at all, and thus make no contribution to ground-level ozone formation. Others, such as methane, react and contribute to ozone formation, but react so slowly that their practical effect on ozone formation in urban atmospheres is negligible. Obviously, it does not make sense to regulate such compounds as ozone precursors. In recognition of this, the EPA has exempted certain compounds from such regulations on the basis of having "negligible" effects on ozone formation. Although the EPA has no formal policy on what constitutes "negligible" reactivity, in practice it has used the ozone formation potential of ethane as the standard in this regard. This is because ethane is the most reactive of the compounds that the EPA has exempted to date. Therefore, the ozone formation potential of a compound relative to ethane is of particular interest when assessing whether it might be a likely candidate for exemption from regulation as an ozone precursor.

The dibasic esters, of which dimethyl succinate [$CH_3OC(O)CH_2CH_2C(O)OCH_3$, DBE-4], dimethyl glutarate [$CH_3OC(O)CH_2CH_2CH_2C(O)OCH_3$, DBE-5], and dimethyl adipate [$CH_3OC(O)CH_2CH_2CH_2CH_2$-$C(O)OCH_3$, DBE-6], are representative examples, are useful compounds which are of interest to the Dibasic Esters Group of the Synthetic Organic Chemicals Manufacturing Association (SOCMA). They are sufficiently volatile that their use might result in their being emitted into the atmosphere, and thus they

would be subject to regulation as a VOC ozone precursor unless they can be shown to have negligible ozone reactivity. The Dibasic Esters Group of SOCMA contracted with the Statewide Air Pollution Research Center (SAPRC) and the College of Engineering Center for Environmental Research and Technology (CE-CERT) at the University of California at Riverside to carry out a program to assess this. This program involved measuring the rate constants for the atmospheric reactions of the three representative dibasic esters, estimating their likely atmospheric reaction mechanisms, carrying out environmental chamber experiments to directly measure the actual ozone impacts of two of these compounds, DBE-4 and DBE-5, using the results to establish which of the estimated mechanisms can actually predict their ozone impacts in the atmosphere, and then using the experimentally-validated mechanisms to obtain estimates of the ozone impacts of these compounds which could serve as a basis for regulatory decision making. This report describes the results of this program.

EXPERIMENTAL AND DATA ANALYSIS METHODS

Kinetic Studies

The major atmospheric sink for the dibasic esters is expected to be reaction with the OH radical. The experimental methods used to measure the OH radical rate constants for the selected dibasic esters were generally similar to those used in our previous study of the atmospheric chemistry of a series of carbamates and lactates (Kwok et al., 1996). Experiments were carried out in a 7900 liter all-Teflon chamber, equipped with two parallel banks of Sylvania F40/350BL blacklamps for irradiation, at 298 ± 3 K and 740 Torr total pressure of purified air at ~5% relative humidity. The chamber is fitted with a Teflon-coated fan for rapid mixing of reactants during their introduction into the chamber.

Rate constants for the OH radical reactions were determined using a relative rate method in which the relative disappearance rates of the dibasic esters and a reference compound, whose OH radical reaction rate constant is reliably known, were measured in the presence of OH radicals. Providing that the dibasic esters and reference compound reacted only with OH radicals, then

$$\ln\left\{\frac{[DBE]_{t_o}}{[DBE]_t}\right\} = \frac{k_1}{k_2} \ln\left\{\frac{[reference\ compound]_{t_o}}{[reference\ compound]_t}\right\} \quad \text{(I)}$$

where $[DBE]_{t_o}$ and $[\text{reference compound}]_{t_o}$ are the concentrations of the dibasic ester and reference compound, respectively, at time t_o, $[DBE]_t$ and $[\text{reference compound}]_t$ are the corresponding concentrations at time t, and k_1 and k_2 are the rate constants for reactions (1) and (2), respectively.

$$\text{OH + dibasic ester} \rightarrow \text{products} \quad (1)$$
$$\text{OH + reference compound} \rightarrow \text{products} \quad (2)$$

Hence plots of $\ln([DBE]_{t_o}/[DBE]_t)$ against $\ln([\text{reference compound}]_{t_o}/[\text{reference compound}]_t)$ should be straight lines with slope k_1/k_2 and zero intercept.

OH radicals were generated by the photolysis of methyl nitrite (CH_3ONO) in air at wavelengths greater than 300 nm (Atkinson et al., 1981).

$$CH_3ONO + h\nu \rightarrow CH_3O + NO$$
$$CH_3O + O_2 \rightarrow HCHO + HO_2$$
$$HO_2 + NO \rightarrow OH + NO_2$$

NO was added to the reactant mixtures to suppress the formation of O_3, and hence of NO_3 radicals (Atkinson et al., 1981). Cyclohexane was used as the reference compound, and the initial reactant concentrations (in molecule cm^{-3} units) were: CH_3ONO, 2.4 x 10^{14}; NO, 2.4 x 10^{14}; dibasic esters and cyclohexane, ~2.4 x 10^{13} each. Irradiations were carried out at 20% of the maximum light intensity for 15-45 min (with this light intensity corresponding to an NO_2 photolysis rate of ~2 x 10^{-3} s^{-1}).

The concentrations of the dibasic esters and cyclohexane were measured by gas chromatography with flame ionization detection (GC-FID) during the experiments. For the analysis of the dibasic esters, 100 cm^3 volume gas samples were collected from the chamber onto Tenax-TA solid adsorbent, with subsequent thermal desorption at ~225 C onto a 30 m DB-1701 megabore column held at 40° C and then temperature programmed to 200° C at 8° C min^{-1}. For the analysis of cyclohexane, gas samples were collected from the chamber in 100 cm^3 all-glass, gas-tight syringes and transferred via a 1 cm^3 stainless steel loop and gas sampling valve onto a 30 m DB-5 megabore column held at -25° C and then temperature programmed at 8 ^oC min^{-1}. Based on five independent sets of duplicate or triplicate analyses in the dark (prior to the irradiations), the maximum GC-FID measurement uncertainties for the three dibasic esters were in the ranges 0.2-2.9% for DBE-4, 0.9-5.7% for DBE-5 and 3.2-13.8% for DBE-6. The NO and initial NO_2 concentrations were measured using a Thermo Environmental Instruments, Inc., Model 42 chemiluminescent NO-NO_x analyzer.

Photolysis of a dibasic ester - cyclohexane - air mixture (with the dibasic ester and cyclohexane concentrations being the same as in the OH radical reaction rate constant determinations, of ~2.4 x 10^{13} molecule cm^{-3} each) was also carried out at 20% of the maximum light intensity for 15-45 min to check that photolysis of the dibasic esters was not occurring under blacklamp irradiation.

The chemicals used, and their stated purities, were: cyclohexane (high-purity solvent grade), American Burdick and Jackson; dimethyl succinate [DBE-4] (98.4%), dimethyl glutarate [DBE-5] (99%), and dimethyl adipate [DBE-6] (98.7%), DuPont Nylon; and NO (≥99%), Liquid Carbonic. Methyl nitrite was prepared and stored as described previously (Atkinson et al., 1981).

Environmental Chamber Studies

Overall Experimental Approach

Most of the environmental chamber experiments for this program consisted of measurements of "incremental reactivities" of the dibasic esters under various conditions. These involve two types of irradiations of model photochemical smog mixtures. The first is a "base case" experiment where a mixture of reactive organic gases (ROGs) representing those present in polluted atmospheres (the "ROG surrogate") is irradiated in the presence of oxides of nitrogen (NO_x) in air. The second is the "test" experiment which consists of repeating the base case irradiation except that the VOC whose reactivity is being assessed is

added. The differences between the results of these experiments provide a measure of the atmospheric impact of the test compound, and the difference relative to the amount added is a measure of its reactivity.

To provide data concerning the reactivities of the test compound under varying atmospheric conditions, three types of base case experiments were carried out:

1. Mini-Surrogate Experiments. This base case employed a simplified ROG surrogate and relatively low ROG/NO_x ratios. Low ROG/NO_x ratios represent "maximum incremental reactivity" (MIR) conditions, which are most sensitive to VOC effects. This is useful because it provides a sensitive test for the model, and also because it is most important that the model correctly predict a VOC's reactivity under conditions where the atmosphere is most sensitive to the VOCs. The ROG mini-surrogate mixture employed consisted of ethene, n-hexane, and m-xylene. This same surrogate was employed in our previous studies (Carter et al, 1993a,b; 1995a.), and was found to provide a more sensitive test of the mechanism than the more complex surrogates which more closely represent atmospheric conditions (Carter et al, 1995a). This high sensitivity to mechanistic differences makes the mini-surrogate experiments most useful for mechanism evaluation.

2. Full Surrogate Experiments. This base case employed a more complex ROG surrogate under somewhat higher, though still relatively low, ROG/NO_x conditions. While less sensitive to the mechanism employed, experiments with a more representative ROG surrogate are needed to evaluate the mechanism under conditions that more closely resembling the atmosphere. The ROG surrogate employed was the same as the 8-component "lumped molecule" surrogate as employed in our previous study (Carter et al. 1995a), and consists of n-butane, n-octane, ethene, propene, trans-2-butene, toluene, m-xylene, and formaldehyde. Calculations have indicated that use of this 8-component mixture will give essentially the same results in incremental reactivity experiments as actual ambient mixtures (Carter et al. 1995a).

3. Full Surrogate, low NO_x Experiments. This base case employing the same 8-component lumped molecule surrogate as the full surrogate experiments described above, except that lower NO_x levels (higher ROG/NO_x ratios) were employed to represent NO_x-limited conditions. Such experiments are necessary to assess the ability of the model to properly simulate reactivities under conditions where NO_x is low. The initial ROG and NO_x reactant concentrations were comparable to those employed in our previous studies (Carter et al. 1995a).

An appropriate set of control and characterization experiments necessary for assuring data quality and characterizing the conditions of the runs for mechanism evaluation were also carried out. These are discussed where relevant in the results or modeling methods sections.

Environmental Chamber

The environmental chamber system employed in this study was the CE-CERT dual-reactor Xenon Arc Teflon Chamber (CTC). This consists of two 4' x 4' x 8' FEP Teflon reaction bags located adjacent to each other at one end of an 8' x 12' room with reflective aluminum paneling on all surfaces. The two reactors are referred to as the two "sides" of the chamber (Side A and Side B) in the subsequent discussion. Four 6.5 KW xenon arc are lights were mounted on the wall opposite the reaction bags, all in a room with walls and ceiling covered with reflective aluminum paneling to maximize light intensity and homogeneity. The reaction bags were interconnected with two ports, each containing a fan to exchange the contents of the bags to assure that the common reactants were adequately mixed. This was important in order to evaluate the effect of adding a test compound to a standard mixture. Two separate fans were also employed to mix the contents within each chamber. As discussed elsewhere (Carter et al. 1995b,c), this light source gives the closest approximation available of the ground-level solar spectrum for an indoor chamber. The chamber was very similar to the Statewide Air Pollution Research Center's Xenon arc Teflon Chamber (SAPRC XTC) which is described in detail elsewhere (Carter et al. 1995b,c).

Experimental Procedures

The reaction bags were flushed with dry air produced by an AADCO air purification system for 14 hours (6pm-8am) on the nights before experiments. The continuous monitors were connected prior to reactant injection and the data system began logging data from the continuous monitoring systems. The reactants were injected as described below (see also Carter et al, 1993a,, 1995b). The common reactants were injected in both sides simultaneously using a three-way (one inlet and two outlets connected to side A and B respectively) bulb of 2 liters in the injection line and were well mixed before the chamber was divided. The contents of each side were blown into the other using two box fans located between them. Mixing fans were used to mix the reactants in the chamber during the injection period, but these were turned off prior to the irradiation. The sides were then separated by closing the ports which connected them, after turning all the fans off to allow their pressures to equalize. After that, reactants for specific sides (the test compound in the case of reactivity experiments) were injected and mixed. The lights are turned on after lowering a metal baffle between the lights and the reactors, and the lights are allowed to warm up for at least 30 minutes. Irradiation in the chamber is begun by raising the baffle between the lights and the reactors, and the irradiation proceeds for 6 hours. After the run, the contents of the chamber were emptied by allowing the bags to collapse, and then was flushed with purified air. The contents of the reactors were vented into a fume hood.

The procedures for injecting the various types of reactants were as follows. The NO and NO_2 were prepared for injection using a high vacuum rack. Known pressure of NO, measured with MKS Baratron capacitance manometers, were expanded into Pyrex bulbs with known volumes, which were then filled with nitrogen (for NO) or oxygen (for NO_2). The contents of the bulbs were then flushed into the chamber with AADCO air. The gaseous reactants were prepared for injection either using a high vacuum

rack or a gas-tight syringes whose amounts were calculated. The gas reactants in a gas-tight syringe were usually diluted to 100-ml with nitrogen in a syringe. The volatile liquid reactants were injected, using a micro syringe, into a 1-liter Pyrex bulb equipped with stopcocks on each end and a port for the injection of the liquid. The port was then closed and one end of the bulb was attached to the injection port of the chamber and the other to a dry air source. The stopcocks were then opened, and the contents of the bulb were flushed into the chamber with a combination of dry air and heat gun for approximately 5 minutes. Formaldehyde was prepared in a vacuum rack system by heating paraformaldehyde in an evacuated bulb until the pressure corresponded to the desired amount of formaldehyde. The bulb was then closed and detached from the vacuum system and its contents were flushed into the chamber with dry air through the injection port.

Since DBE-4 and DBE-5 have relatively high boiling points, and may condense in cold spots using usual liquid injection, a heated injection system was employed. This was done by placing the desired quantity of DBE-4 or DBE-5 (typical 150 µl) in a three-way glass tube which was surrounded with heat tape. The liquid DBE was placed into the tube through one of the ports, and tube was heated to around 200˚C, and the evaporating DBE was flushed into chamber with purified dry air at 2 liters/minute for about 15 minutes.

Analytical Methods

Ozone and nitrogen oxides (NO_x) were continuously monitored using commercially available continuous analyzers with Teflon sample lines inserted directly into the chambers. The sampling lines from each side of the chamber were connected to solenoids which switched from side to side every 20 minutes, so the instruments alternately collected data from each side. Ozone was monitored using a Dasibi 1003AH UV photometric ozone analyzer and NO and total oxides of nitrogen (including HNO_3 and organic nitrates) were monitored using a Teco Model 14B chemiluminescent NO/NO_x monitor. The output of these instruments, along with that from the temperature sensors and the and formaldehyde instrument, were attached to a computer data acquisition system, which recorded the data at 10 minutes intervals for ozone, NO and temperature, and at 20 minute intervals for formaldehyde, using 30 second averaging times. This yielded a sampling interval of 20 or 40 minutes for taking data from each side.

The NO_x and CO analyzers were calibrated with a certified NO and CO source and CSI gas-phase dilution system. It was done prior to chamber experiment for each run. The NO_2 converter efficiency check was carried out in regular intervals. The ozone analyzer was calibrated against transfer standard ozone analyzer using transfer standard method in a interval of three months and was check with CSI ozone generator (set to 400 ppb) for each experiment to assure that the instrument worked properly. The details were discussed elsewhere (Carter et al, 1995b)

Organic reactants other than formaldehyde were measured by gas chromatography with FID and ECD detections as described elsewhere (Carter et al. 1993a; 1995b). GC samples were taken for analysis at intervals from 20 to 30 minutes either using 100 ml gas-tight glass syringes or by collecting the 100 ml sample from the chamber onto Tenax-GC solid adsorbent cartridge. These samples were taken from ports directly connected to the chamber after injection and before irradiation and at regular intervals after irradiation. The sampling method employed for injecting the sample onto the GC column depended on the volatility or "stickiness" of the compound. For analysis of the more volatile species, the contents of the syringe were flushed through a 2 ml or 3 ml stainless steel or 1/8' Teflon tube loop and subsequently injected onto the column by turning a gas sample valve.

The DBE-4 and DBE-5 were found to be too "sticky" to be satisfactorily sampled using the loop analysis method. Instead, samples for DBE analyses were taken by passing 100 ml of air from the chamber through a glass cartridge filled with Tenax-GC solid absorbent. The tube was then placed in a specially modified GC injection port, which was then heated to 300˚C to desorb the sample onto the GC column for analysis.

The calibrations for the GC analyses for most compounds were carried out by sampling from chambers or vessels of known volume into which known amounts of the reactants were injected, as described previously (Carter et al, 1995b).

Characterization Methods

Three temperature thermocouples for each chamber were used to monitor the chamber temperature, two of which were located in the sampling line of continuous analyzers to monitor the temperature in each side. The third one was located in the outlet of the air conditioning system used to control the chamber temperature. The temperature in these experiment were typically 25-30° C.

The spectrum of the xenon arc light source was measured several (usually five) times during each experiment using a LiCor LI-1800 spectraradiometer. The absolute light intensity in this chamber was measured by "photostationary state" NO_2 actinometry experiments and by Cl_2 actinometry. The photostationary state experiments (which were carried out prior to the period of the experiments for this report) consisted of simultaneous measurements of photostationary state concentrations of NO, NO_2, and O_3 in otherwise pure air, with the NO_2 photolysis rate being calculated from the $[NO][O_3]/[NO_2]$ ratio (Carter et al. 1997). The Cl_2 actinometry experiments consisted of photolyzing ~0.1 ppm of Cl_2 in ~1 ppm of n-butane, calculating the Cl_2 photolysis rate from the rate of consumption of n-butane, and then calculating the corresponding NO_2 photolysis rate from the absorption cross sections and quantum yields for NO_2 and Cl_2 (assuming unit quantum yields for Cl_2) and the spectral distribution of the light source (Carter et al, 1997). The results of these two methods are generally in good agreement, and were used

to place the somewhat more precise data of the relative light intensity methods, discussed below, on an absolute basis (Carter et al, 1997).

Relative trends in light intensity with time are obtained using the quartz tube method of Zafonte et al. (1977), modified as discussed by Carter et al. (1995b; 1997), and from absolute intensities of spectra taken several times during each run using a Li-Cor LI-1800 spectraradiometer. Because the quartz tube during the actinometry experiments was located closer to the lights than the reaction bags, the NO_2 photolysis rates obtained using this method were corrected by multiplying them by a factor of 0.79 to make them consistent with the absolute values obtained using the steady state or Cl_2 actinometry methods (Carter et al, 1997). The LiCor data gave the most precise indication of the relative trend in light intensity, and NO_2 photolysis rates calculated using it (and NO_2 absorption cross sections and quantum yields) were used as the primary method for determining how the light intensity varied with time. These data indicated that the NO_2 photolysis rates declined slowly with time, with the data being fit by a curve giving an NO_2 photolysis rates of around 0.174 min^{-1} during the period of this study.

The dilution of the CTC chamber due to sampling is expected to be small because the flexible reaction bags can collapse as samples are withdrawn for analysis. Also, the chamber was designed to operate under slightly positive pressure, so any small leaks would result in reducing the bag volume rather than diluting the contents of the chamber. Information concerning dilution in an experiment can be obtained from relative rates of decay of added VOCs which react with OH radicals with differing rate constants (Carter et al. 1993a; 1995b). Most experiments had a more reactive compounds such as m-xylene and n-octane present either as a reactant or added in trace amounts to monitor OH radical levels. Trace amounts (~0.1 ppm) of n-butane were also added to experiments if needed to provide a less reactive compound for monitoring dilution. In addition, specific dilution check experiments such as CO irradiations were carried out. Based on these results, the dilution rate was found to be negligible in this chamber during this period, being less than 0.3% per hour in all runs, and usually less than 0.1% per hour.

Reactivity Data Analysis Methods

As indicated above, most of the experiments for this program consisted of simultaneous irradiation of a "base case" reactive organic gas (ROG) surrogate - NO_x mixture in one of the dual reaction chambers, together with an irradiation, in the other reactor, of the same mixture with added. The results are analyzed to yield two measures of VOC reactivity: the effect of the added VOC on the amount of NO reacted plus the amount of ozone formed, and integrated OH radical levels. These are discussed in more detail below.

The first measure of reactivity is the effect of the VOC on the change in the quantity $[O_3]$-[NO], or $([O_3]_t$-$[NO]_t)$-$([O_3]_0$-$[NO]_0)$, which is abbreviated as $d(O_3$-NO) in the subsequent discussion. As discussed elsewhere (e.g., Johnson, 1983; Carter and Atkinson, 1987; Carter and Lurmann, 1990, 1991, Carter et al, 1993a, 1995a,d), this gives a direct measure of the amount of conversion of NO to NO_2 by

peroxy radicals formed in the photooxidation reactions, which is the process that is directly responsible for ozone formation in the atmosphere. (Johnson calls it "smog produced" or "SP".) The incremental reactivity of the VOC relative to this quantity, which is calculated for each hour of the experiment, is given by

$$IR[d(O_3\text{-}NO)]_t^{VOC} = \frac{d(O_3\text{-}NO)_t^{test} - d(O_3\text{-}NO)_t^{base}}{[VOC]_0} \qquad (I)$$

where $d(O_3\text{-}NO)_t^{test}$ is the $d(O_3\text{-}NO)$ measured at time t from the experiment where the test VOC was added, $d(O_3\text{-}NO)_t^{base}$ is the corresponding value from the corresponding base case run, and $[VOC]_0$ is the amount of test VOC added. An estimated uncertainty for $IR[d(O_3\text{-}NO)]$ is derived based on assuming an ~3% uncertainty or imprecision in the measured $d(O_3\text{-}NO)$ values. This is consistent with the results of the side equivalency test, where equivalent base case mixtures are irradiated on each side of the chamber.

Note that reactivity relative to $d(O_3\text{-}NO)$ is essentially the same as reactivity relative to O_3 in experiments where O_3 levels are high, because under such conditions $[NO]_t^{base} \approx [NO]_t^{test} \approx 0$, so a change $d(O_3\text{-}NO)$ caused by the test compound is due to the change in O_3 alone. However, $d(O_3\text{-}NO)$ reactivity has the advantage that it provides a useful measure of the effect of the VOC on processes responsible for O_3 formation even in experiments where O_3 formation is suppressed by relatively high NO levels.

The second measure of reactivity is the effect of the VOC on integrated hydroxyl (OH) radical concentrations in the experiment, which is abbreviated as "IntOH" in the subsequent discussion. This is an important factor affecting reactivity because radical levels affect how rapidly all VOCs present, including the base ROG components, react to form ozone. If a compound is present in the experiment which reacts primarily with OH radicals, then the IntOH at time t can be estimated from

$$IntOH_t = \int_0^t [OH]_\tau \, d\tau = \frac{\ln\left(\frac{[tracer]_0}{[tracer]_t}\right) - D\,t}{kOH^{tracer}}, \qquad (II)$$

where $[tracer]_0$ and $[tracer]_t$ are the initial and time=t concentrations of the tracer compound, kOH^{tracer} its OH rate constant, and D is the dilution rate in the experiments. The latter was found to be small and was neglected in our analysis. The concentration of tracer at each hourly interval was determined by linear interpolation of the experimentally measured values. *m*-Xylene was used as the OH tracer in these experiments because it is a surrogate component present in all experiments, its OH rate constant is known (the value used was 2.36×10^{-11} cm^3 $molec^{-1}$ s^{-1} [Atkinson, 1989]), and it reacts relatively rapidly.

The effect of the VOC on OH radicals can thus be measured by its IntOH incremental reactivity, which is defined as

$$IR[IntOH]_t = \frac{IntOH_t^{test} - IntOH_t^{base}}{[VOC]_0} \quad \text{(III)}$$

where $IntOH_t^{test}$ and $IntOH_t^{base}$ are the IntOH values measured at time t in the added VOC and the base case experiment, respectively. The results are reported in units of 10^6 min. The uncertainties in IntOH and IR[IntOH] are estimated based on assuming an ~2% imprecision in the measurements of the m-xylene concentrations. This is consistent with the observed precision of results of replicate analyses of this compound.

CHEMICAL MECHANISMS AND MODELING METHODS

Chemical Mechanism

General Atmospheric Photooxidation Mechanism

The chemical mechanism used in the environmental chamber and atmospheric model simulations in this study is given in Appendix A to this report. This mechanism is based on that documented by Carter (1990), with a number of updates as discussed below. It can explicitly represent a large number of different types of organic compounds, but it lumps together species reacting with similar rate constants and mechanisms in simulations of atmospheric mixtures, and it uses a condensed representation for many of the reactive organic products. The reactions of inorganics, CO, formaldehyde, acetaldehyde, peroxyacetyl nitrate, propionaldehyde, peroxypropionyl nitrate, glyoxal and its PAN analog, methylglyoxal and several other product compounds are represented explicitly. In addition, the reactions of unknown photoreactive products formed in the reactions of aromatic hydrocarbons are represented by model species whose yields and photolysis parameters are adjusted based on fits of model simulations to environmental chamber experiments. A chemical operator approach is used to represent peroxy radical reactions, as discussed in detail by Carter (1990). Generalized reactions with variable rate constants and product yields are used to represent the primary emitted alkane, alkene, aromatic and other VOCs, with rate constants and product yields appropriate for the individual compounds being represented in each simulation). The tables in the Appendix list only those VOCs (or groups of VOCs) used in the simulations in this work. Most of the higher molecular weight oxygenated product species are represented using the "surrogate species" approach, where simpler molecules such as propionaldehyde or 2-butanone are used to represent the reactions of higher molecular weight analogues that are assumed to react similarly.

Several aspects of the Carter (1990) mechanism were updated prior to this work to account for new kinetic and mechanistic information for certain classes of compounds as described by Carter et. al. (1993b) and Carter (1995), and further modifications were made to the uncertain portions of the mechanisms for the aromatic hydrocarbons to satisfactorily simulate results of experiments carried out using differing light sources (Carter et al. 1997). The latest version of the general mechanism is discussed by Carter et al. 1997).

Estimated Atmospheric Reactions of the Dibasic Esters

These dibasic esters are expected to react in the atmosphere primarily with OH radicals. Data in Calvert and Pitts (1966) indicate that esters do not absorb light to a significant extent in the wavelength region important in the lower atmosphere, nor was there any indication of significant loss by photolysis is the kinetic data obtained in this study. Since ozone does not react to a significant extent with aldehydes and ketones (Atkinson and Carter, 1984), one would not expect ozone reaction with esters to be important.

There are no data concerning the reactions of esters with NO_3 radicals, though, based on data for other compound and group-additivity methods, one would not expect the reactions to be rapid (Atkinson, 1991).

The rate constants for the OH radical reactions with the three dibasic esters considered here were measured in this work to be (1.5±0.6), (3.5±1.1) and (8.8±2.6) x 10^{-12} cm^3 $molec^{-1}$ s^{-1} for DBE-4, DBE-5, and DBE-6, respectively (see below). Since these are the only available data concerning these rate constants, these values were used in all the model simulations discussed in this report.

Reaction with OH radicals would involve H-abstraction from one of the two possible positions on DBE-4, or one of three possible positions for DBE-5 and DBE-6. Based on structure-reactivity estimates (Kwok and Atkinson, 1995), the total rate constant for reaction at a CH_3 group is estimated to be 4.4 x 10^{-13} cm^3 $molec^{-1}$ s^{-1} in each of these molecules, so this mode of initial reaction is estimated to occur ~30%. ~13%, and ~5% of the time for DBE-4, DBE-5 and DBE-6, respectively. The remaining 70% of the reaction for DBE-2 is at the α-CH_2 group, i.e., the group next to the carbonyl. If OH reaction at α-CH_2 this position occurs with the same rate constant (i.e., 1.1 x 10^{-12} cm^3 $molec^{-1}$ s^{-1}) in the other dibasic esters as it does for DBE-4, then this reaction would be expected to occur respectively ~30% and ~12% of the time for DBE-5 and DBE-6. This means that reaction at the β-CH_2 group would occur ~57% and ~83% of the time for these two compounds.

Tables 1-3 give summaries of the sets of products expected to be formed following the reactions of OH radicals at the various positions of these dibasic esters. The assumed or alternative mechanisms used to derive these product distributions are discussed below. In the case of DBE-4, several alternative mechanisms are evaluated against the chamber data, and the products predicted by these alternatives are included in Table 1.

Reaction at the CH_3 Group in DBE-4

The initial reactions following OH attack on the methyl group on DBE-4 are expected to be:

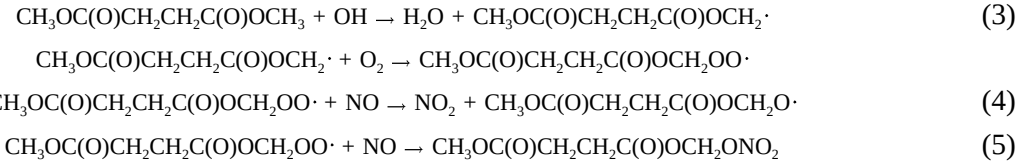

$$CH_3OC(O)CH_2CH_2C(O)OCH_3 + OH \rightarrow H_2O + CH_3OC(O)CH_2CH_2C(O)OCH_2\cdot \quad (3)$$

$$CH_3OC(O)CH_2CH_2C(O)OCH_2\cdot + O_2 \rightarrow CH_3OC(O)CH_2CH_2C(O)OCH_2OO\cdot$$

$$CH_3OC(O)CH_2CH_2C(O)OCH_2OO\cdot + NO \rightarrow NO_2 + CH_3OC(O)CH_2CH_2C(O)OCH_2O\cdot \quad (4)$$

$$CH_3OC(O)CH_2CH_2C(O)OCH_2OO\cdot + NO \rightarrow CH_3OC(O)CH_2CH_2C(O)OCH_2ONO_2 \quad (5)$$

The extent of alkyl nitrate formation via peroxy + NO reactions such as Reaction (5) will be discussed separately below. Based on reactions of analogous species (e.g., Atkinson, 1990, 1994, and references

Table 1. Summary of products and model species used in the alternative mechanisms for the atmospheric reactions of DBE-4.

Products	Model Species	Yields Assumed			
		Model A	Model B	Model C	Model D
Alkyl NItrate Formation [a]					
-NO + Organic Nitrate	RO2-N.	0.12	0.14	0.28	0.10
Propigation routes [b]					
Reaction at -CH_3 group (~30% assumed)					
-NO + NO_2 + HO_2	RO2-R.	0.30	0.30	0.30	0.30
$CH_3OC(O)CH_2CH_2C(O)OH$	MEK	0.30	0.30	0.30	0.30
CO	CO	0.30	0.30	0.30	0.30
Reaction at -CH_2 group (~70% assumed)					
Assume reaction (17) (isomerization) dominates					
-NO + NO_2 + HO_2	RO2-R.	0.70			
-NO + NO_2 (secondary radicals)	R2O2.	0.70			
$CH_3OC(O)CH_2CH_2(OH)C(O)OH$	MEK	0.70			
CO	CO	0.70			
Assume reaction (15) (decomposition) dominates					
-NO + NO_2 + HO_2	RO2-R.		0.70		
-NO + NO_2 (secondary radicals)	R2O2.		0.70		
$CH_3OC(O)CH_2CHO$	RCHO		0.70		
HCHO	HCHO		0.70		
CO_2	CO_2		0.70		
Assume reaction (14) (O_2 reaction) dominates					
Assume high reactivity α-keto ester					
-NO + NO_2 + HO_2	RO2-R.			0.70	
$CH_3OC(O)CH_2C(O)C(O)OCH_3$	BACL			0.70	
Assume low reactivity α-keto ester					
-NO + NO_2 + HO_2	RO2-R				0.70
$CH_3OC(O)CH_2C(O)C(O)OCH_3$	MEK				0.70

[a] The overall alkyl nitrate yields for the alternative mechanisms were derived to give best fits to the results of the mini-surrogate + DBE-4 experiments (see Results section.)

[b] The yields shown for the various propitation routes are relative to total propigation only, i.e., not counting nitrate formation. Therefore, the actual yields used in the model calculations (see Appendix A) are the tabulated yields x (1 - the overall nitrate yields).

Table 2. Summary of products and model species used in the assumed mechanism for the atmospheric reactions of DBE-5.

Products	Model Species	Yields Assumed
Alkyl NItrate Formation [a]		
-NO + Organic Nitrate	RO2-N.	0.25
Propigation routes [b]		
Reaction at -CH_3 group (~13% assumed)		
-NO + NO_2 + HO_2	RO2-R.	0.13
$CH_3OC(O)CH_2CH_2CH_2C(O)OH$	MEK	0.13
CO	CO	0.13
Reaction at α-CH_2 group (~30% Assumed) Assume isomerization (Reaction 17 analogue) dominates		
-NO + NO_2 + HO_2	RO2-R.	0.30
-NO + NO_2 (secondary radicals)	R2O2.	0.30
$CH_3OC(O)CH_2CH_2CH_2(OH)C(O)OH$	MEK	0.30
CO	CO	0.30
Reaction at b-CH_2 group (~57% assumed)		
Reaction 26 (O_2 reaction) (~45% assumed)		
-NO + NO_2 + HO_2	RO2-R.	0.28
$CH_3OC(O)CH_2C(O)CH_2C(O)OCH_3$	MEK	0.28
Reaction (27) (decomposition) (~55% assumed)		
-NO + NO_2 + HO_2	RO2-R.	0.34
-2 NO + 2 NO_2 (secondary radicals)	R2O2.	0.68
$CH_3OC(O)CH_2CHO$	RCHO	0.34
$HOCH_2C(O)OH$	MEK	0.34
CO	CO	0.34

[a] The overall alkyl nitrate yield was derived to give best fits to the results of the mini-surrogate + DBE-5 experiments (see Results section.)

[b] The yields shown for the various propitation routes are relative to total propigation only, i.e., not counting nitrate formation. Therefore, the actual yields used in the model calculations (see Appendix A) are the tabulated yields x (1 - the overall nitrate yield).

Table 3. Summary of products and model species used in the assumed mechanism for the atmospheric reactions of DBE-6.

Products	Model Species	Yields Assumed
Alkyl NItrate Formation [a]		
-NO + Organic Nitrate	RO2-N.	0.33
Propigation routes [b]		
Reaction at -CH_3 group (~5% assumed)		
-NO + NO_2 + HO_2	RO2-R.	0.05
$CH_3OC(O)CH_2CH_2CH_2CH_2C(O)OH$	MEK	0.05
CO	CO	0.05
Reaction at α-CH_2 group (~12% Assumed)		
Reaction 22 (isomerization from CH_3) (~34% assumed)		
-NO + NO_2 + HO_2	RO2-R.	0.04
-NO + NO_2 (secondary radicals)	R2O2.	0.04
$CH_3OC(O)CH_2CH_2CH_2CH_2(OH)C(O)OH$	MEK	0.04
CO	CO	0.04
Reaction 23 (isomerization from CH_2) (~66% assumed). High reactivity α-keto ester assumed.		
-NO + NO_2 + HO_2	RO2-R.	0.08
-NO + NO_2 (secondary radicals)	R2O2.	0.08
$CH_3OC(O)CH(OH)CH_2CH_2C(O)C(O)OCH_3$	BACL	0.08
Reaction at β-CH_2 group (~83% assumed)		
Reaction 32 (O_2 reaction) (~27% assumed)		
-NO + NO_2 + HO_2	RO2-R.	0.22
$CH_3OC(O)CH_2CH_2C(O)CH_2C(O)OCH_3$	MEK	0.28
Reaction 33 (decomposition) (~73% assumed)		
-NO + NO_2 + HO_2	RO2-R.	0.61
-NO + NO_2 (secondary radicals)	R2O2.	0.61
2 $CH_3OC(O)CH_2CHO$	RCHO	1.22

[a] The overall alkyl nitrate yield was derived as discussed in the text (see Results section.)

[b] The yields shown for the various propitation routes are relative to total propigation only, i.e., not counting nitrate formation. The actual yields used in the model calculations (see Appendix A) are the tabulated yields x (1 - the overall nitrate yield).

therein) the alkoxy radical formed in Reaction (4) can either react with O_2, decompose, or undergo 1,4 hydrogen shift isomerization,

$$CH_3OC(O)CH_2CH_2C(O)OCH_2O\cdot + O_2 \rightarrow CH_3OC(O)CH_2CH_2C(O)OCHO + HO_2 \quad (6)$$

$$CH_3OC(O)CH_2CH_2C(O)OCH_2O\cdot \rightarrow CH_3OC(O)CH_2CH_2C(O)O\cdot + HCHO \quad (7)$$

$$CH_3OC(O)CH_2CH_2C(O)OCH_2O\cdot \rightarrow CH_3OC(O)CH_2CH(\cdot)C(O)OCH_2OH \quad (8)$$

The current estimation methods (Carter and Atkinson, 1985; Atkinson, 1997) predict that 1,4-H shift isomerization (Reaction 8) will dominate. However, studies with ethyl acetate, where analogous to the above reactions are all possible, indicate that an alternative route, involving an internal shift of the α-alkoxy H atom to the carbonyl group via a 5-member ring transition state,

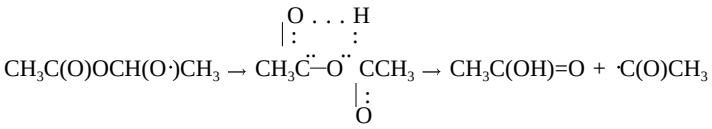

$$CH_3C(O)OCH(O\cdot)CH_3 \rightarrow CH_3C(OH)=O + \cdot C(O)CH_3 \quad (9)$$

apparently dominates over 1,4-H shift isomerization in the case of this compound (unpublished results from this laboratory). The evidence from this comes from the fact that (1) acetic acid is observed as a major product in the photoxidation of ethyl acetate, and (2) the ozone reactivity and PAN yield results in environmental chamber experiments with ethyl acetate can only be simulated if the model assumes the photoxidation process involves significant formation of acetyl ($CH_3CO\cdot$) radicals. Based on these results, it is reasonable to expect that the analogous reactions dominate in the DBE systems. In the case of DBE-4, the analogous reaction is,

$$CH_3OC(O)CH_2CH_2C(O)OCH_2O\cdot \rightarrow CH_3OC(O)CH_2CH_2C(O)OH + HCO\cdot \quad (10)$$

followed by

$$HCO + O_2 \rightarrow HO_2 + CO$$

Note, however, that this is somewhat uncertain, because the competing isomerization process (e.g., Reaction 7 for DBE-4), would be expected to be somewhat faster in the DBE system than for ethyl acetate, since in the DBE system isomerization involves abstraction from a weaker secondary C-H bond, while in the ethyl acetate system abstraction would be from a primary C-H bond in the CH_3 group. No information is currently available concerning the rate constants for these "ester re-arrangement" reactions (e.g., Reactions 9 or 10), but we tentatively assume that they are rapid and compete over dominating processes in systems where they are possible.

The products assumed to be formed in the reaction of OH radicals with the CH_3 group in DBE-4 are shown on Table 1. As discussed above, this involves the formation of CO and the acid monoester

along with conversion of one molecule of NO to NO_2, along with some consumption of NO to form an alkyl nitrate as discussed below.

Reaction at the CH_3 Group in DBE-5 and DBE-6

The reactions following OH attack on the methyl groups of DBE-5 and DBE-6 are expected to be exactly analogous to those for DBE-4, except that the corresponding higher molecular weight monoester acid is formed. The specific sets of products are shown on Tables 2 and 3, respectively.

Reaction at the α-CH_2 Group in DBE-4

The initial reactions following OH attack on the CH_2 group next to the carbonyl in DBE-4 would be expected to proceed as follows:

$$CH_3OC(O)CH_2CH_2C(O)OCH_3 + OH \rightarrow H_2O + CH_3OC(O)CH_2CH(\cdot)C(O)OCH_3 \quad (11)$$

$$CH_3OC(O)CH_2CH(\cdot)C(O)OCH_3 + O_2 \rightarrow CH_3OC(O)CH_2CH(OO\cdot)C(O)OCH_3$$

$$CH_3OC(O)CH_2CH(OO\cdot)C(O)OCH_3 + NO \rightarrow NO_2 + CH_3OC(O)CH_2CH(O\cdot)C(O)OCH_3 \quad (12)$$

$$CH_3OC(O)CH_2CH(OO\cdot)C(O)OCH_3 + NO \rightarrow CH_3OC(O)CH_2CH(ONO_2)C(O)OCH_3 \quad (13)$$

with the alkoxy radical again being able to react either with O_2 or by decomposition or isomerization:

$$CH_3OC(O)CH_2CH(O\cdot)C(O)OCH_3 + O_2 \rightarrow CH_3OC(O)CH_2C(O)C(O)OCH_3 + HO_2 \quad (14)$$

$$0CH_3OC(O)CH_2CH(O\cdot)C(O)OCH_3 \rightarrow CH_3OC(O)CH_2CHO + \cdot C(O)OCH_3 \quad (15)$$

$$0CH_3OC(O)CH_2CH(O\cdot)C(O)OCH_3 \rightarrow CH_3OC(O)CH_2\cdot HC(O)C(O)OCH_3 \quad (16)$$

$$CH_3OC(O)CH_2CH(O\cdot)C(O)OCH_3 \rightarrow CH_3OC(O)CH_2CH(OH)C(O)OCH_2\cdot \quad (17)$$

Based on the estimation methods of Carter and Atkinson (1985), as updated by Atkinson (1997), reaction with O_2 and decomposition (Reactions 14-16) are expected to be minor, and 1,4-H shift isomerization (Reaction 17) is expected to be the major process. However, this estimation method was based on data for alkanes and alkenes, and its applicability to radicals formed in ester systems is highly uncertain. The estimation that Reaction (16) is unimportant is probably not uncertain given the relatively high estimated endothermicity, but the uncertainties of the estimates for the other three reactions are such that none of them can be entirely ruled out. Therefore, all three possibilities are considered.

The radical formed in the decomposition via Reaction (15) is expected to rapidly decompose to CO_2 and methyl radicals, with the latter ultimately forming formaldehyde and HO_2 after an additional NO to NO_2 conversion.

$$CH_3OC(O)\cdot \rightarrow CH_3\cdot + CO_2$$
$$CH_3\cdot + O_2 \rightarrow CH_3OO\cdot$$
$$CH_3OO\cdot + NO \rightarrow NO_2 + CH_3O\cdot$$
$$CH_3O\cdot + O_2 \rightarrow HCHO + HO_2$$

The radical formed after isomerization (Reaction 17) is expected to form, after addition of O_2 and conversion of an additional NO to NO_2 conversion, an alkoxy radical analogous to that formed when OH reacts at the CH_3 group in the DBE, as well as possibly an additional alkyl nitrate formation:

$$CH_3OC(O)CH_2CH(OH)C(O)OCH_2\cdot + O_2 \rightarrow CH_3OC(O)CH_2CH(OH)C(O)OCH_2OO\cdot$$
$$CH_3OC(O)CH_2CH(OH)C(O)OCH_2OO\cdot + NO \rightarrow NO_2 + CH_3OC(O)CH_2CH(OH)C(O)OCH_2O\cdot \quad (19)$$
$$CH_3OC(O)CH_2CH(OH)C(O)OCH_2OO\cdot + NO \rightarrow CH_3OC(O)CH_2CH(OH)C(O)OCH_2ONO_2 \quad (20)$$

Since this alkoxy radical can undergo the "ester rearrangement" which appears to dominate over competing processes in the ethyl acetate system, we assume that this rearrangement, or

$$CH_3OC(O)CH_2CH(OH)C(O)OCH_2O\cdot \rightarrow CH_3OC(O)CH_2CH(OH)C(O)OH + HCO\cdot \quad (21)$$

dominates in this system as well. Note that the $HCO\cdot$ forms HO_2 and CO as shown above.

Table 1 gives the overall products predicted assuming the various alternatives concerning the relative importances of Reactions (14), (15), and (17). Model calculations were carried out using all three of these alternatives.

Reaction at the α-CH_2 Group in DBE-5

The reactions following OH attack on the α-CH_2 groups in DBE-5 and DBE-6 would also be expected to be similar to those discussed above for DBE-4. However, in the case of these compounds, we consider only the case where the isomerizations of the initially formed alkoxy radicals (analogues to Reaction 17) is the dominant process, as predicted by the application of the estimation methods of Atkinson (1997). This is based on the results of the model simulations of the DBE-4 experiments discussed later in this report. In the case of DBE-5, the assumed reactions are exactly analogous to Reactions (11-13, 17, 19-20), above, except that the higher analogue intermediates or product are involved. Table 2 gives the overall products and processes predicted to occur.

Reaction at the α-CH_2 Group in DBE-6

The initial reactions following OH attack on the α-CH_2 group in DBE-6 would also be expected to be similar to those discussed above for DBE-4 and DBE-5. The difference in this case is that the alkoxy radical has a two possible isomerization routes,

$$CH_3OC(O)CH_2CH_2CH_2CH(O\cdot)C(O)OCH_3 \rightarrow CH_3OC(O)CH_2CH_2CH_2CH(OH)C(O)OCH_2\cdot \quad (22)$$

$$CH_3OC(O)CH_2CH_2CH_2CH(O\cdot)C(O)OCH_3 \rightarrow CH_3OC(O)CH(\cdot)CH_2CH_2CH(OH)C(O)OCH_3 \quad (23)$$

where Reaction (22) is analogous to those which can occur in the DBE-4 and DBE-5 systems (e.g., Reaction 17, above), but where Reaction (23) has no analogue for the lower DBE's. Based on application of an estimation method similar to that of Atkinson (1997), we estimate that Reaction (22) occurs ~34% of the time, with the remaining 66% being via Reaction (23). The subsequent reactions assumed for the radical formed following Reaction (22) are exactly analogous to those assumed for the radical formed in Reaction (17) in the DBE-4 system. The radical formed in Reaction (23) is expected to react as follows,

$$CH_3OC(O)CH(\cdot)CH_2CH_2CH(OH)C(O)OCH_3 + O_2 \rightarrow CH_3OC(O)CH(OO\cdot)CH_2CH_2CH(OH)C(O)OCH_3$$

$$CH_3OC(O)CH(OO\cdot)CH_2CH_2CH(OH)C(O)OCH_3 + NO \rightarrow NO_2 + CH_3OC(O)CH(O\cdot)CH_2CH_2CH(OH)C(O)OCH_3$$

$$CH_3OC(O)CH(O\cdot)CH_2CH_2CH(OH)C(O)OCH_3 \rightarrow CH_3OC(O)CH(OH)CH_2CH_2C(OH)(\cdot)C(O)OCH_3$$

$$CH_3OC(O)CH(OH)CH_2CH_2C(OH)(\cdot)C(O)OCH_3 + O_2 \rightarrow HO_2 + CH_3OC(O)CH(OH)CH_2CH_2C(O)C(O)OCH_3$$

The overall products formed in these assumed reactions are summarized in Table 3.

Reaction at the β-CH_2 Group in DBE-5

The initial reactions following OH attack on the β-CH_2 group in DBE-5 are expected to be:

$$CH_3OC(O)CH_2CH_2CH_2C(O)OCH_3 + \cdot OH \rightarrow H_2O + CH_3OC(O)CH_2CH(\cdot)CH_2C(O)OCH_3 \quad (24)$$

$$CH_3OC(O)CH_2CH(\cdot)CH_2C(O)OCH_3 + O_2 \rightarrow CH_3OC(O)CH_2CH(OO\cdot)CH_2C(O)OCH3$$

$$CH_3OC(O)CH_2CH(OO\cdot)CH_2C(O)OCH_3 + NO \rightarrow NO_2 + CH_3OC(O)CH_2CH(O\cdot)CH_2C(O)OCH_3 \quad (25)$$

$$CH_3OC(O)CH_2CH(OO\cdot)CH_2C(O)OCH_3 + NO \rightarrow CH_3OC(O)CH_2CH(ONO_2)CH_2C(O)OCH_3 \quad (26)$$

The alkoxy radical formed in Reaction (25) can react with O_2 or undergo decomposition, though it cannot undergo 1,4-H shift isomerizations analogous to those shown above.

$$CH_3OC(O)CH_2CH(O\cdot)CH_2C(O)OCH_3 + O_2 \rightarrow CH_3OC(O)CH_2C(O)CH_2C(O)OCH_3 + HO_2\cdot \quad (27)$$

$$CH_3OC(O)CH_2CH(O\cdot)CH_2C(O)OCH_3 \rightarrow CH_3OC(O)CH_2\cdot + CH_3OC(O)CH_2CHO \quad (28)$$

If the estimation methods developed by Atkinson (1997) to alkoxy radicals formed in alkane and alkane systems are applied, then Reactions (27) and (28) are estimated to occur ~45% and ~55% of the time, respectively. This estimation method is somewhat less uncertain in the case of this radical because the reacting center is somewhat isolated from the ester centers, but the rate constant ratio is probably still uncertain by at least a factor of two, and thus can be used as an adjustable parameter in the model simulations if necessary. However, the data did not justify such adjustments, so the initial estimates are used in the model simulations discussed in this work.

Table 2 shows the overall products and processes expected following Reactions (27) and (28). The products shown for the decomposition route is based on assuming that the radical formed in Reaction (28) reacts with O_2 and NO to form another alkoxy radical,

$$CH_3OC(O)CH_2\cdot + O_2 \rightarrow CH_3OC(O)CH_2OO\cdot$$
$$CH_3OC(O)CH_2OO\cdot + NO \rightarrow NO_2 + CH_3OC(O)CH_2O\cdot$$

which can react with O_2, decompose, or isomerize.

$$CH_3OC(O)CH_2O\cdot + O_2 \rightarrow CH_3OC(O)CHO + HO_2 \quad (29)$$
$$CH_3OC(O)CH_2O\cdot \rightarrow CH_3OC(O)\cdot + HCHO \quad (30)$$
$$CH_3OC(O)CH_2O\cdot \rightarrow HOCH_2C(O)OCH_2\cdot \quad (31)$$

Decomposition via Reaction (30) is estimated to be too endothermic for this reaction to be important, and the estimation method developed by Atkinson (1997) for alkanes and alkenes predicts that isomerization (Reaction 31) would dominate over O_2 reaction (Reaction 29). Although the applicability of this estimation method to this system is uncertain (see above), the modeling of the DBE-4 system, discussed in the Results section, tends to support this estimation. If this is assumed, then the subsequent reactions are as follows.

$$HOCH_2C(O)OCH_2\cdot + O_2 \rightarrow HOCH_2C(O)OCH_2OO\cdot$$
$$HOCH_2C(O)OCH_2OO\cdot + NO \rightarrow NO_2 + HOCH_2C(O)OCH_2O\cdot$$
$$HOCH_2C(O)OCH_2O\cdot \rightarrow HOCH_2C(O)OH + HCO$$
$$HCO + O_2 \rightarrow HO_2 + CO$$

Note that an alkoxy radical which can undergo the "ester rearrangement" is predicted to be formed, and again this rearrangement is assumed to be the dominant reaction for this radical.

Reaction at the β-CH_2 Group in DBE-6

The reactions immediately following OH attack on the β-CH_2 in DBE-6 are also expected to be analogous to those discussed above for DBE-5. However, in this case, the alkoxy radical formed can react as follows,

$$CH_3OC(O)CH_2CH_2CH(O\cdot)CH_2C(O)OCH_3 + O_2 \rightarrow CH_3OC(O)CH_2CH_2C(O)CH_2C(O)OCH_3 + HO_2\cdot \quad (32)$$
$$CH_3OC(O)CH_2CH_2CH(O\cdot)CH_2C(O)OCH_3 \rightarrow CH_3OC(O)CH_2CH_2\cdot + CH_3OC(O)CH_2CHO \quad (33)$$
$$CH_3OC(O)CH_2CH_2CH(O\cdot)CH_2C(O)OCH_3 \rightarrow CH_3OC(O)CH_2CH_2CHO + CH_3OC(O)CH_2\cdot \quad (34)$$

where again the radical cannot undergo isomerization. Note that in this case there are two possible decompositions instead of one (because of the less symmetrical nature of the molecule), and also the

estimated rates of these decompositions are somewhat different. The application of the estimation method of Atkinson (1997) to this system predicts that the relative importances of the O_2 reaction (Reaction 32) and the two decomposition pathways (Reactions 33 and 34) are 26%, 70%, and 4%, respectively. For modeling purposes, we neglect the minor pathway (Reaction 35), and assume that the relative importances of Reactions 32 and 33 are respectively 73% and 27%, respectively. The expected reactions for the radical formed in Reaction (33) are,

$$CH_3OC(O)CH_2CH_2\cdot + O_2 \rightarrow CH_3OC(O)CH_2CH_2OO\cdot$$
$$CH_3OC(O)CH_2CH_2OO\cdot + NO \rightarrow NO_2 + CH_3OC(O)CH_2CH_2O\cdot$$
$$CH_3OC(O)CH_2CH_2O\cdot + O_2 \rightarrow CH_3OC(O)CH_2CHO + HO_2\cdot$$

with the competing decomposition,

$$CH_3OC(O)CH_2CH_2O\cdot \rightarrow CH_3OC(O)CH_2\cdot + HCHO$$

being predicted to be of negligible importance. Table 6 gives the overall products predicted by these reactions.

Organic Nitrate Formation

Organic nitrate formation via processes such as Reactions 5, 13, 20, and 26 above, also needs to be considered because they are radical and NO_x terminating processes, which, if sufficiently rapid, can significantly affect predictions of ozone impacts. Alkyl nitrate formation is well characterized only for the n-alkanes (Carter and Atkinson, 1989a; Atkinson, 1997), where it has been found to become increasingly important as the size of the molecule increases, and to significantly affect atmospheric reactivities for compounds larger than n-butane (e.g., see Carter and Atkinson, 1989b; Carter, 1994). Some data for organic nitrate yields from branched alkanes are also available, suggesting that organic nitrate yields may be somewhat lower for primary and tertiary peroxy radicals than for the secondary peroxy radicals which dominate in the n-alkane photooxidation systems (Carter and Atkinson, 1989a, and references therein.) There are no quantitative direct measurements of nitrate yields from any of the peroxy radicals expected to be formed in photooxidations of compounds such as esters or ethers, but indirect estimates of overall nitrate yields can be obtained from model simulations of environmental chamber incremental reactivity experiments which are highly sensitive to this parameter (Carter et al, 1993a; Carter, 1995). Model simulations of experiments involving methyl t-butyl ether (Carter et al, 1993a) and several other compounds (unpublished results from this laboratory) suggest that nitrate yields from oxygenated compounds are probably less than those estimated for alkanes of the same molecular weight, but may be comparable to those for alkanes with the same number of carbons. Based on this, we would estimate overall nitrate yields of ~18%, ~27%, and ~36% for DBE-4, DBE-5 and DBE-6, respectively.

As discussed later in this report, the DBE-4 reactivity experiments are best fit assuming nitrate yields in the 10-14% range, depending on what other mechanistic assumptions are used. This is somewhat lower than the initially estimated yields of 18%. On the other hand, the DBE-5 experiments are reasonably well fit assuming nitrate yields of ~25%, only slightly lower than the initially estimated value of ~17%. Based on the DBE-5 results, we estimate that the nitrate yields for DBE-6 will be only slightly lower than the ~36% estimated based on the number of carbons. For atmospheric modeling purposes we use a nitrate yield of ~33% for DBE-6, which is derived based on assuming that the optimum/estimated nitrate yield ratio for DBE-6 is the same as that for DBE-5.

Representation of DBE and DBE Products in the Model

As discussed above, the general chemical mechanism used in the model simulations in this report uses a condensed representation for the reactions of many of the organic products, and a chemical operator approach for representing the net effects of the peroxy radicals with NO_x, HO_2, and other peroxy radicals (Carter, 1990). Tables 1-3 show the specific model species used to represent the various processes predicted to be involved in the DBE photooxidations, and the overall reactions used for the DBE species are given in Appendix A. The model species used for the products include the chemical operators "RO2-R.", "RO2-N.", and "R2O2.", where RO2-R. represents the net effect of peroxy radical reactions which, in the presence of NO_x, involve an NO to NO_2 conversion followed by HO_2 formation, RO2-N. represents the net effect of peroxy radicals which react with NO to form an alkyl nitrate (the latter being represented by the model species "RNO3"), and R2O2. represents the extra NO to NO_2 conversions involved in multi-step mechanisms where additional peroxy radicals are formed, such as those involving alkoxy radical decompositions or isomerizations (Carter, 1990). The products CO, CO2, and formaldehyde are represented explicitly. The model species "MEK" (methyl ethyl ketone) is used to represent higher ketones or other products which are less reactive than aldehydes and more reactive than acetone. This would include products such as the monoacid esters, non-α-dicarbonyl keto esters, and hydroxy keto esters and hydroxy acids as shown on Tables 1-3. This may be a highly approximate representation in some cases, but these low or moderate reactivity products make relatively little contribution to the overall reactivity of the system. The model species "RCHO" (propionaldehyde) is used to represent C_{3+} aldehydes, of which the CH_3OCOCH_2CHO formed in these DBE systems is an example. The reactions used for these model species are given in Appendix A.

The main uncertainty concerns the appropriate representation of α-keto ester species such as the $CH_3OC(O)(CH_2)_nC(O)C(O)OCH_3$ predicted to be formed following reaction at the α-CH_2 group if the reaction of O_2 with the alkoxy radical formed (e.g., Reaction 14 in the DBE-4 system) occurred. If these species are formed and photolyze as rapidly under atmospheric conditions as the simpler α-dicarbonyls such as biacetyl, then they would significantly enhance the overall reactivities of the DBEs. However, esters photolyze at lower wavelengths than do ketones (Calvert and Pitts, 1966), suggesting that α-keto esters may be less photoreactive than biacetyl. On the other hand, Calvert and Pitts (1966) report that α-

keto esters undergo photodecomposition 3660 A, which is a longer wavelength than where ketones and esters absorb, but which is consistent with what would be expected for α-dicarbonyls such as biacetyl. Because of this, we consider it likely that the α-keto esters are relatively photoreactive, though they may be less so than other α-dicarbonyls. For model evaluation purposes, we consider two possibilities, which should bracket the overall uncertainty range: one where the α-keto esters are assumed to photolyze with comparable reactivity as biacetyl and thus may be appropriately represented by the BACL (biacetyl) model species, and the second where they are assumed to have only low or moderate reactivity, and be appropriately represented by MEK. This is shown on Table 1.

Modeling Methods

Environmental Chamber Simulations

The ability of the chemical mechanisms to appropriately simulate the atmospheric impacts of DBE-4 and DBE-5 was evaluated by conducting model simulations of the environmental chamber experiments from this study. This requires including in the model appropriate representations of chamber-dependent effects such as wall reactions and characteristics of the light source. The methods used are based on those discussed in detail by Carter and Lurmann (1990, 1991), updated as discussed by Carter et al. (1995b,c; 1997). The photolysis rates were derived from results of NO_2 actinometry experiments and measurements of the relative spectra of the light source. In the case of the xenon arc lights used in the CTC, the spectra were derived from those measured during the individual experiments, assuming continuous linear changes in relative intensity at the various wavelengths, as discussed by Carter et al. (1997). The thermal rate constants were calculated using the temperatures measured during the experiments, with the small variations in temperature with time during the experiment being taken into account. The computer programs and modeling methods employed are discussed in more detail elsewhere (Carter et al, 1995b). The specific values of the chamber-dependent parameters used in the model simulations of the experiments for this study are given in Table A-4 in Appendix A.

In the case of DBE-4, four alternative mechanisms were used in the environmental chamber simulations to see which of these alternatives were most consistent with the data. These are labeled Models "A" through "D", as indicated in Table 1. In addition, for each of these models, the overall alkyl nitrate yields (as shown on Table 1) were adjusted to give the best fit between experimental and calculated $d(O_3\text{-NO})$ and IntOH reactivities measured in the DBE-4 mini-surrogate reactivity experiments. The mini-surrogate experiments were used for this purpose because experiments and model simulations indicate that they are the most sensitive to this parameter of the three types of reactivity experiments which were we carry out (Carter et al, 1995a). In the case of DBE-5, only a single alternative mechanism was employed, but again the overall nitrate yield (as shown on Table 2) was adjusted based on the model simulations of the mini-surrogate + DBE-5 experiments.

Atmospheric Reactivity Simulations

To estimate its effects on ozone formation under conditions more representative of polluted urban atmospheres, incremental reactivities, defined as the change in O_3 caused by adding small amounts of a compound to the emissions, were calculated for ethane, the three dibasic esters, and the mixture representing the VOCs emitted from all sources. The scenarios employed were those used by Carter (1994a) to develop various reactivity scales to quantify impacts of VOCs on ozone formation in various environments. These were based on a series of single-day EKMA box model scenarios (EPA, 1984) derived by the EPA to represent 39 different urban ozone exceedence areas around the United States (Baugues, 1990). It was found that NO_x levels are the most important factor affecting differences in relative ozone impacts among VOCs, and that the ranges of relative reactivities in the various scales can be reasonably well represented by ranges in relative reactivities in three "averaged conditions" scenarios representing three different NO_x conditions. These scenarios were derived by averaging the inputs to the 39 EPA scenarios, except for the NO_x emissions. In the "maximum reactivity" scenario, the NO_x inputs were adjusted such that the final O_3 level is most sensitive to changes in VOC emissions; in the "maximum ozone" scenario the NO_x inputs were adjusted to yield the highest maximum O_3 concentration; and in the "equal benefit" scenario the NO_x inputs were adjusted such that relative changes in VOC and NO_x emissions had equal effect on ozone formation. As discussed by Carter (1994a), there represent respectively the high, medium and low ranges of NO_x conditions which are of relevance when assessing VOC control strategies for reducing ozone.

The DBE mechanisms used in the atmospheric simulations were those which best fit the results of the chamber experiments, as discussed below. The mechanisms for the reactions of the other species were the same as employed in the chamber simulations, except that the reactions representing chamber effects were removed, and the reactions for the full variety of VOCs emitted into the scenarios (Carter, 1994a) were represented (see Appendix A). Most of the emitted VOCs (other than the test compound whose reactivity is being calculated) are not represented in the model explicitly, but are represented using lumped model species whose rate constants and product yield parameters are derived based on the mixture of compounds they represent. The rate constants and mechanistic parameters for the emitted species in the scenarios were the same as those used previously (Carter et al, 1993b), except for the aromatics, whose unknown photoreactive product yields were reoptimized in a manner analogous to that discussed above for toluene and m-xylene (Carter et al. 1997). The listings on Appendix A give the lumped model species used to represent the emissions into the scenarios, indicate the types of species each is used to represent, and give their rate constants and product yield parameters.

RESULTS AND DISCUSSION

Kinetic Results

Irradiation of a dibasic esters - cyclohexane - air mixture at 20% of the maximum light intensity for 45 min resulted in a measured loss of <2% of any of the three dibasic esters. Photolysis of the dibasic esters was therefore negligible during the CH_3ONO - NO - dibasic ester - cyclohexane - air irradiations used for the OH radical reaction rate constants determinations.

The data obtained from the CH_3ONO - NO - dibasic ester - cyclohexane - air irradiations are plotted in accordance with Equation (I) in Figure 1. Reasonably good straight line plots are observed, and least-squares analyses of these data lead to the rate constant ratios given in Table 4. These rate constant ratios are placed on an absolute basis by use of a rate constant k_2 for the reaction of the OH radical with cyclohexane at 298 K of 7.49×10^{-12} cm^3 $molecule^{-1}$ s^{-1} (±25%) (Atkinson, 1989, 1994), and the resulting rate constants k_1 are also given in Table 1.

The rate constants estimated using the structure-reactivity approach of Kwok and Atkinson (1995), updated as discussed by Kwok et al. (1996), leads to calculated rate constants of 1.15×10^{-12}, 2.56×10^{-12} and 3.97×10^{-12} cm^3 $molecule^{-1}$ s^{-1} for DBE-4, DBE-5 and DBE-6, respectively. The rate constants calculated for DBE-4 and DBE-5 are in reasonable agreement with the measured values, but the calculated rate constant for DBE-6 is lower than the measured value by a factor of 2.2.

Apart from the formation of cyclohexanone and cyclohexyl nitrate from cyclohexane, the GC-FID analyses showed the formation of no other significant product peaks. Note, however that the formation of formaldehyde could not be ruled out because it is not detectable by GC-FID, and it is formed from methyl nitrite photolysis in any case.

Environmental Chamber Results

Summary of Experiments

Table 5 gives a chronological listing of all the experiments carried out for this program. These consisted primarily of incremental reactivity experiments, whose conditions and selected results are summarized on Table 6. Control experiments were conducted to assure consistency with previous results, and side equivalency tests were conducted to assure that essentially equivalent results were obtained when equal mixtures were simultaneously irradiated in each of the dual reaction bags. Table 5 summarizes relevant results from these characterization and control runs.

Table 4. Results of rate constant measurements for the reactions of OH radicals with selected dibasic esters at 298 ± 3 K and 740 Torr of air.

Dibasic Ester	k(DBE) / k(cyclohexane)[a]	10^{12} x k(DBE) (cm^3 $molecule^{-1}$ s^{-1})[b]
$CH_3OC(O)CH_2CH_2C(O)OCH_3$ (DBE-4)	0.195 ± 0.057	1.5 ± 0.6
$CH_3OC(O)CH_2CH_2CH_2C(O)OCH_3$ (DBE-5)	0.464 ± 0.084	3.5 ± 1.1
$CH_3OC(O)CH_2CH_2CH_2CH_2C(O)OCH_3$ (DBE-6)	1.17 ± 0.18	8.8 ± 2.6

[a] Indicated errors are two least-squares standard deviations.

[b] Placed on an absolute basis by use of a rate constant for the reaction of the OH radical with cyclohexane at 298 K of k_2 = 7.49 x 10^{-12} cm^3 $molecule^{-1}$ s^{-1} (±25%) (Atkinson, 1989, 1994). Indicated error limits include the estimated uncertainty in the cyclohexane rate constant.

The results of the characterization and control runs were generally as expected based on our previous experience with these and similar chambers in our laboratories (Carter et al. 1995b and references therein). Good side equivalency was observed when equivalent surrogate - NO_x (not shown on Table 5), propene - NO_x, CO - NO_x, or n-butane - NO_x mixtures were simultaneously irradiated in the dual reactors. The results of the CO - NO_x and n-butane - NO_x experiments, which are highly sensitive to the magnitude of the chamber radical source assumed in the model (see Table A-4 in Appendix A), were sufficiently well simulated by the model to indicate that the model was appropriately representing this effect for these runs. Most of the actinometry results agreed with the extrapolated values based on results of previous determinations, to within the variability of these determinations. The anomalously low Cl_2 actinometry result in run CTC-190 was inconsistent with the result of the NO_2 actinometry experiment carried out at the same time and with the results of other Cl_2 actinometry experiments carried out during the period of the experiments for this program.

Results of The Reactivity Experiments and Mechanism Evaluations

Summaries of the conditions and results of the incremental reactivity experiments are given on Table 6, and figures shown later in this section give time series plots for relevant measurements used for mechanism evaluation. These include concentrations of d(O_3-NO) and m-xylene in the base case and test experiments, concentrations of the DBE in the test experiment, and the d(O_3-NO) and IntOH incremental reactivities derived from the differences between the two sides. Results of model calculations, discussed below, are also shown in these figures.

Both DBE-4 and DBE-5 were observed to inhibit rates of NO oxidation and O_3 formation in the mini-surrogate experiments, and to inhibit OH radical levels in all of the reactivity runs, though the inhibiting effect was greater for DBE-5 than for DBE-4. On the other hand, both DBEs had positive

Figure 1. Plots of Equation (I) for the gas-phase reactions of the OH radical with dimethyl succinate (DBE-4), dimethyl glutarate (DBE-5) and dimethyl adipate (DBE-6), with cyclohexane as the reference organic.

Table 5. Chronolological listing of the environmental chamber experiments carried out for this program.

RunID	Date	Title	Comments
CTC174	11/22/96	Pure air irradiation	After 6 hours of irriadiation, approximately 22 ppb O_3 formed on side A and 24 on side B. Results are within the normal range, and were consistent with the predictions of the chamber effects model.
CTC177	11/27/96	NO2 and Chlorine Actinometry.	In-chamber NO_2 photolysis rates from the NO_2/N_2 tube and the n-butane - Cl_2 method were calculated to be 0.185 and 0.174 min^{-1}, respectively. These are in reasonably good agreement with other actinometry measurements in this chamber.
CTC189	12/23/96	n-Butane + NOx	Control run to measure the chamber radical source. NO consumption rate was slightly slower than predictions of the chamber model, but within the expected range.
CTC190	1/3/97	NO2 and Chlorine Actinometry.	NO_2 photolysis rates from the NO_2/N_2 tube and the n-butane - Cl_2 method were calculated to be 0.160 and 0.107 min^{-1}, respectively. The latter is anomalously low, but the former is within the range observed in other actinometry experiments.
CTC191	1/7/97	Propene + NOx	Control run for comparison with other propene runs carried out in this and other chambers. Good side equivalency was observed. The ozone formation rate was slightly slower than predicted by the model, but within the expected range.
CTC197	1/21/97	Mini Surrogate + DBE-4	DBE-4 in Side B. See Table 6 and Figure 3.
CTC198	1/22/97	Full Surrogate + DBE-4	DBE-4 in Side A. See Table 6 and Figure 5.
CTC199	1/23/97	Low NOx full surrogate + DBE-4	DBE-4 in Side B. See Table 6 and Figure 6.
CTC200	1/24/97	CO + NOx	Control run to measure the chamber radical source. NO consumption rate well fit by predictions of the chamber model. CO data indicated that dilution was negligible.
CTC201	1/28/97	Mini Surrogate + DBE-5	DBE-5 in Side A. See Table 6 and Figure 10.

Table 5 (continued)

RunID	Date	Title	Comments
CTC202	1/30/97	Full Surrogate + DBE-4	DBE-4 in Side B. One of the lamps failed during the run. Also, the ozone monitor malfunctioned and there was no ozone data for most of the run. Run not usable.
CTC203	1/31/97	Propene + NOx	Control run for comparison with other propene runs carried out in this and other chambers. Good side equivalency was observed. The final ozone yield was slightly higher than predicted by the model, but within the expected range.
CTC204	2/4/97	Full Surrogate + DBE-5	DBE-5 in Side A. See Table 6 and Figure 11.
CTC205	2/5/97	Low NOx Full Surrogate + DBE-5	DBE-5 in Side B. See Table 6 and Figure 14.
CTC206	2/6/97	n-Butane + NOx	Control run to measure the chamber radical source. NO consumption rate was slightly slower than predictions of the chamber model, but within the expected range.
CTC207	2/7/97	NO2 and Chlorine Actinometry.	In-chamber NO_2 photolysis rates from the NO_2/N_2 tube and the n-butane - Cl_2 method were calculated to be 0.156 and 0.175 min^{-1}, respectively. These are in reasonably good agreement with other actinometry measurements in this chamber.
CTC208	2/11/97	Full Surrogate + DBE-4	DBE-4 in Side A. See Table 6 and Figure 4.
CTC209	2/12/97	Mini Surrogate + DBE-5	DBE-5 in Side B. See Table 6 and Figure 9.
CTC210	2/13/97	Low NOx Full Surrogate + DBE-4	DBE-4 in Side A. See Table 6 and Figure 7.
CTC211	2/14/97	Mini Surrogate + DBE-4	DBE-4 in Side B. See Table 6 and Figure 2.
CTC212	2/20/97	Full Surrogate + DBE-5	DBE-5 in Side B. See Table 6 and Figure 12.
CTC213	3/28/97	n-Butane + NOx	Control run to measure the chamber radical source. NO consumption rate was slightly slower than predictions of the chamber model, but within the expected range.
CTC214	3/31/97	Low NOx Full Surrogate + DBE-5	DBE-5 in Side B. Lamp failed during run. Run not used.

Table 5 (continued)

RunID	Date	Title	Comments
CTC215	4/7/97	Low NOx Full Surrogate + DBE-5	DBE-5 in Side A. See Table 6 and Figure 13.
CTC218	4/10/97	NO2 and Chlorine Actinometry.	In-chamber NO_2 photolysis rates from the NO_2/N_2 tube and the n-butane - Cl_2 method were calculated to be 0.189 and 0.145 min^{-1}, respectively. These are in the range of results of other actinometry measurements in this chamber.
CTC219	4/11/97	Propene + NOx	Control run for comparison with other propene runs carried out in this and other chambers. Good side equivalency was observed. The results are in the expected range and in good agreement with model predictions.
CTC224	4/21/97	CO + NOx	Control run to measure dilution and the chamber radical source. Results are consistent with predictions of chamber model. No measurable dilution observed.

effects on d(O_3-NO) in both the high NO_x and the low NO_x full surrogate runs, indicating a significant effect of base ROG surrogate on the ozone reactivities of these compounds. This is similar to results observed in reactivity experiments with high molecular weight alkanes and other compounds whose atmospheric reactions tend to both inhibit radical levels and yet react to form radicals which cause direct ozone formation by converting NO to NO_2 (Carter et al, 1995a). The radical inhibition effect causes the uniformly negative IntOH reactivities, and also causes the negative d(O_3-NO) reactivities in the mini-surrogate experiments, which are highly sensitive to radical inhibition/initiation effects. Because the full surrogate contains radical initiating species such as formaldehyde (which forms radicals upon photolysis) and higher alkenes (which form radicals when reacting with O_3), they tend to be less sensitive to radical initiation or inhibition effects of the test VOCs. Consequently, these runs are more sensitive to effects such as NO to NO_2 conversions caused by the test VOCs' direct reactions (Carter et al, 1995a). In the case of these DBEs, the sensitivity to the inhibition effect becomes sufficiently reduced that the positive effects of the NO to NO_2 conversions in the DBEs' reactions becomes more important, resulting in positive net d(O_3-NO) incremental reactivities.

Table 6. Summary of conditions and selected results of the incremental reactivity experiments.

As with the alkanes (Cater et al, 1993a, 1995a,d) the radical inhibition effect for the DBEs is attributed to alkyl nitrate formation in the RO_2+NO reactions such as in Reactions 5, 13, 20, and 26 above. The greater level of inhibition observed for DBE-5 than for DBE-4 is consistent with the predicted higher nitrate yields for DBE-5, based on the larger size of the molecule. Note that the predicted polyfunctional organic nitrate products cannot be detected using the GC techniques employed in this study, so the occurrence of this process can only be inferred based on its apparent effect on d(O_3-NO) and IntOH levels.

Because the actual overall alkyl nitrate yields in the DBE photooxidation systems are unknown, the nitrate yields used for atmospheric reactivity estimation purposes were determined by adjusting them to fit the environmental chamber data. Since the mini-surrogate experiments are the most sensitive to the

Table 6. Summary of conditions and results of the incremental reactivity experiments.

Run	Initial Reactants (ppm)			t=6 d(O_3-NO) (ppm)			t=6 IntOH (10^{-6} min)		
	NOx	Surg [a]	DBE	Base	Test	IR [b]	Base	Test	IR
				DBE-4					
Mini-Surrogate									
CTC-211(B)	0.23	5.0	8.6	0.54	0.50	-0.005	19	8	-1.2
CTC-197(B)	0.27	5.1	16.5	0.57	0.51	-0.004	18	6	-0.7
Full Surrogate - High NOx									
CTC-208(A)	0.46	6.4	9.1	0.70	0.99	0.032	24	18	-0.6
CTC-198(A)	0.41	6.1	16.4	0.71	1.09	0.023	23	12	-0.7
Full Surrogate - Low NOx									
CTC-199(B)	0.16	5.8	8.4	0.44	0.56	0.014	21	12	-1.0
CTC-210(A)	0.17	6.0	13.3	0.44	0.60	0.011	21	10	-0.8
				DBE-5					
Mini-Surrogate									
CTC-209(B)	0.27	5.0	4.2	0.55	0.33	-0.052	17	5	-3.0
CTC-201(A)	0.25	4.9	8.7	0.51	0.22	-0.033	15	2	-1.4
Full Surrogate - High NOx									
CTC-204(A)	0.48	6.3	4.5	0.71	0.88	0.038	-	15	-
CTC-212(B)	0.46	6.0	5.2	0.66	0.81	0.029	22	14	-1.5
Full Surrogate - Low NOx									
CTC-215(A)	0.19	5.5	7.1	0.47	0.58	0.015	22	10	-1.7
CTC-205(B)	0.17	6.2	4.5	0.47	0.54	0.017	22	11	-2.3

Notes

[a] Total base ROG surrogate in ppmC.

[b] Incremental reactivity

radical inhibiting effects of the organic nitrate formation process, simulations of those experiments were used for this purpose. The ability of the models to predict the results of the other types of experiments can then be used to evaluate other aspects of the mechanisms, such as the assumed numbers of NO to NO_2 conversions and the reactivities of the assumed products, which will have differing effects on model simulations of the different types of experiments.

Evaluation of the Alternative DBE-4 Mechanisms

As discussed in the previous section, four alternative DBE-4 photooxidation mechanisms, employing differing assumptions concerning uncertain aspects of the mechanism, were evaluated. Because the different alternative mechanisms predict different amounts of NO to NO_2 conversions and different levels of radical initiation from the products formed, the alkyl nitrate yields which best fit the mini-surrogate experiments differed depending on which mechanism was assumed. The best fit nitrate yields for each of the four mechanisms are given in Table 1, above, and are in the 10-14% range for Models A, B, and D, and are 28% for Model C. The much higher nitrate yield for Model C is because that mechanism predicts relatively high yields of a highly photoreactive product (represented by biacetyl in the model), which provides significant radical initiation which must be balanced by additional termination of higher nitrate yields to yield the same results as models which assume that such a highly photoreactive product is not formed.

Figures 2 and 3 show experimental and calculated d(O_3-NO) and IntOH data for the DBE-4 mini-surrogate experiments, and Figures 4-7 show plots of these data for the full surrogate DBE-4 runs. Figures 2 and 3 show that with appropriately adjusted nitrate yields all four of the alternative DBE-4 mechanisms can fit the mini-surrogate data to within the experimental uncertainty. However, Figures 4-7 show that Model C does not satisfactorily simulate the d(O_3-NO) results of the full surrogate experiments, and therefore can be ruled out on this basis. On the other hand, the Models A, B, and D perform reasonably well in simulating the full surrogate experiments, though Model D tends to slightly underpredict d(O_3-NO) reactivities in the higher NO_x runs, while Model A tends to slightly overpredict in the lower NO_x runs. However, these discrepancies between model simulations and experimental data are not sufficiently large to rule out any of these three alternatives.

Model B differs from the other DBE-4 mechanisms in that it predicts significant amounts of formaldehyde formation in the DBE-4 reactions. This was not consistent with the results of our experiments. Figure 8 shows the experimental concentration-time plots for formaldehyde in all of the DBE-4 reactivity runs, where they are compared with those calculated using the three models which are not inconsistent with the d(O_3-NO) data. It can be seen that Model B significantly overpredicts the formaldehyde yields in the added DBE experiments, while the formaldehyde levels predicted by the models assuming no formaldehyde formation from DBE-4 are quite consistent with the data. Note that

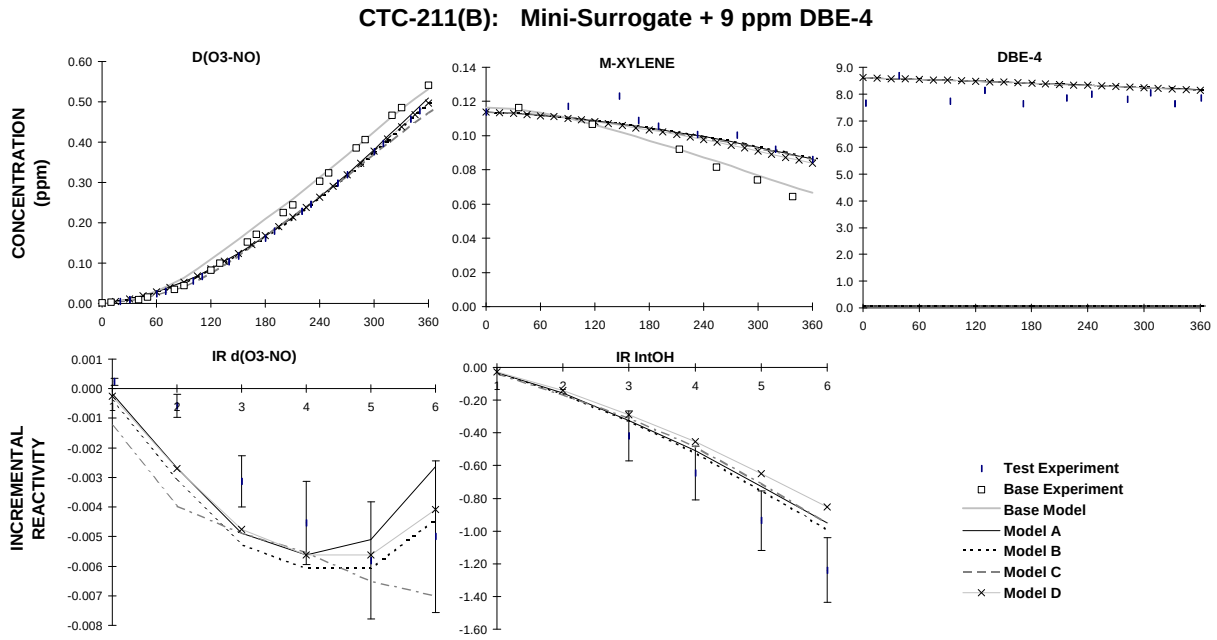

Figure 2. Plots of selected results of the mini-surrogate + DBE-4 run CTC-211.

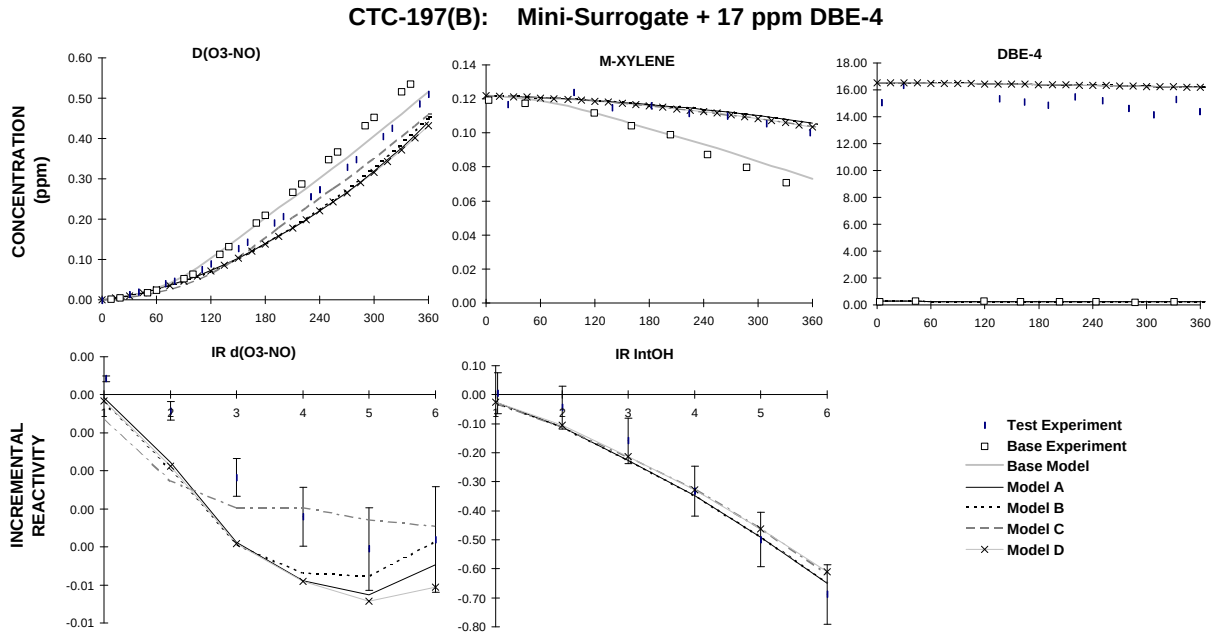

Figure 4. Plots of selected results of the mini-surrogate + DBE-4 run CTC-197.

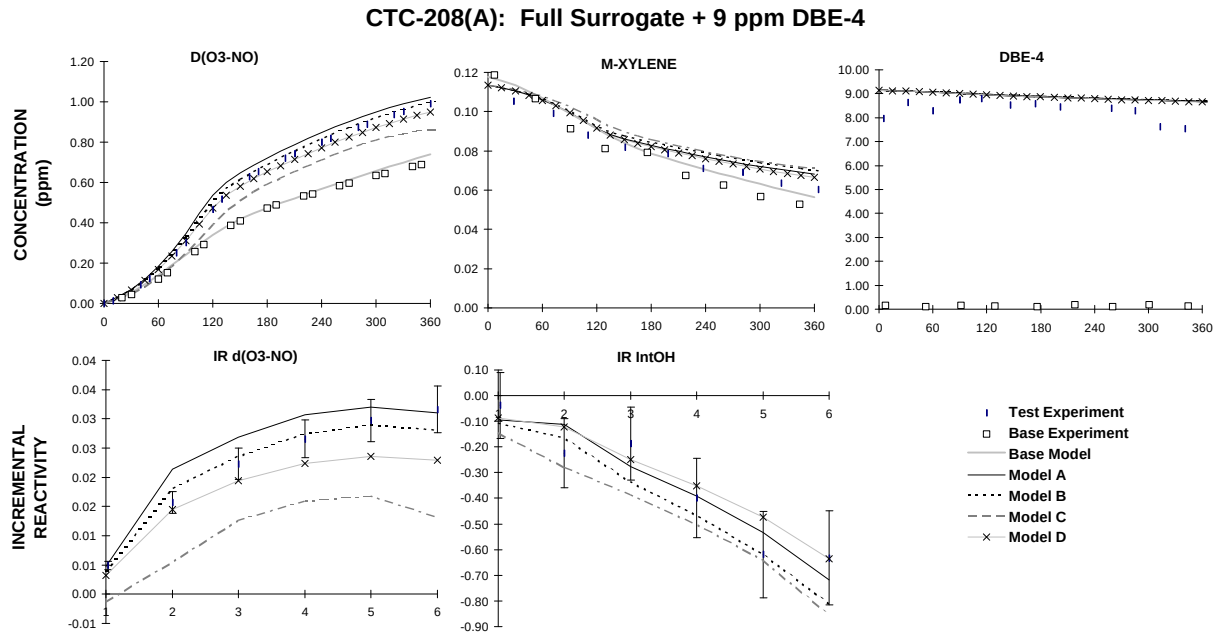

Figure 4. Plots of selected results of the full surrogate + DBE-4 run CTC-208.

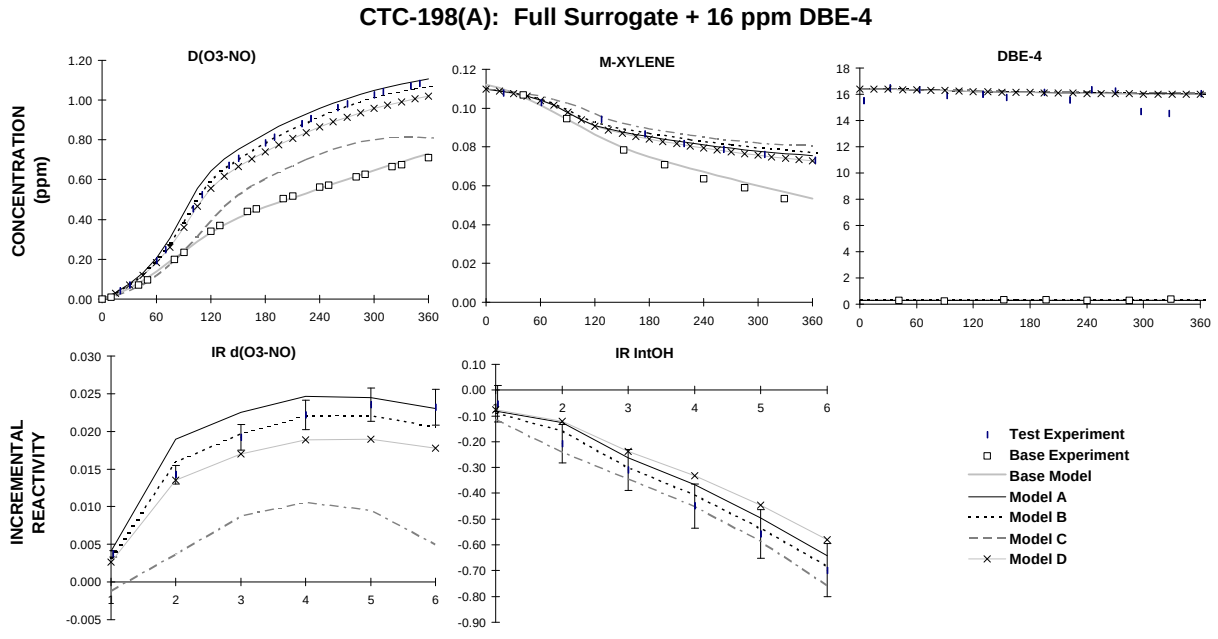

Figure 5. Plots of selected results of the full surrogate + DBE-4 run CTC-198.

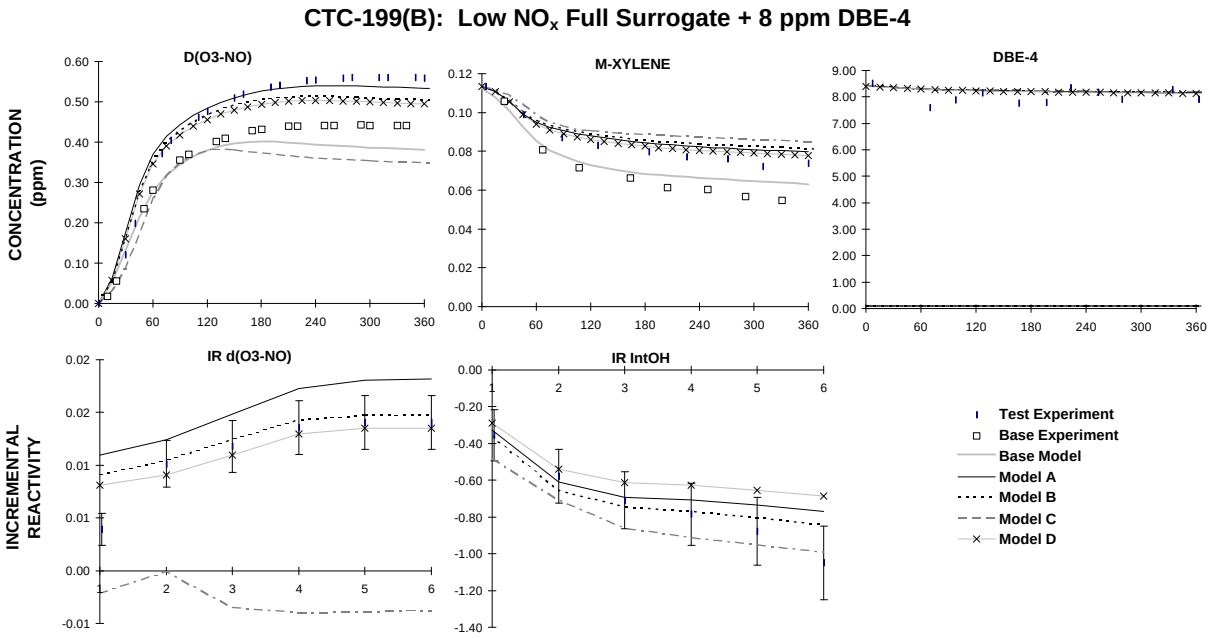

Figure 6. Plots of selected results of the low NO_x full surrogate + DBE-4 run CTC-199.

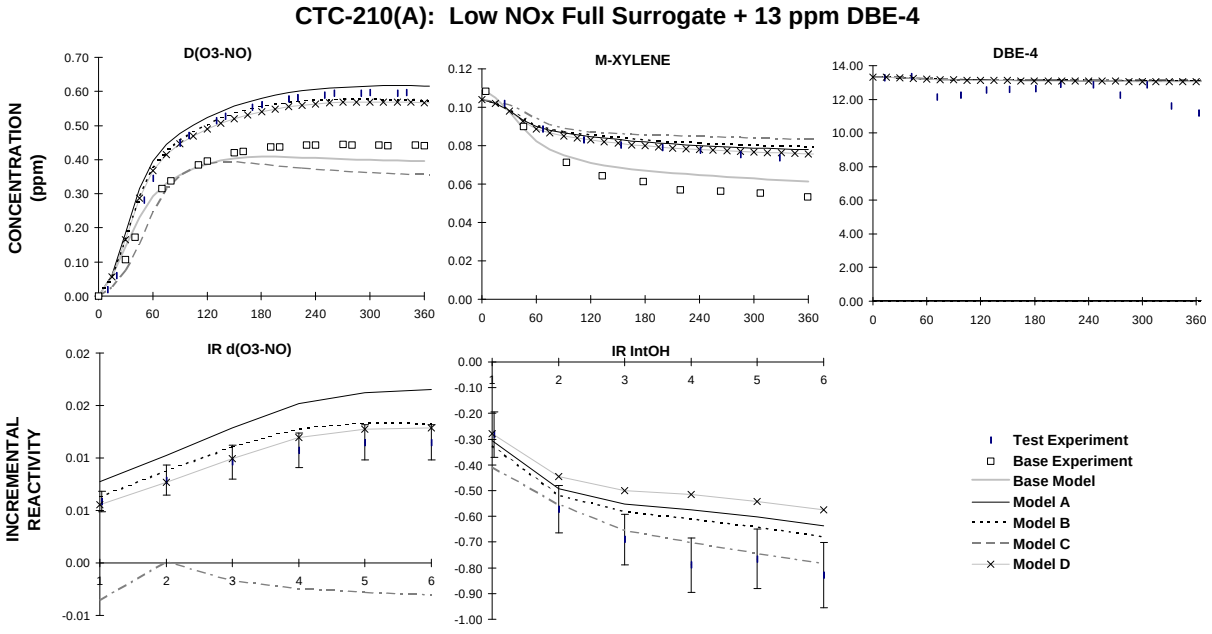

Figure 7. Plots of selected results of the low NO_x full surrogate + DBE-4 run CTC-210.

Figure 8. Plots of experimental and calculated concentration-time data for formaldehyde in the DBE-4 reactivity experiments.

the suppression in the formaldehyde levels caused by adding DBE-4 to the mini-surrogate is attributed to the suppression of overall radical levels by DBE-4, which reduces the rate of the OH + ethene reaction, the primary formaldehyde source in these experiments. Although Model B also predicts a suppression in the formaldehyde formation in the added DBE-4 mini-surrogate runs, this suppression was far less than was observed experimentally.

Therefore, the chamber data rule out DBE-4 models B and C, but are not inconsistent with wither Models A and D. However, Model A is considered to be somewhat more likely to be correct based on fundamental mechanistic considerations. In the first place, as discussed above it is unlikely that the α-keto ester product is really as unreactive as estimated in Model D, even if may be less reactive than biacetyl, as assumed in Model C. In addition, the estimation methods developed for the alkanes and alkenes (Atkinson, 1997) predict not only that reaction of the $CH_3OC(O)CH_2CH(O\cdot)C(O)OCH_3$ radical with O_2, which is assumed to dominate in Models C and D, is not only slower than its isomerization (as assumed by Model A), but is also slower than its decomposition via Reaction (15), which, based on the formaldehyde data, has been shown not to be important. Since the chamber data are not inconsistent with Model A, and

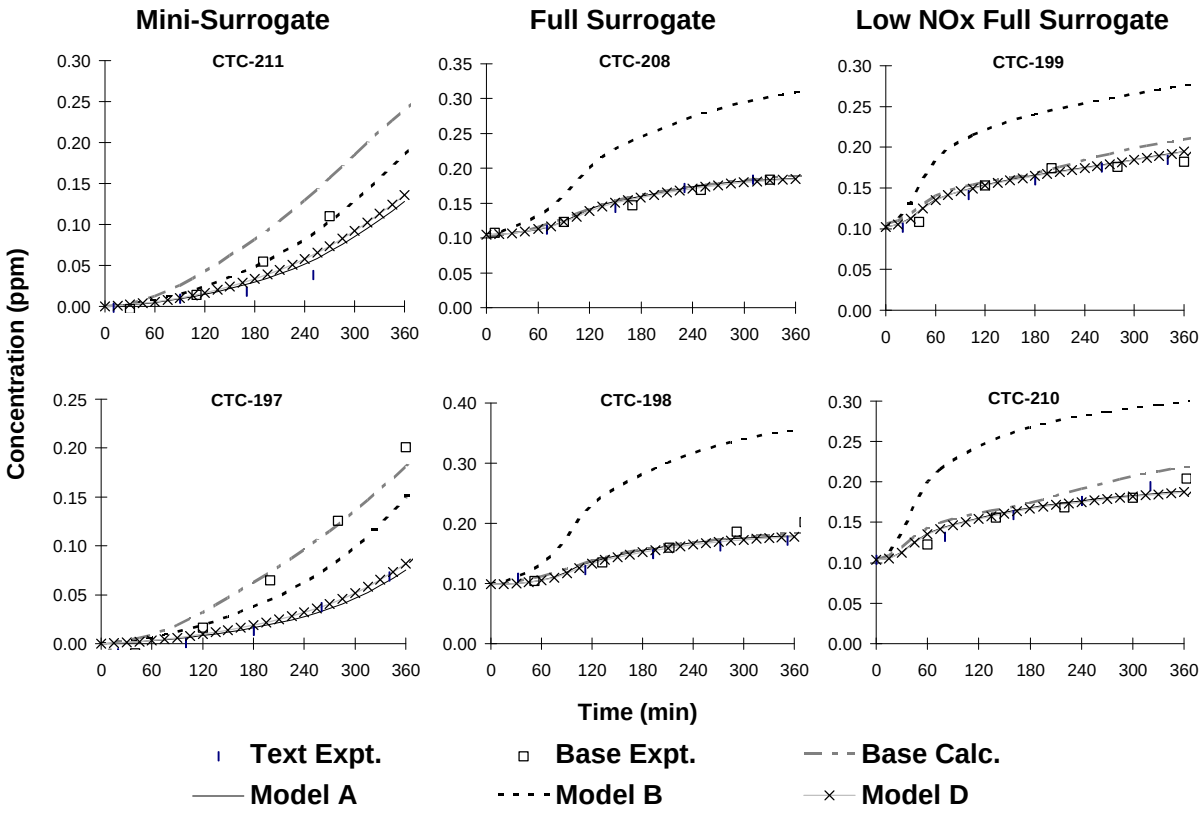

Figure 8. Plots of experimental and calculated concentration-time data for formaldehyde in the DBE-4 reactivity experiments.

since this model is predicted to be most reasonable based on current estimation methods, we assume that this is the most likely mechanism to be correct, and we assume that the analogous isomerization also dominates in the estimated DBE-5 and DBE-6 mechanisms (as shown in Tables 2 and 3, above). Note that this assumption is less important in the DBE-5 and DBE-6 systems, because reaction at the β-CH_2 route, which is not involved in the DBE-4 system, is a major or dominant process for the higher DBEs.

Evaluation of the DBE-5 Mechanism

Figures 9-14 show plots of the experimental and calculated d(O_3-NO) and IntOH reactivity results for the DBE-5 reactivity experiments, and plots of experimental and calculated formaldehyde data are shown on Figure 15. As with DBE-4, the overall organic nitrate yield was adjusted to yield the best fits to the mini-surrogate experiments, though in this case the best fit overall nitrate yield, 25%, was relatively close to the initial estimate of ~26%. As shown on Figures 9 and 10, the adjusted mechanism slightly overpredicts the inhibition of d(O_3-NO) run CTC-209(B), but overpredicts it by about the same amount in run CTC-201(A). This is within the expected variability of these experiments. Figures 11-14 show that the results of the full surrogate experiments are reasonably well simulated by the model, though there is a slight tendency for the model to underpredict the d(O_3-NO) reactivities in the low NO_x runs. This discrepancy is not sufficiently large to justify further adjustments of the assumed DBE-5 mechanism, particularly in view of the fact that the adjusted nitrate yield model slightly underpredicts O_3 yields in the base case experiments, which may result in small biases in the simulations of incremental reactivities of added VOCs.

The assumed mechanism predicts that the photoxidation of DBE-5 does not result in significant formaldehyde formation. Figure 15 shows that the addition of DBE-5 suppresses formaldehyde yields in the mini-surrogate experiments, but has no significant effect on formaldehyde formation in the full surrogate runs. This is essentially the same as observed with DBE-4 (see Figure 8). As with DBE-4, the suppression in formaldehyde yields in the mini-surrogate experiments is due to the suppression in overall radical levels caused by the nitrate formation in the DBE-5 reaction slowing down the rate of formaldehyde formation in the oxidation of ethene. These results are consistent with the predictions of the estimated DBE-5 mechanism, which assumes no formaldehyde formation from DBE-5.

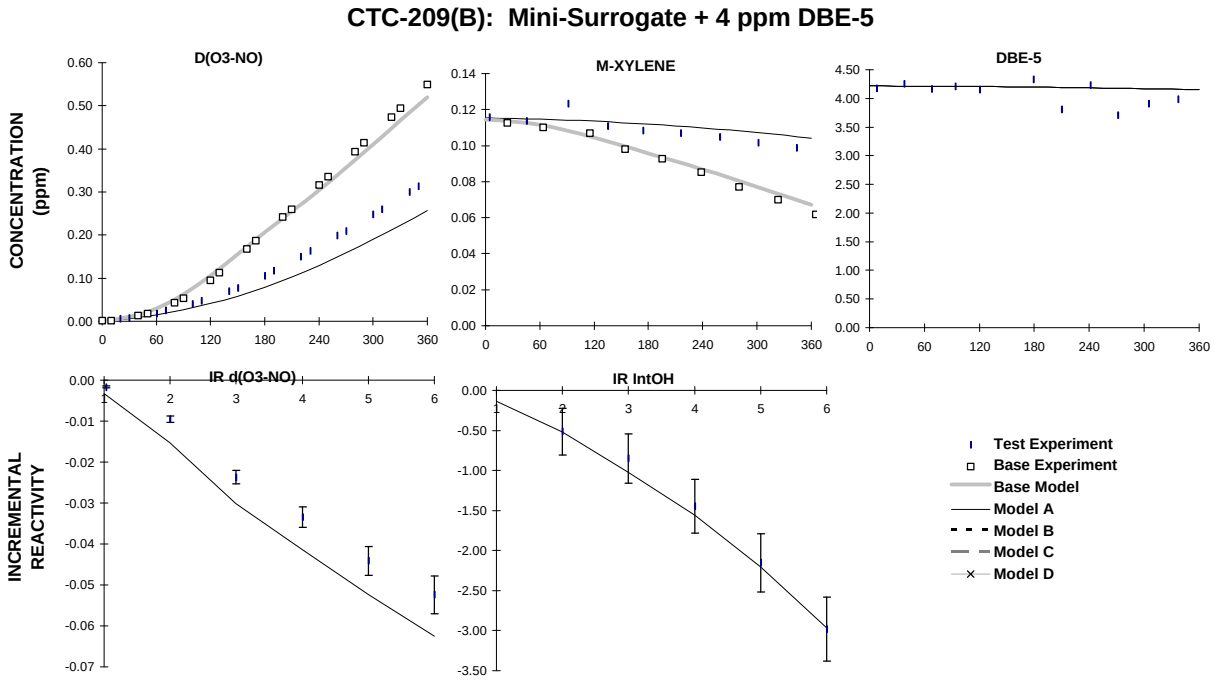

Figure 9. Plots of selected results of the mini-surrogate + DBE-5 run CTC-209.

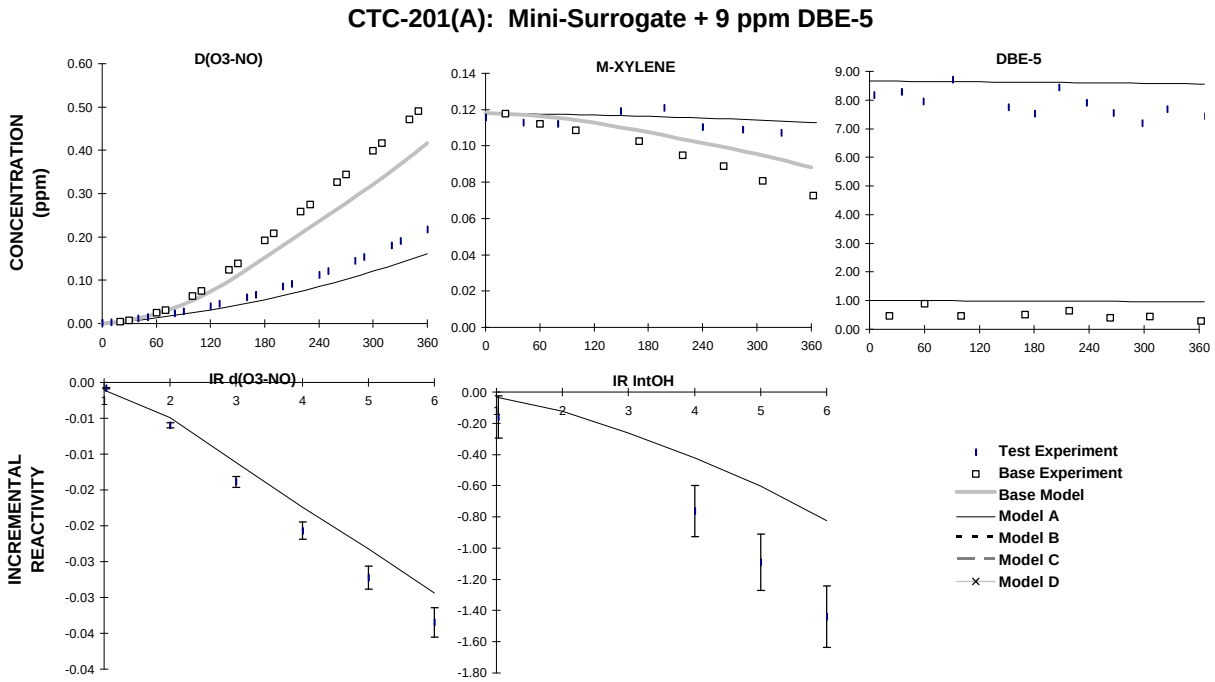

Figure 10. Plots of selected results of the mini-surrogate + DBE-5 run CTC-201.

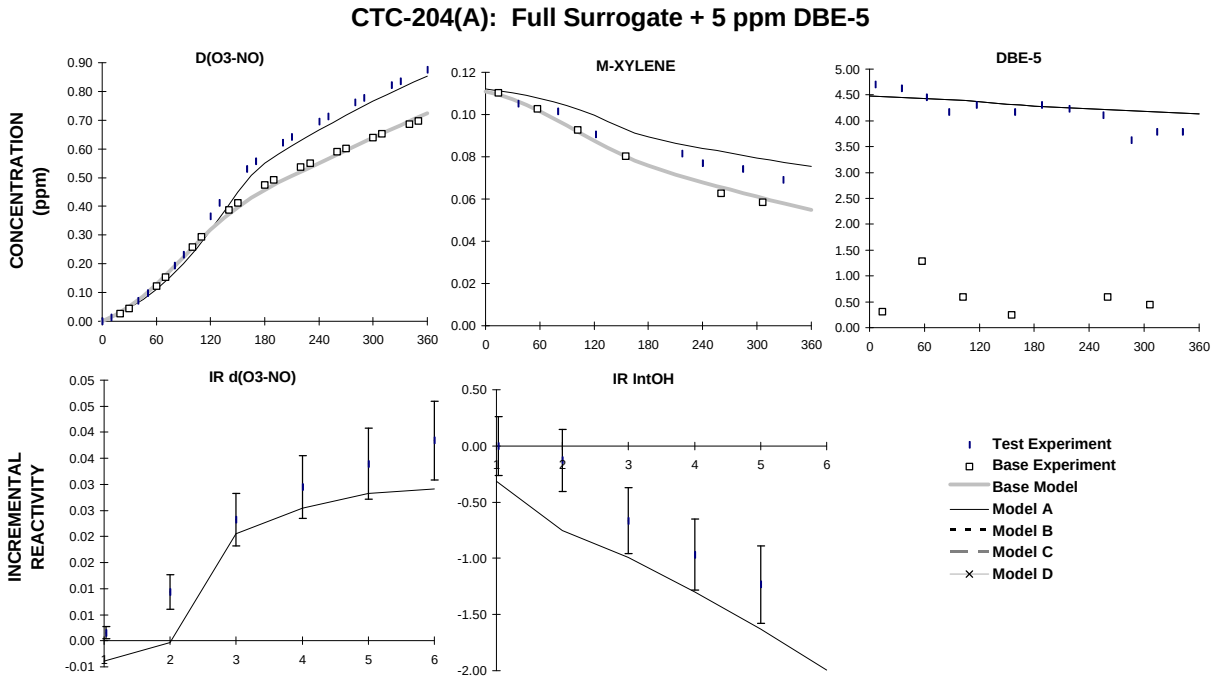

Figure 11. Plots of selected results of the full surrogate + DBE-5 run CTC-204.

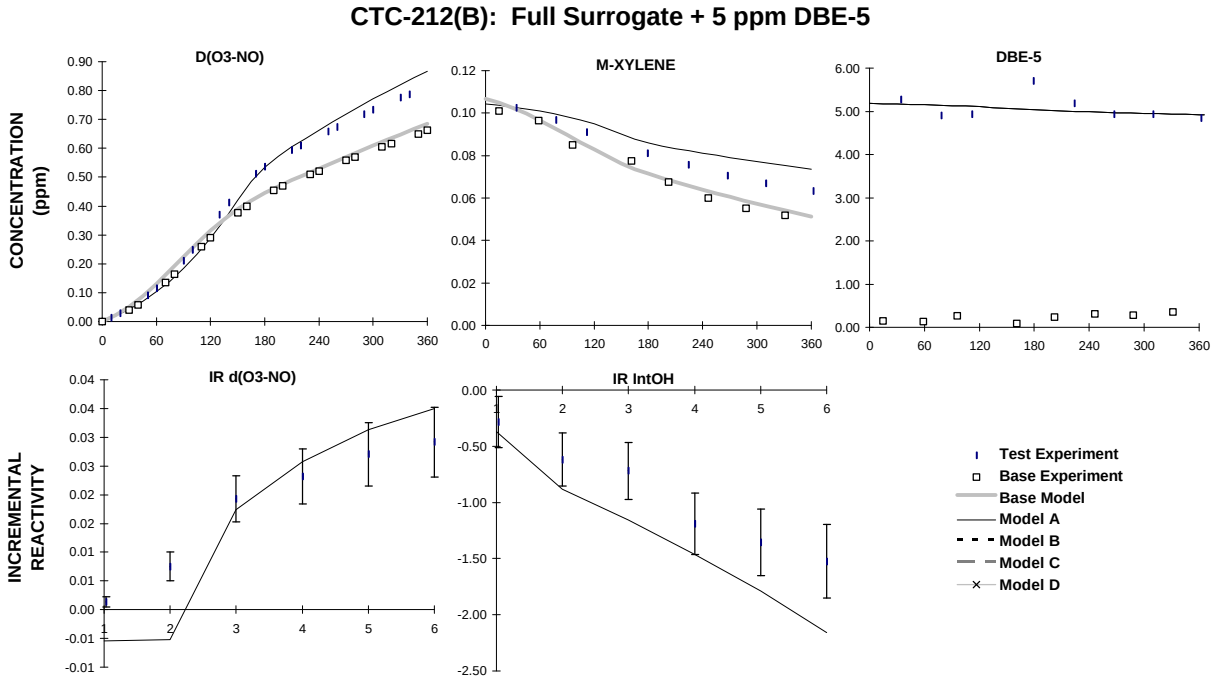

Figure 12. Plots of selected results of the full surrogate + DBE-5 run CTC-212.

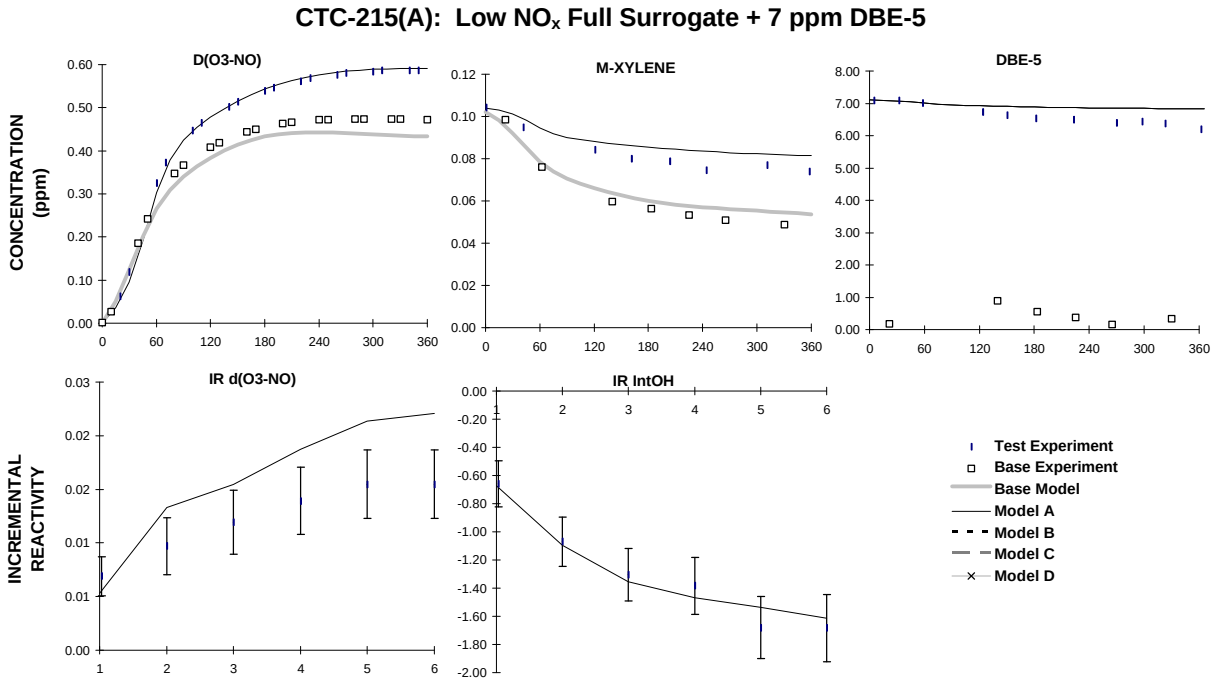

Figure 13. Plots of selected results of the low NO_x full surrogate + DBE-5 run CTC-215.

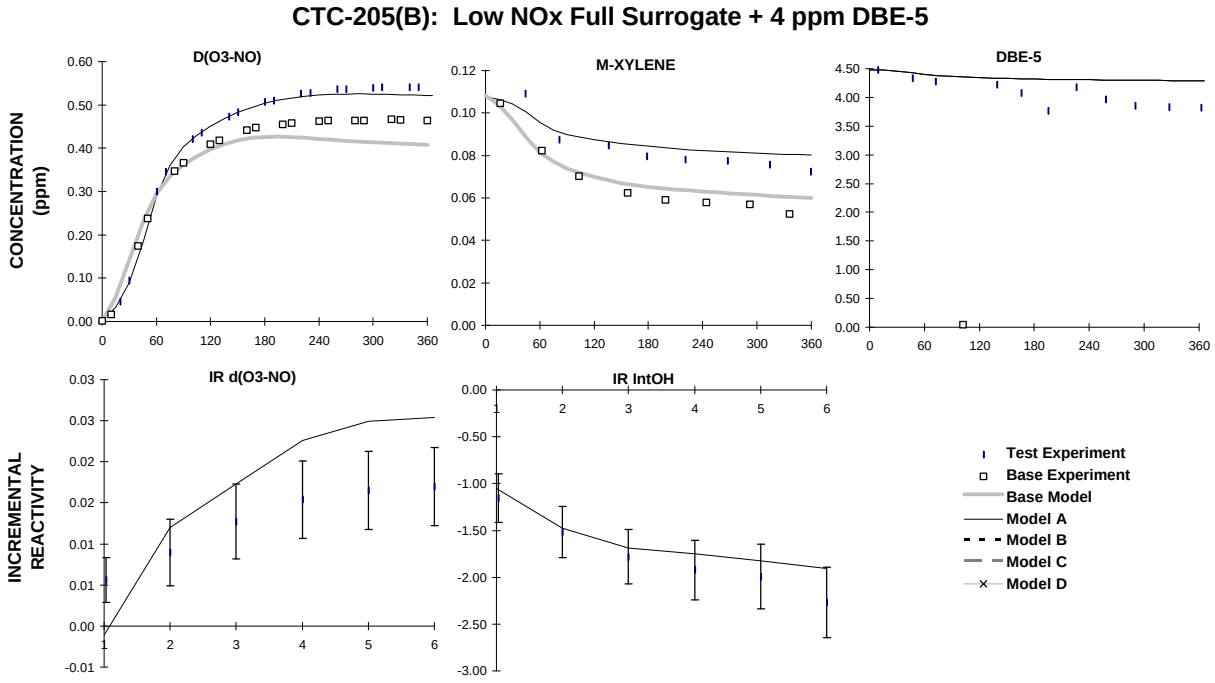

Figure 14. Plots of selected results of thelow NO_x full surrogate + DBE-5 run CTC-205.

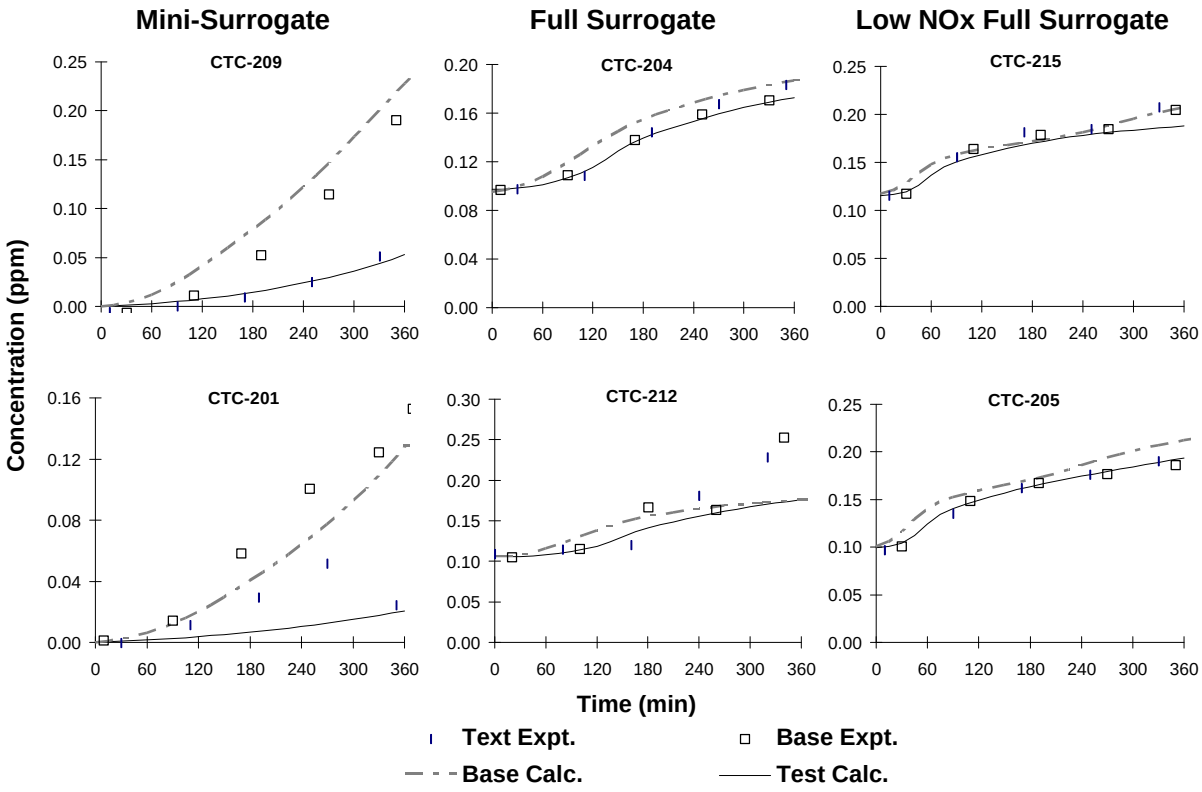

Figure 15. Plots of experimental and calculated concentration-time data for formaldehyde in the DBE-5 reactivity experiments.

ATMOSPHERIC REACTIVITY CALCULATIONS

Incremental reactivities of VOCs have been shown to be highly dependent on environmental conditions, so reactivities measured in environmental chamber experiments cannot necessarily be assumed to be the same as those under atmospheric conditions (Carter and Atkinson, 1989b; Carter et al, 1995a). Because of this, the only method available to obtain quantitative estimates of incremental reactivities of VOCs in ambient air pollution episodes is to conduct airshed model simulations of the episodes. Since these simulations cannot be any more reliable than the chemical mechanisms used, the major objective of this program was to assess the reliability of the DBE-4 and DBE-5 mechanisms for use in such calculations. This was discussed in the previous sections. In this section, we discuss the results of model simulations of the incremental reactivities of the DBE's in a variety of model scenarios representing ozone exceedence episodes in various areas in the United States, and compare the results to incremental reactivities calculated for ethane, the compound used by the EPA as the criterion for determining "negligible" reactivity, and for the base ROG, the mixture representing total ROG emissions from all sources. Because the data from the DBE-4 experiments are insufficient to distinguish between models A and D, which are both reasonably consistent with most of the data, both models will be used in the atmospheric reactivity calculations for this compound. Although atmospheric reactivity estimates are also presented for DBE-6, the DBE-6 must be considered to be more uncertain because no chamber data were obtained to evaluate the predictive capability of the assumed mechanism for this compound.

Scenarios Used for Reactivity Assessment

The set of airshed scenarios employed to assess the DBE reactivities for this study is the same as those used for calculating the MIR and other reactivity scales (Carter, 1994a; Carter et al, 1993b). The objective is to use a set of scenarios which represents, as much as possible, a comprehensive distribution of the environmental conditions where unacceptable levels of ozone are formed. Although a set of scenarios has not been developed for the specific purpose of VOC reactivity assessment, the EPA developed an extensive set of scenarios for conducting analyses of effects of ROG and NO_x controls on ozone formation using the EKMA modeling approach (Gipson et al. 1981; Gipson and Freas, 1983; EPA, 1984; Gery et al. 1987; Baugues, 1990). The EKMA approach involves the use of single-cell box models to simulate how the ozone formation in one day episodes is affected by changes in ROG and NO_x inputs. Although single-cell models cannot represent realistic pollution episodes in great detail, they can represent dynamic injection of pollutants, time-varying changes of inversion heights, entrainment of pollutants from aloft as the inversion height raises, and time-varying photolysis rates, temperatures, and humidities (Gipson and Freas, 1981; EPA, 1984; Gipson, 1984; Hogo and Gery, 1988). Thus, they can be used to simulate a wide range of the chemical conditions which affect ozone formation from ROG and NO_x, and which affect VOC reactivity. Therefore, at least to the extent they are suitable for their intended purpose, an

appropriate set of EKMA scenarios should also be suitable for assessing reactivities over a wide range of conditions.

Base Case Scenarios

The set of EKMA scenarios used in this study were developed by the United States EPA for assessing how various ROG and NO_x control strategies would affect ozone nonattainment in various areas of the country (Baugues, 1990). The characteristics of these scenarios and the methods used to derive their input data are described in more detail elsewhere (Baugues, 1990; Carter, 1994b). Briefly, 39 urban areas in the United States were selected based on geographical representativeness of ozone nonattainment areas and data availability, and a representative high ozone episode was selected for each. The initial non-methane organic carbon (NMOC) and NO_x concentrations, the aloft O_3 concentrations, and the mixing height inputs were based on measurement data for the various areas, the hourly emissions in the scenarios were obtained from the National Acid Precipitation Assessment Program emissions inventory (Baugues, 1990), and biogenic emissions were also included. Table 7 gives a summary of the urban areas represented and other selected characteristics of the scenarios.

Several changes to the scenario inputs were made based on discussions with the California ARB staff and others (Carter, 1994b). Two percent of the initial NO_x and 0.1% of the emitted NO_x in all the scenarios was assumed to be in the form of HONO. The photolysis rates were calculated using solar light intensities and spectra calculated by Jeffries (1991) for 640 meters, the approximate mid-point of the mixed layer during daylight hours. The composition of the NMOCs entrained from aloft was based on the analysis of Jeffries et al. (1989). The composition of the initial and emitted reactive organics was derived as discussed below. Complete listings of the input data for the scenarios are given elsewhere (Carter, 1994b).

This set of 39 EKMA scenarios are referred to as "base case" to distinguish them from the scenarios derived from them by adjusting NO_x inputs to yield standard conditions of NO_x availability as discussed below. No claim is made as to the accuracy of these scenarios in representing any real episode, but they are a result of an effort to represent, as accurately as possible given the available data and the limitations of the formulation of the EKMA model, the range of conditions occurring in urban areas throughout the United States. When developing general reactivity scales it is more important that the scenarios employed represent a realistic distribution of chemical conditions than accurately representing the details of any one particular episode.

The Base ROG mixture is the mixture of reactive organic gases used to represent the chemical composition of the initial and emitted anthropogenic reactive organic gases from all sources in the scenarios. Consistent with the approach used in the original EPA scenarios, the same mixture was used for all scenarios. The speciation for this mixture was derived by Croes (1991) based on an analysis of

Table 7. Summary of conditions of base case scenarios used for atmospheric reactivity assessment.

City, State	Calc. Max O_3 (ppb)	ROG /NO_x	NO_x /NO_x^{MOR}	Final Height (km)	Init.+Emit Base ROG (mmol m^{-2})	Aloft O_3 (ppb)
Atlanta, GA	179	7.3	0.7	2.1	12	63
Austin, TX	175	9.3	0.5	2.1	11	85
Baltimore, MD	326	5.2	1.0	1.2	17	84
Baton Rouge, LA	247	6.8	0.8	1.0	11	62
Birmingham, AL	238	6.9	0.5	1.8	13	81
Boston, MA	195	6.5	0.6	2.6	14	105
Charlotte, NC	143	7.8	0.3	3.0	7	92
Chicago, IL	281	11.6	0.5	1.4	25	40
Cincinnati, OH	198	6.4	0.7	2.8	17	70
Cleveland, OH	251	6.6	0.9	1.7	16	89
Dallas, TX	213	4.7	1.2	2.3	18	75
Denver, CO	211	6.3	1.0	3.4	29	57
Detroit, MI	238	6.8	0.7	1.8	17	68
El Paso, TX	188	6.6	0.9	2.0	12	65
Hartford, CT	169	8.4	0.5	2.3	11	78
Houston, TX	307	6.1	0.9	1.7	25	65
Indianapolis, IN	211	6.6	0.8	1.7	12	52
Jacksonville, FL	156	7.6	0.6	1.5	8	40
Kansas City, MO	154	7.1	0.6	2.2	9	65
Lake Charles, LA	291	7.4	0.6	0.5	7	40
Los Angeles, CA	580	7.6	0.8	0.5	23	100
Louisville, KY	210	5.5	0.8	2.5	14	75
Memphis, TN	225	6.8	0.6	1.8	15	58
Miami, FL	133	9.6	0.4	2.7	9	57
Nashville, TN	166	8.1	0.4	1.6	7	50
New York, NY	363	8.1	0.7	1.5	39	103
Philadelphia, PA	242	6.2	0.9	1.8	19	53
Phoenix, AZ	275	7.6	0.8	3.3	40	60
Portland, OR	165	6.5	0.7	1.6	6	66
Richmond, VA	233	6.2	0.7	1.9	16	64
Sacramento, CA	202	6.6	0.8	1.1	7	60
St Louis, MO	322	6.1	1.0	1.6	26	82
Salt Lake City, UT	184	8.5	0.6	2.2	11	85
San Antonio, TX	132	3.9	1.0	2.3	6	60
San Diego, CA	196	7.1	0.9	0.9	8	90
San Francisco, CA	325	4.8	1.5	0.7	25	70
Tampa, FL	232	4.4	1.0	1.0	8	68
Tulsa, OK	225	5.3	0.9	1.8	15	70
Washington, DC	276	5.3	0.8	1.4	13	99

the EPA database (Jeffries et al. 1989) for the hydrocarbons and the 1987 Southern California Air Quality Study (SCAQS) database for the oxygenates (Croes et al. 1994; Lurmann et al. 1992). This mixture consists of 52% (by carbon) alkanes, 15% alkenes, 27% aromatics, 1% formaldehyde, 2% higher aldehydes, 1% ketones, and 2% acetylene. The detailed composition of this mixture is given elsewhere (Carter, 1994b).

Adjusted NO_x scenarios

Incremental reactivities in the base case scenarios would be expected to vary widely, since incremental reactivities depend on the ROG/NO_x ratio, and that ratio varies widely among the base case scenarios. To obtain reactivity scales for specified NO_x conditions, separate sets of scenarios, designated MIR (for maximum incremental reactivity), MOR (for maximum ozone reactivity), and Equal Benefit Incremental Reactivity (EBIR) were developed (Carter, 1994a). In the MIR scenarios, the NO_x inputs were adjusted so the base ROG mixture (and most other VOCs) have their highest incremental reactivity. This is representative of the highest NO_x conditions of relevance to VOC reactivity assessment because at higher NO_x levels O_3 yields become significantly suppressed, but is also the condition where O_3 is most sensitive to VOC emissions. In the MOR scenarios, the NO_x inputs were adjusted to yield the highest ozone concentration. In the EBIR scenarios, the NO_x inputs were adjusted so that the relative effects of NO_x reductions and total ROG reductions on peak ozone levels were equal. This represents the lowest NO_x condition of relevance for VOC reactivity assessment, because O_3 formation becomes more sensitive to NO_x emissions than VOC emissions at lower NO_x levels. The changes in the base case ROG/NO_x ratios which yielded the MOR scenarios are given in Table 7. As discussed by Carter (1994a) the MIR and EBIR ROG/NO_x ratios are respectively ~1.5 and ~0.7 times those for the MOR scenarios in all cases.

For this study, the MIR, MOIR, and EBIR reactivities were calculated using the "averaged conditions" scenarios with the corresponding adjusted NO_x conditions. As discussed by Carter (1994a), averaged conditions scenarios have all inputs derived by averaging the corresponding inputs of the base case scenarios, except that the NO_x inputs were adjusted to yield the specified NO_x conditions as discussed above. This is slightly different than the approach used by Carter (1994a) to derive the MIR, MOIR, and EBIR scales, which involved adjusting NO_x conditions separately for each of the 39 base case scenarios, and then averaging the reactivities derived from them. Since Carter (1994a) showed that both approaches yield essentially the same result. For this work use of the averaged conditions approach was preferred because it is computationally much more straightforward, and gives an equally a good indication of how the relative reactivities of compounds vary with varying NO_x conditions.

NO_x Conditions in the Base Case Scenarios

The variability of ROG/NO_x ratios in the base case scenarios suggest a variability of reactivity characteristics in those scenarios. However, as discussed previously (Carter, 1994a), the ROG/NO_x ratio is also variable in the MIR or MOR scenarios, despite the fact that the NO_x inputs in these scenarios are

adjusted to yield a specified reactivity characteristic. Thus, the ROG/NO_x ratio, by itself, is not necessarily a good predictor of reactivity characteristics of a particular scenario. The NO_x/NO_x^{MOR} ratio is a much better predictor of this, with values greater than 1 indicating relatively high NO_x conditions where ozone formation is more sensitive to VOCs, and values less than 1 indicating NO_x-limited conditions. NO_x/NO_x^{MOR} ratios less than 0.7 represent conditions where NO_x control is a more effective ozone control strategy than ROG control (Carter, 1994a). Note that more than half of the base case scenarios represent NO_x-limited conditions, and ~25% of them represent conditions where NO_x control is more beneficial than VOC control. A relatively small number of scenarios represent MIR or near MIR conditions. However, as discussed elsewhere (Carter, 1994a), this set of scenarios is based on near-worst-case conditions for ozone formation in each of the airsheds. Had scenarios representing less-than-worst-case conditions been included, one might expect a larger number of MIR or near MIR scenarios. This is because NO_x is consumed more slowly on days with lower light intensity or temperature, and thus the scenario is less likely to become NO_x-limited.

Incremental and Relative Reactivities

The incremental reactivity of a VOC in an airshed scenario is the change in ozone caused by adding the VOC to the emissions, divided by the amount of VOC added, calculated for sufficiently small amounts of added VOC that the incremental reactivity is independent of the amount added. The procedure used to calculate incremental reactivities in a scenario was as discussed in detail elsewhere (Carter, 1994a,b). The incremental reactivities depend on how the amount of VOC added are quantified. In this work, the added VOC was quantified on a mass basis, since this is how VOCs are regulated. In addition, the incremental reactivities also depend on how ozone impacts are quantified (Carter, 1994a). In this work, two different ozone quantifications were used, resulting in two different incremental reactivities being calculated for a VOC in a scenario. These are discussed below.

The "Ozone Yield" incremental reactivities measure the effect of the VOC on the total amount of ozone formed in the scenario at the time of its maximum concentration. In this work, this is quantified as grams O_3 formed per gram VOC added. This gives the same ratios of incremental reactivities as reactivities calculated from peak ozone concentrations, but is preferred because it permits magnitudes of reactivities in scenarios with differing dilutions to be compared on the same basis. Most previous recent studies of incremental reactivity (Dodge, 1984; Carter and Atkinson, 1987, 1989, Chang and Rudy, 1990; Jeffries and Crouse, 1991) have all been based on ozone yield or peak ozone concentration reactivities.

The ozone yield incremental reactivities do not necessarily measure the effect of the VOC on exposure to unacceptable levels of ozone because it does not measure how long high levels of ozone are present. A quantification which reflects this is integrated ozone over the standard, which is defined as the sum of the hourly ozone concentrations for the hours when ozone exceeds the standard in the base case scenarios (Carter 1994a). In the previous work (Carter, 1994a), we used the California ozone standard

of 90 ppb, but in this work we will use the national standard of 0.12 ppm. Reactivities relative to this quantification of ozone are referred to by the abbreviation "IntO_3>0.12" reactivities.

Relative reactivities are ratios of incremental reactivities to incremental reactivities of some standard VOC or mixture. Since these are the quantities which usually are the most relevant to control strategy applications, the results in this work will be given in terms of relative reactivities. In our previous work (Carter 1991, 1994a), we used the incremental reactivity of the base ROG mixture, i.e., the mixture representing ROG pollutants from all sources, as the standard to define relative reactivities. However, because of the tendency within the EPA to consider ethane as the standard to define exempt vs controlled VOCs, in this work we will present reactivity ratios where ethane is used as the standard.

Reactivity Scales

A reactivity scale is a set of incremental or relative reactivities for a particular scenario or group of scenarios. Two types of reactivity scales will be discussed here, "base case" scales and adjusted NO_x scales. Base case scales are simply the set of incremental or relative reactivities in the 39 base case scenarios. Two sets of scales are derived — those based ozone yield reactivities and those based on IntO_3>0.12 reactivities. In the previous work (Carter, 1991, 1994a) we derived various multi-scenario scales from the individual base case scales by averaging or other procedures, to evaluate alternative approaches for developing single reactivity scales for applications requiring single scales. However, the decision of whether to exempt a VOC should not be made based on relative reactivities of a single scale, but on a knowledge of the range of relative reactivities for a variety of conditions. Thus in this work we present the distribution of base case relative reactivities for the 39 individual scenarios rather than developing aggregated or optimum scales which represent the distribution by single numbers.

The adjusted NO_x incremental reactivity scales refer to the MIR (maximum incremental reactivity), MOIR (maximum ozone incremental reactivity), or the EBIR (Equal Benefit Incremental Reactivity) scales. These consist of reactivities in averaged conditions scenarios where NO_x inputs were adjusted to yield MIR, MOR or EBIR conditions, respectively. Reactivities in the MIR scale are of interest because the California Air Resources Board utilized an MIR scale to calculate reactivity adjustment factors in its clean fuels/low emissions vehicle regulations (CARB, 1993). The justification for using this scale in applications requiring a single scale (such as the CARB vehicle regulations) is that it reflects conditions where ozone is most sensitive to changes in VOC emissions, and complements NO_x control, which is most effective for reducing ozone under conditions where the MIR scale is least applicable (Carter, 1994a). The MOIR scale is preferred by many as an alternative for such applications because it reflects conditions which are most favorable for ozone, and is more representative of the distribution of conditions in the base case scenarios (Carter 1994a). Most other alternative reactivity scales which might be appropriate for assessing VOC control strategies (i.e., excluding scales representing highly NO_x-limited conditions where ozone is more sensitive to NO_x than VOCs) tend to fall in the range defined by the MIR and MOIR scales.

Since the EBIR scale represents lower NO_x conditions where O_3 is less sensitive to VOCs, its use in applications requiring a single scale has not been considered. However, it is useful for assessing how reactivities depend on NO_x conditions.

Note that the MIR, MOIR, EBIR and base case scales derived in this work are somewhat different from those calculated previously (Carter, 1994a; Carter et al, 1993b) because an updated chemical mechanism was used. In addition, as indicated above, for computational efficiency the MIR, MOIR and EBIR scales were calculated using a single averaged conditions scenario, rather than the average of the adjusted NO_x base case scenarios as done previously (Carter, 1994a).

Calculated Relative Reactivities of the DBEs

Table 8 gives the incremental reactivities calculated for the three dibasic esters, relative to ethane, for the various scenarios and scales. Also shown for comparison purposes are the relative reactivities of the base ROG mixture, which can be considered to be the weighted average reactivity for all VOCs measured in polluted urban atmospheres. The reactivities are given in an ozone formed per mass VOC emitted basis, and were calculated using effects of the VOCs on both peak ozone yields and on integrated ozone over the current U.S. standard of 0.12 ppm.

The atmospheric reactivity calculations for DBE-4 were carried out using both models "A" and "D" because they were both equally consistent with the chamber data. However, since we consider model A to be more chemically reasonable, calculations using that model are considered more likely to be correct. The results using Model A indicate that DBE-4 is about 65-80% as reactive as ethane on an ozone per gram basis, with the reactivity calculated using Model D being ~20-25% lower. The DBE-4 relative reactivities are not strongly dependent on scenario conditions or how O_3 is quantified, though the relative reactivities calculated using Model A tend to increase slightly as NO_x is reduced, and the relative reactivities in the low NO_x scenarios calculated using Model D are somewhat higher if ozone is quantified by integrated ozone over the standard. However, in all but one scenario DBE-4 is calculated to have a lower ozone impact per gram than ethane, with the only exception being the New York scenario, where Model A predicts the DBE-4 ozone impact is ~25% greater than that of ethane.

DBE-5 is calculated to be ~1 - 1.25 times more reactive than ethane, on an ozone per gram basis. In contrast with DBE-4, the relative reactivities for DBE-5 are the highest in the high NO_x MIR scenario, and tend to decline as NO_x is reduced. As with DBE-4, the DBE-5 reactivities do not appear to be significantly affected by how ozone is quantified. Although DBE-5 is slightly more reactive than ethane in most scenarios, in no scenario is it more reactive than 1.5 times than of ethane, and it is less reactive than ethane in ~25% of the base case scenarios. Given that the DBE-5 mechanism tends to somewhat overpredict the d(O_3-NO) reactivities in the low NO_x full surrogate scenarios (see Figures 13

Table 8. Summary of calculated incremental reactivities (gram basis) for the dibasic esters and the average for all ambient VOCs relative to ethane.

Scenario	O_3 Yield Relative Reactivities					$IntO_3$ >0.12 Relative Reactivities				
	DBE-4 [a]		DBE-5	DBE-6	Base	DBE-4		DBE-5	DBE-6	Base
	A	D			ROG	A	D			ROG
Averaged Conditions										
Max React	0.65	0.53	1.27	4.2	13.1	0.67	0.58	1.29	4.3	14.4
Max Ozone	0.75	0.59	1.27	3.3	6.9	0.77	0.90	1.23	3.4	10.4
Equal Benefit	0.74	0.55	1.01	2.6	5.3	0.82	0.84	0.97	2.4	8.1
Base Case										
Average	**0.75**	**0.57**	**1.12**	**2.9**	**6.3**	**0.80**	**0.59**	**1.06**	**2.7**	**9.3**
St.Dev	**0.11**	**0.07**	**0.22**	**0.6**	**2.4**	**0.11**	**0.07**	**0.23**	**0.8**	**2.7**
ATL GA	0.74	0.55	1.02	2.7	6.0	0.83	0.59	1.01	2.4	8.4
AUS TX	0.69	0.53	0.82	2.3	5.2	0.83	0.61	0.80	1.8	7.3
BAL MD	0.78	0.60	1.37	3.6	6.5	0.78	0.59	1.32	3.7	11.5
BAT LA	0.83	0.62	1.13	2.5	6.6	0.91	0.67	1.10	2.3	9.7
BIR AL	0.67	0.52	1.03	2.8	4.3	0.73	0.54	0.92	2.5	7.7
BOS MA	0.78	0.59	1.22	2.9	5.0	0.84	0.62	1.18	2.8	8.1
CHA NC	0.65	0.49	0.75	2.2	4.9	0.72	0.52	0.69	1.8	6.1
CHI IL	0.75	0.56	0.60	1.4	3.7	0.93	0.65	0.58	0.7	7.3
CIN OH	0.71	0.54	1.19	3.2	5.3	0.74	0.55	1.14	3.2	8.2
CLE OH	0.78	0.58	1.19	3.1	6.8	0.81	0.60	1.18	3.2	11.3
DAL TX	0.70	0.56	1.21	3.4	8.5	0.72	0.56	1.16	3.4	11.6
DEN CO	0.84	0.60	1.22	3.2	9.2	0.84	0.61	1.22	3.3	13.7
DET MI	0.73	0.58	1.25	3.2	5.1	0.76	0.58	1.19	3.1	8.9
ELP TX	0.73	0.55	1.07	3.1	8.9	0.79	0.58	1.05	3.0	12.7
HAR CT	0.64	0.49	0.92	2.7	4.9	0.71	0.53	0.86	2.4	6.9
HOU TX	0.79	0.61	1.28	3.1	5.4	0.82	0.61	1.22	3.1	9.0
IND IN	0.72	0.55	1.12	3.0	6.4	0.75	0.56	1.05	2.9	9.4
JAC FL	0.76	0.55	0.85	2.2	6.2	0.82	0.58	0.76	1.8	7.6
KAN MO	0.67	0.53	1.13	3.1	5.2	0.73	0.55	1.06	2.9	7.1
LAK LA	0.92	0.68	1.08	2.0	4.5	1.02	0.72	0.90	1.2	7.4
LOS CA	0.93	0.66	1.35	3.1	6.9	0.88	0.63	1.18	2.9	11.8
LOU KY	0.75	0.59	1.24	2.9	5.4	0.79	0.60	1.17	2.8	7.5
MEM TN	0.78	0.59	1.17	2.8	4.9	0.83	0.61	1.12	2.7	7.6
MIA FL	0.60	0.43	0.36	1.4	5.6	0.62	0.43	0.32	1.2	5.9
NAS TN	0.65	0.50	0.89	2.4	4.3	0.66	0.47	0.70	1.9	5.2
NEW NY	1.25	0.89	1.38	2.0	5.9	1.23	0.87	1.45	2.3	11.4
PHI PA	0.78	0.60	1.27	3.1	6.0	0.81	0.61	1.22	3.1	9.0
PHO AZ	0.69	0.54	1.19	3.4	6.2	0.71	0.55	1.12	3.3	10.5
POR OR	0.70	0.54	1.06	2.7	5.8	0.77	0.57	1.02	2.5	7.2
RIC VA	0.73	0.56	1.22	3.2	5.4	0.77	0.58	1.20	3.2	8.7
SAC CA	0.65	0.50	1.10	3.0	5.9	0.67	0.50	1.00	2.9	8.4
SAI MO	0.80	0.61	1.32	3.4	7.1	0.80	0.60	1.26	3.4	12.2
SAL UT	0.63	0.48	0.97	2.9	5.4	0.70	0.50	0.91	2.7	8.6
SAN TX	0.68	0.52	1.16	3.3	8.0	0.68	0.52	1.13	3.3	8.6
SDO CA	0.85	0.60	1.14	2.7	8.5	0.90	0.64	1.12	2.6	10.9
SFO CA	0.72	0.57	1.36	4.8	18.3	0.73	0.58	1.36	4.8	20.2
TAM FL	0.80	0.62	1.26	3.0	7.5	0.82	0.63	1.20	3.1	10.9
TUL OK	0.81	0.63	1.35	3.2	5.6	0.81	0.61	1.30	3.3	9.0
WAS DC	0.76	0.60	1.28	3.1	5.2	0.79	0.60	1.21	3.1	8.9

[a] Results are shown for alternative mechanisms "A" and "D". Model A is considered to be more likely.

and 14, above), this mechanism may be slightly overestimating the DBE-5 reactivities in some of the lower NO_x scenarios. However, the model performed reasonably well in simulating the DBE-5 reactivities in the higher NO_x experiments more representative of or MIR scenario where DBE-5 is calculated to have the highest reactivities relative to ethane.

DBE-6 is calculated to have significantly higher ozone impacts than the other two dibasic esters, being ~3 - 4.5 times more reactive than ethane, depending on conditions. However, it is still not a highly reactive compound, since it is still calculated to be significantly less reactive than the mixture of VOCs measured in urban air (the "Base ROG" on Table 8). As with the other DBE's, the DBE-6 reactivities are not significantly affected by how ozone is quantified, though they are somewhat more dependent on NO_x conditions, tending to decline as NO_x is reduced. This higher reactivity for DBE-6 can be attributed to its relatively high rate constant, combined with the fact that it is predicted to form somewhat more reactive products than the other two DBEs. In particular, most of the reactive products predicted for DBE-4 and DBE-5 are various keto-esters or ester-acids, DBE-6 is predicted to form significant yields of aldehydes and α-keto esters, which are believed to be more reactive. These two factors are enough to counter the effect of the somewhat higher nitrate yield predicted for DBE-6, which would tend to reduce its net reactivity.

CONCLUSIONS

The decision whether it is appropriate to regulate a compound as an ozone precursor requires a qualitative assessment of its ozone impacts under a variety of environmental conditions. This involves developing a chemical mechanism for the gas-phase compounds atmospheric reactions which can be reliably used in airshed models to predict its atmospheric reactivity. Until this study, there was no information available concerning the atmospheric reaction rates or mechanisms for any of the dibasic esters. The objectives of this study was to measure the atmospheric reaction rates for the three representative dibasic esters, estimate their atmospheric reaction mechanisms, and to provide the data needed to verify the capabilities of those mechanisms to predict the atmospheric impacts for DBE-4 and DBE-5. We believe this program successfully addressed these objective.

The only significant gas-phase reaction of the dibasic esters under atmospheric conditions is reaction with OH radicals. The rate constants for the OH radical reaction were found to be (1.5±0.6) x 10^{-12}, (3.5±1.1) x 10^{-12} and (8.8±2.6) x 10^{-12} cm^3 $molecule^{-1}$ s^{-1} for DBE-4, DBE-5 and DBE-6, respectively. The rate constants measured for DBE-4 and DBE-5 agree reasonably well with those predicted using structure-reactivity relationships (Kwok and Atkinson, 1995; Kwok et al. 1996), but the measured rate constant for DBE-6 exceeds the estimated value by almost a factor of two. Although these OH radical rate constants are higher than the rate constant of 2.7 x 10^{-13} cm^3 $molec^{-1}$ s^{-1} for ethane (Atkinson, 1989), the compound used by the EPA as the informal standard for determining "negligible" reactivity, on a per-mass basis the rate constants relative to ethane are respectively 0.9, 2.4, and 5.6. This means that if the amount reacted is quantified by mass, then DBE-4 reacts more slowly in the atmosphere than does ethane, but the other two DBEs are more reactive than ethane in this respect.

The mechanisms of the DBE reactions following OH attack are fairly complex and uncertain because the OH radicals can attack at two different positions for DBE-4 and three for DBE-5 and DBE-6, and because alkoxy radicals are predicted to be formed which can undergo a number of competing reactions, whose branching ratios are unknown. In addition, the overall organic nitrate yields from peroxy + NO reactions, an important factor affecting ozone reactivities of higher molecular weight compounds, are unknown. However, estimated mechanisms for DBE-4 and DBE-5, derived by applying structure-reactivity estimates for estimating relative rates of OH reaction at the different positions, and by applying alkoxy radical rate constant estimation methods developed for alkanes and alkenes, were found give reasonably satisfactory predictions of results of the environmental chamber experiments carried out under differing conditions, provided that the overall organic nitrate yields were optimized within their uncertainty range to fit the chamber data. The chamber data are not consistent with alternative mechanisms which predict significant formation of formaldehyde from DBE-4 or DBE-5, nor are they not consistent with

mechanisms which predict formation of significant yields of highly photoreactive products, as might be expected if compounds such as α-keto esters were formed.

Both DBE-4 and DBE-5 tend to be OH radical inhibitors in atmospheric simulation systems, though not enough so that they are ozone inhibitors under most atmospheric conditions. This radical inhibition is attributed to the formation of organic nitrates in the reactions of peroxy radicals with NO. The DBE-4 and DBE-5 chamber data were best fit by models assuming overall nitrate yields of respectively 12% and 25%. These are not outside the expected uncertainty range for these compounds, and are respectively ~33% less and about the same as the nitrate yields formed from alkanes with the same number of carbons. This suggests that the nitrate yields of alkanes with the same number of carbons might be an appropriate basis for estimating the nitrate yields for DBE-6 and other esters for which there are no data. Based this, the nitrate yields for DBE-6 are estimated to be ~33%.

Although the DBE-4 and DBE-5 mechanisms are uncertain in their details, the reasonably good performance of these mechanisms in simulating the results of the chamber experiments, using two different ROG surrogates and NO_x levels, suggests that they should give reasonable predictions of relative ozone impacts under various atmospheric conditions. The two alternative DBE-4 mechanisms which were consistent with the chamber data gave atmospheric reactivity predictions which differed by ~25-30% from each other. Although the DBE-4 mechanism giving the higher set of reactivity predictions is considered to be the more chemically reasonable, the ~30% difference between these two mechanisms give an indication of the effect of the chemical uncertainty in these atmospheric reactivity estimates. It is unlikely that chemically reasonable mechanisms could differ by much more than that in their atmospheric reactivity predictions and still be consistent with the chamber data.

When applied to atmospheric ozone impact simulations, the model predicted that DBE-4 is about 65% - 80% as reactive as ethane on an ozone formed per gram emitted basis, while DBE-5 is predicted to be about 1 - 1.25 times more reactive than ethane. The relative reactivities were not strongly dependent on scenario conditions or how ozone impacts are quantified. DBE-6 is predicted to be ~3 - 4.5 times more reactive than ethane, with the relative reactivity depending somewhat more on environmental conditions. The chamber data suggest that the DBE-4 and DBE-5 mechanisms may be slightly overestimating their ozone reactivities in the lower NO_x scenarios, but as indicated above the error is unlikely to be greater than ~30%, and at present these represent our best estimates. Based on these results, we can conclude that DBE-4 is slightly less reactive than ethane on an ozone formed per gram basis, while DBE-5 is of comparable or only slightly higher reactivity. The estimated atmospheric reactivity for DBE-6 is more uncertain because the mechanism has not been experimentally tested, but it is reasonable to conclude that it is almost certainly more reactive than ethane, though less reactive than the average of all VOC emissions.

REFERENCES

Atkinson, R. (1989): "Kinetics and Mechanisms of the Gas-Phase Reactions of the Hydroxyl Radical with Organic Compounds," J. Phys. Chem. Ref. Data, Monograph 1, 1-246.

Atkinson, R. (1990): "Gas-Phase Tropospheric Chemistry of Organic Compounds: A Review," Atmos. Environ., 24A, 1-24.

Atkinson, R. (1991): "Kinetics and Mechanisms of the Gas-Phase Reactions of the NO_3 Radical with Organic Compounds," J. Phys. Chem. Ref. Data, 20, 459-507.

Atkinson, R. (1994): Gas-phase tropospheric chemistry of organic compounds, J. Phys. Chem. Ref. Data, Monograph 2, 1-216.

Atkinson, R. (1997): "Gas Phase Tropospheric Chemistry of Volatile Organic Compounds: 1. Alkanes and Alkenes," J. Phys. Chem. Ref. Data, 26, 215-290.

Atkinson, R., W. P. L. Carter, A. M. Winer, and J. N. Pitts, Jr. (1981): An experimental protocol for the determination of OH radical rate constants with organics using methyl nitrite photolysis as an OH radical source, J. Air Pollut. Control Assoc., 31, 1090-1092.

Atkinson, R. and W. P. L. Carter (1984): "Kinetics and Mechanisms of the Gas-Phase Reactions of Ozone with Organic Compounds under Atmospheric Conditions," Chem. Rev. 1984, 437-470.

Baugues, K. (1990): "Preliminary Planning Information for Updating the Ozone Regulatory Impact Analysis Version of EKMA," Draft Document, Source Receptor Analysis Branch, Technical Support Division, U. S. Environmental Protection Agency, Research Triangle Park, NC, January.

CARB (1993): "Proposed Regulations for Low-Emission Vehicles and Clean Fuels — Staff Report and Technical Support Document," California Air Resources Board, Sacramento, CA, August 13, 1990. See also Appendix VIII of "California Exhaust Emission Standards and Test Procedures for 1988 and Subsequent Model Passenger Cars, Light Duty Trucks and Medium Duty Vehicles," as last amended September 22, 1993. Incorporated by reference in Section 1960.1 (k) of Title 13, California Code of Regulations.

Calvert, J. G., and J. N. Pitts, Jr. (1966): Photochemistry, John Wiley and Sons, New York.

Carter, W. P. L. (1990): "A Detailed Mechanism for the Gas-Phase Atmospheric Reactions of Organic Compounds," Atmos. Environ., 24A, 481-518.

Carter, W. P. L. (1991): "Development of Ozone Reactivity Scales for Volatile Organic Compounds", EPA-600/3-91/050, August.

Carter, W. P. L. (1994a): "Development of Ozone Reactivity Scales for Volatile Organic Compounds," J. Air & Waste Manage. Assoc., 44, 881-899.

Carter, W. P. L. (1994b): "Calculation of Reactivity Scales Using an Updated Carbon Bond IV Mechanism," Draft Report Prepared for Systems Applications International Under Funding from the Auto/Oil Air Quality Improvement Research Program, April 12.

Carter, W. P. L. (1995): "Computer Modeling of Environmental Chamber Measurements of Maximum Incremental Reactivities of Volatile Organic Compounds," Atmos. Environ., 29, 2513-2517.

Carter, W. P. L., and R. Atkinson (1985): "Atmospheric Chemistry of Alkanes", J. Atmos. Chem., 3, 377-405, 1985.

Carter, W. P. L. and R. Atkinson (1987): "An Experimental Study of Incremental Hydrocarbon Reactivity," Environ. Sci. Technol., 21, 670-679

Carter, W. P. L. and R. Atkinson (1989a): "Alkyl Nitrate Formation from the Atmospheric Photooxidation of Alkanes; a Revised Estimation Method," J. Atm. Chem. 8, 165-173.

Carter, W. P. L. and R. Atkinson (1989b): "A Computer Modeling Study of Incremental Hydrocarbon Reactivity", Environ. Sci. Technol., 23, 864.

Carter, W. P. L., and F. W. Lurmann (1990): "Evaluation of the RADM Gas-Phase Chemical Mechanism," Final Report, EPA-600/3-90-001.

Carter, W. P. L. and F. W. Lurmann (1991): "Evaluation of a Detailed Gas-Phase Atmospheric Reaction Mechanism using Environmental Chamber Data," Atm. Environ. 25A, 2771-2806.

Carter, W. P. L., J. A. Pierce, I. L. Malkina, D. Luo and W. D. Long (1993a): "Environmental Chamber Studies of Maximum Incremental Reactivities of Volatile Organic Compounds," Report to Coordinating Research Council, Project No. ME-9, California Air Resources Board Contract No. A032-0692; South Coast Air Quality Management District Contract No. C91323, United States Environmental Protection Agency Cooperative Agreement No. CR-814396-01-0, University Corporation for Atmospheric Research Contract No. 59166, and Dow Corning Corporation. April 1.

Carter, W. P. L, D. Luo, I. L. Malkina, and J. A. Pierce (1993b): "An Experimental and Modeling Study of the Photochemical Ozone Reactivity of Acetone," Final Report to Chemical Manufacturers Association Contract No. KET-ACE-CRC-2.0. December 10.

Carter, W. P. L., D. Luo, I. L. Malkina, and J. A. Pierce (1995a): "Environmental Chamber Studies of Atmospheric Reactivities of Volatile Organic Compounds. Effects of Varying ROG Surrogate and NO_x," Final report to Coordinating Research Council, Inc., Project ME-9, California Air Resources Board, Contract A032-0692, and South Coast Air Quality Management District, Contract C91323. March 24.

Carter, W. P. L., D. Luo, I. L. Malkina, and D. Fitz (1995b): "The University of California, Riverside Environmental Chamber Data Base for Evaluating Oxidant Mechanism. Indoor Chamber Experiments through 1993," Report submitted to the U. S. Environmental Protection Agency, EPA/AREAL, Research Triangle Park, NC., March 20..

Carter, W. P. L., D. Luo, I. L. Malkina, and J. A. Pierce (1995c): "Environmental Chamber Studies of Atmospheric Reactivities of Volatile Organic Compounds. Effects of Varying Chamber and Light Source," Final report to National Renewable Energy Laboratory, Contract XZ-2-12075, Coordinating Research Council, Inc., Project M-9, California Air Resources Board, Contract A032-0692, and South Coast Air Quality Management District, Contract C91323, March 26.

Carter, W. P. L., J. A. Pierce, D. Luo, and I. L. Malkina (1995d): "Environmental Chamber Study of Maximum Incremental Reactivities of Volatile Organic Compounds," Atmos. Environ. 29, 2499-2511.

Carter, W. P. L., D. Luo, and I. L. Malkina (1997): "Environmental Chamber Studies for Development of an Updated Photochemical Mechanism for VOC Reactivity Assessment," Draft final report to California Air Resources Board Contract 92-345, Coordinating Research Council Project M-9, and National Renewable Energy Laboratory Contract ZF-2-12252-07. March 10.

Chang, T. Y. and S. J. Rudy (1990): "Ozone-Forming Potential of Organic Emissions from Alternative-Fueled Vehicles," Atmos. Environ., 24A, 2421-2430.

Croes, B. E., Technical Support Division, California Air Resources Board, personal communication (1991).

Croes, B. E., et al. (1994): "Southern California Air Quality Study Data Archive," Research Division, California Air Resources Board.

Dodge, M. C. (1984): "Combined effects of organic reactivity and NMHC/NOx ratio on photochemical oxidant formation -- a modeling study," Atmos. Environ., 18, 1657.

EPA (1984): "Guideline for Using the Carbon Bond Mechanism in City-Specific EKMA," EPA-450/4-84-005, February.

Gery, M. W., R. D. Edmond and G. Z. Whitten (1987): "Tropospheric Ultraviolet Radiation. Assessment of Existing Data and Effects on Ozone Formation," Final Report, EPA-600/3-87-047, October.

Gipson, G. L., W. P. Freas, R. A. Kelly and E. L. Meyer (1981): "Guideline for Use of City-Specific EKMA in Preparing Ozone SIPs, EPA-450/4-80-027, March.

Gipson, G. L. and W. P. Freas (1983): "Use of City-Specific EKMA in the Ozone RIA," U. S. Environmental Protection Agency, July.

Gipson, G. L. (1984): "Users Manual for OZIPM-2: Ozone Isopleth Plotting Package With Optional Mechanism/Version 2," EPA-450/4-84-024, August.

Hogo, H. and M. W. Gery (1988): "Guidelines for Using OZIPM-4 with CBM-IV or Optional Mechanisms. Volume 1. Description of the Ozone Isopleth Plotting Package Version 4", Final Report for EPA Contract No. 68-02-4136, Atmospheric Sciences Research Laboratory, Research Triangle Park, NC. January.

Jeffries, H. E., K. G. Sexton, J. R. Arnold, and T. L. Kale (1989): "Validation Testing of New Mechanisms with Outdoor Chamber Data. Volume 2: Analysis of VOC Data for the CB4 and CAL Photochemical Mechanisms," Final Report, EPA-600/3-89-010b.

Jeffries, H. E. and R. Crouse (1991): "Scientific and Technical Issues Related to the Application of Incremental Reactivity. Part II: Explaining Mechanism Differences," Report prepared for Western States Petroleum Association, Glendale, CA, October.

Jeffries, H. E. (1991): "UNC Solar Radiation Models," unpublished draft report for EPA Cooperative Agreements CR813107, CR813964 and CR815779". Undated.

Johnson, G. M. (1983): "Factors Affecting Oxidant Formation in Sydney Air," in "The Urban Atmosphere -- Sydney, a Case Study." Eds. J. N. Carras and G. M. Johnson (CSIRO, Melbourne), pp. 393-408.

Kwok, E. S. C. and R. Atkinson (1995): "Estimation of hydroxyl radical reaction rate constants for gas-phase organic compounds using a structure-reactivity relationship: An update." Atmos. Environ., 29, 1685-1695.

Kwok, E. S. C.; S. M. Aschmann, and R. Atkinson (1996): "Rate constants for the gas-phase reactions of the OH radical with selected carbamates and lactates," Environ. Sci. Technol., 30, 329-334.

Lurmann, F. W. and H. H. Main (1992): "Analysis of the Ambient VOC Data Collected in the Southern California Air Quality Study," Final Report to California Air Resources Board Contract No. A832-130, February.

Pitts, J. N., Jr., E. Sanhueza, R. Atkinson, W. P. L. Carter, A. M. Winer, G. W. Harris, and C. N. Plum (1984): "An Investigation of the Dark Formation of Nitrous Acid in Environmental Chambers," Int. J. Chem. Kinet., 16, 919-939.

Tuazon, E. C., R. Atkinson, C. N. Plum, A. M. Winer, and J. N. Pitts, Jr. (1983): "The Reaction of Gas-Phase N_2O_5 with Water Vapor," Geophys. Res. Lett. 10, 953-956.

Zafonte, L., P. L. Rieger, and J. R. Holmes (1977): "Nitrogen Dioxide Photolysis in the Los Angeles Atmosphere," Environ. Sci. Technol. 11, 483-487.

APPENDIX A
LISTING OF THE CHEMICAL MECHANISM

The chemical mechanism used in the environmental chamber and atmospheric model simulations discussed in this report is given in Tables A-1 through A-4. Table A-1 lists the species used in the mechanism, Table A-2 gives the reactions and rate constants, Table A-3 gives the parameters used to calculate the rates of the photolysis reactions, and Table A-4 gives the values and derivations of the chamber-dependent parameters used when modeling the environmental chamber experiments. Footnotes to Table A-2 indicate the format used for the reaction listing.

Table A-1. List of species in the chemical mechanism used in the model simulations for this study.

Name	Description
Constant Species.	
O2	Oxygen
M	Air
H2O	Water
Active Inorganic Species.	
O3	Ozone
NO	Nitric Oxide
NO2	Nitrogen Dioxide
NO3	Nitrate Radical
N2O5	Nitrogen Pentoxide
HONO	Nitrous Acid
HNO3	Nitric Acid
HNO4	Peroxynitric Acid
HO2H	Hydrogen Peroxide
Active Radical Species and Operators.	
HO2.	Hydroperoxide Radicals
RO2.	Operator to Calculate Total Organic Peroxy Radicals
RCO3.	Operator to Calculate Total Acetyl Peroxy Radicals
Active Reactive Organic Product Species.	
CO	Carbon Monoxide
HCHO	Formaldehyde
CCHO	Acetaldehyde
RCHO	Lumped C3+ Aldehydes
ACET	Acetone
MEK	Lumped Ketones

Table A-1, (continued)

Name	Description
PHEN	Phenol
CRES	Cresols
BALD	Aromatic aldehydes (e.g., benzaldehyde)
GLY	Glyoxal
MGLY	Methyl Glyoxal
BACL	Biacetyl or other lumped α-dicarbonyls, including α-keto esters
AFG1	Reactive Aromatic Fragmentation Products from benzene and naphthalene
AFG2	Other Reactive Aromatic Fragmentation Products
AFG3	Aromatic Fragmentation Products used in adjusted m-xylene mechanism
RNO3	Organic Nitrates
NPHE	Nitrophenols
ISOPROD	Lumped isoprene product species
PAN	Peroxy Acetyl Nitrate
PPN	Peroxy Propionyl Nitrate
GPAN	PAN Analogue formed from Glyoxal
PBZN	PAN Analogues formed from Aromatic Aldehydes
-OOH	Operator Representing Hydroperoxy Groups
Non-Reacting Species	
CO2	Carbon Dioxide
-C	"Lost Carbon"
-N	"Lost Nitrogen"
H2	Hydrogen
Steady State Species and Operators.	
HO.	Hydroxyl Radicals
O	Ground State Oxygen Atoms
O*1D2	Excited Oxygen Atoms
RO2-R.	Peroxy Radical Operator representing NO to NO_2 conversion with HO_2 formation.
RO2-N.	Peroxy Radical Operator representing NO consumption with organic nitrate formation.
RO2-NP.	Peroxy Radical Operator representing NO consumption with nitrophenol formation
R2O2.	Peroxy Radical Operator representing NO to NO_2 conversion.
CCO-O2.	Peroxy Acetyl Radicals
C2CO-O2.	Peroxy Propionyl Radicals
HCOCO-O2.	Peroxyacyl Radical formed from Glyoxal
BZ-CO-O2.	Peroxyacyl Radical formed from Aromatic Aldehydes
HOCOO.	Intermediate formed in Formaldehyde + HO_2 reaction
BZ-O.	Phenoxy Radicals
BZ(NO2)-O.	Nitratophenoxy Radicals
HOCOO.	Radical Intermediate formed in the HO_2 + Formaldehyde system.
(HCHO2)	Excited Criegee biradicals formed from $=CH_2$ groups
(CCHO2)	Excited Criegee biradicals formed from $=CHCH_3$ groups
(RCHO2)	Excited Criegee biradicals formed from =CHR groups, where R not CH_3
(C(C)CO2)	Excited Criegee biradicals formed from $=C(CH_3)_2$ groups

Table A-1, (continued)

Name	Description
(C(R)CO2)	Excited Criegee biradicals formed from $=C(CH_3)R$ or CR_2 groups
(BZCHO2)	Excited Criegee biradicals formed from styrenes
(C:CC(C)O2)	Excited Criegee biradicals formed from isoprene
(C:C(C)CHO2)	Excited Criegee biradicals formed from isoprene
(C2(O2)CHO)	Excited Criegee biradicals formed from isoprene products
(HOCCHO2)	Excited Criegee biradicals formed from isoprene products
(HCOCHO2)	Excited Criegee biradicals formed from isoprene products
(C2(O2)COH)	Excited Criegee biradicals formed from isoprene products
Primary Organics Represented explicitly	
CH4	Methane
ISOP	Isoprene
APIN	α-Pinene
UNKN	Unknown biogenics.
DBE-4	Dimethyl Succinate, $CH_3OC(O)CH_2CH_2C(O)OCH_3$
DEE-5	Dimethyl Glutarate, $CH_3OC(O)CH_2CH_2CH_2C(O)OCH_3$
DEB-6	Dimethyl Adipate, $CH_3OC(O)CH_2CH_2CH_2CH_2C(O)OCH_3$
Lumped species used to represent the Base ROG mixture in the EKMA model simulations.	
ALK1	Alkanes and other saturated compounds with $k_{OH} < 10^4$ ppm^{-1} min^{-1}.
ALK2	Alkanes and other saturated compounds with $k_{OH} \geq 10^4$ ppm^{-1} min^{-1}.
ARO1	Aromatics with $k_{OH} < 2x10^4$ ppm^{-1} min^{-1}.
ARO2	Aromatics with $k_{OH} \geq 2x10^4$ ppm^{-1} min^{-1}.
OLE2	Alkenes (other than ethene) with $k_{OH} < 7x10^4$ ppm^{-1} min^{-1}.
OLE3	Alkenes with $k_{OH} \geq 7x10^4$ ppm^{-1} min^{-1}.

Table A-2. List of reactions in the chemical mechanism used in the model simulations for this study.

Rxn. Label	Kinetic Parameters [a] k(300)	A	Ea	B	Reactions [b]
Inorganic Reactions					
1	(Phot. Set = NO2)				NO2 + HV = NO + O
2	6.00E-34	6.00E-34	0.00	-2.30	O + O2 + M = O3 + M
3A	9.69E-12	6.50E-12	-0.24	0.00	O + NO2 = NO + O2
3B	1.55E-12	(Falloff Kinetics)			O + NO2 = NO3 + M
	k0 =	9.00E-32	0.00	-2.00	
	kINF =	2.20E-11	0.00	0.00	
		F= 0.60	n= 1.00		
4	1.88E-14	2.00E-12	2.78	0.00	O3 + NO = NO2 + O2
5	3.36E-17	1.40E-13	4.97	0.00	O3 + NO2 = O2 + NO3
6	2.80E-11	1.70E-11	-0.30	0.00	NO + NO3 = 2 NO2
7	1.92E-38	3.30E-39	-1.05	0.00	NO + NO + O2 = 2 NO2
8	1.26E-12	(Falloff Kinetics)			NO2 + NO3 = N2O5
	k0 =	2.20E-30	0.00	-4.30	
	kINF =	1.50E-12	0.00	-0.50	
		F= 0.60	n= 1.00		
9	5.53E+10	9.09E+26	22.26	0.00	N2O5 + #RCON8 = NO2 + NO3
10	1.00E-21	(No T Dependence)			N2O5 + H2O = 2 HNO3
11	4.17E-16	2.50E-14	2.44	0.00	NO2 + NO3 = NO + NO2 + O2
12A	(Phot. Set = NO3NO)				NO3 + HV = NO + O2
12B	(Phot. Set = NO3NO2)				NO3 + HV = NO2 + O
13A	(Phot. Set = O3O3P)				O3 + HV = O + O2
13B	(Phot. Set = O3O1D)				O3 + HV = O*1D2 + O2
14	2.20E-10	(No T Dependence)			O*1D2 + H2O = 2 HO.
15	2.92E-11	1.92E-11	-0.25	0.00	O*1D2 + M = O + M
16	4.81E-12	(Falloff Kinetics)			HO. + NO = HONO
	k0 =	7.00E-31	0.00	-2.60	
	kINF =	1.50E-11	0.00	-0.50	
		F= 0.60	n= 1.00		
17	(Phot. Set = HONO)				HONO + HV = HO. + NO
18	1.13E-11	(Falloff Kinetics)			HO. + NO2 = HNO3
	k0 =	2.60E-30	0.00	-3.20	
	kINF =	2.40E-11	0.00	-1.30	
		F= 0.60	n= 1.00		
19	1.03E-13	6.45E-15	-1.65	0.00	HO. + HNO3 = H2O + NO3
21	2.40E-13	(No T Dependence)			HO. + CO = HO2. + CO2
22	6.95E-14	1.60E-12	1.87	0.00	HO. + O3 = HO2. + O2
23	8.28E-12	3.70E-12	-0.48	0.00	HO2. + NO = HO. + NO2
24	1.37E-12	(Falloff Kinetics)			HO2. + NO2 = HNO4
	k0 =	1.80E-31	0.00	-3.20	
	kINF =	4.70E-12	0.00	-1.40	
		F= 0.60	n= 1.00		
25	7.92E+10	4.76E+26	21.66	0.00	HNO4 + #RCON24 = HO2. + NO2
27	4.61E-12	1.30E-12	-0.75	0.00	HNO4 + HO. = H2O + NO2 + O2
28	2.08E-15	1.10E-14	0.99	0.00	HO2. + O3 = HO. + 2 O2
29A	1.73E-12	2.20E-13	-1.23	0.00	HO2. + HO2. = HO2H + O2
29B	5.00E-32	1.90E-33	-1.95	0.00	HO2. + HO2. + M = HO2H + O2
29C	3.72E-30	3.10E-34	-5.60	0.00	HO2. + HO2. + H2O = HO2H + O2 + H2O
29D	2.65E-30	6.60E-35	-6.32	0.00	HO2. + HO2. + H2O = HO2H + O2 + H2O
30A	1.73E-12	2.20E-13	-1.23	0.00	NO3 + HO2. = HNO3 + O2
30B	5.00E-32	1.90E-33	-1.95	0.00	NO3 + HO2. + M = HNO3 + O2
30C	3.72E-30	3.10E-34	-5.60	0.00	NO3 + HO2. + H2O = HNO3 + O2 + H2O
30D	2.65E-30	6.60E-35	-6.32	0.00	NO3 + HO2. + H2O = HNO3 + O2 + H2O
31	(Phot. Set = H2O2)				HO2H + HV = 2 HO.
32	1.70E-12	3.30E-12	0.40	0.00	HO2H + HO. = HO2. + H2O
33	9.90E-11	4.60E-11	-0.46	0.00	HO. + HO2. = H2O + O2
Peroxy Radical Operators					
B1	7.68E-12	4.20E-12	-0.36	0.00	RO2. + NO = NO
B2	2.25E-11	(Falloff Kinetics)			RCO3. + NO = NO
	k0 =	5.65E-28	0.00	-7.10	
	kINF =	2.64E-11	0.00	-0.90	
		F= 0.27	n= 1.00		
B4	1.04E-11	(Falloff Kinetics)			RCO3. + NO2 = NO2
	k0 =	2.57E-28	0.00	-7.10	
	kINF =	1.20E-11	0.00	-0.90	
		F= 0.30	n= 1.00		
B5	4.90E-12	3.40E-13	-1.59	0.00	RO2. + HO2. = HO2. + RO2-HO2-PROD
B6	4.90E-12	3.40E-13	-1.59	0.00	RCO3. + HO2. = HO2. + RO2-HO2-PROD
B8	1.00E-15	(No T Dependence)			RO2. + RO2. = RO2-RO2-PROD
B9	1.09E-11	1.86E-12	-1.05	0.00	RO2. + RCO3. = RO2-RO2-PROD

Table A-2 (continued)

Rxn. Label	Kinetic Parameters [a] k(300)	A	Ea	B	Reactions [b]
B10	1.64E-11	2.80E-12	-1.05	0.00	RCO3. + RCO3. = RO2-RO2-PROD
B11	(Same k as for RO2.)				RO2-R. + NO = NO2 + HO2.
B12	(Same k as for RO2.)				RO2-R. + HO2. = -OOH
B13	(Same k as for RO2.)				RO2-R. + RO2. = RO2. + 0.5 HO2.
B14	(Same k as for RO2.)				RO2-R. + RCO3. = RCO3. + 0.5 HO2.
B19	(Same k as for RO2.)				RO2-N. + NO = RNO3
B20	(Same k as for RO2.)				RO2-N. + HO2. = -OOH + MEK + 1.5 -C
B21	(Same k as for RO2.)				RO2-N. + RO2. = RO2. + 0.5 HO2. + MEK + 1.5 -C
B22	(Same k as for RO2.)				RO2-N. + RCO3. = RCO3. + 0.5 HO2. + MEK + 1.5 -C
B15	(Same k as for RO2.)				R2O2. + NO = NO2
B16	(Same k as for RO2.)				R2O2. + HO2. =
B17	(Same k as for RO2.)				R2O2. + RO2. = RO2.
B18	(Same k as for RO2.)				R2O2. + RCO3. = RCO3.
B23	(Same k as for RO2.)				RO2-XN. + NO = -N
B24	(Same k as for RO2.)				RO2-XN. + HO2. = -OOH
B25	(Same k as for RO2.)				RO2-XN. + RO2. = RO2. + 0.5 HO2.
B26	(Same k as for RO2.)				RO2-XN. + RCO3. = RCO3. + HO2.
G2	(Same k as for RO2.)				RO2-NP. + NO = NPHE
G3	(Same k as for RO2.)				RO2-NP. + HO2. = -OOH + 6 -C
G4	(Same k as for RO2.)				RO2-NP. + RO2. = RO2. + 0.5 HO2. + 6 -C
G5	(Same k as for RO2.)				RO2-NP. + RCO3. = RCO3. + HO2. + 6 -C
Excited Criegee Biradicals					
RZ1	(fast)				(HCHO2) = 0.7 HCOOH + 0.12 "HO. + HO2. + CO" + 0.18 "H2 + CO2"
RZ2	(fast)				(CCHO2) = 0.25 CCOOH + 0.15 "CH4 + CO2" + 0.6 HO. + 0.3 "CCO-O2. + RCO3." + 0.3 "RO2-R. + HCHO + CO + RO2."
RZ3	(fast)				(RCHO2) = 0.25 CCOOH + 0.15 CO2 + 0.6 HO. + 0.3 "C2CO-O2. + RCO3." + 0.3 "RO2-R. + CCHO + CO + RO2." + 0.55 -C
RZ4	(fast)				(C(C)CO2) = HO. + R2O2. + HCHO + CCO-O2. + RCO3. + RO2.
RZ5	(fast)				(C(R)CO2) = HO. + CCO-O2. + CCHO + R2O2. + RCO3. + RO2.
RZ6	(fast)				(CYCCO2) = 0.3 "HO. + C2CO-O2. + R2O2. + RCO3. + RO2." + 0.3 RCHO + 4.2 -C
RZ8	(fast)				(BZCHO2) = 0.5 "BZ-O. + R2O2. + CO + HO."
ISZ1	(fast)				(C:CC(C)O2) = HO. + R2O2. + HCHO + C2CO-O2. + RO2. + RCO3.
ISZ2	(fast)				(C:C(C)CHO2) = 0.75 RCHO + 0.25 ISOPROD + 0.5 -C
MAZ1	(fast)				(C2(O2)CHO) = HO. + R2O2. + HCHO + HCOCO-O2. + RO2. + RCO3.
M1Z1	(fast)				(HOCCHO2) = 0.6 HO. + 0.3 "CCO-O2. + RCO3." + 0.3 "RO2-R. + HCHO + CO + RO2." + 0.8 -C
M2Z1	(fast)				(HCOCHO2) = 0.12 "HO2. + 2 CO + HO." + 0.74 -C + 0.51 "CO2 + HCHO"
M2Z2	(fast)				(C2(O2)COH) = HO. + MGLY + HO2. + R2O2. + RO2.
Organic Product Species					
B7	(Phot. Set = CO2H)				-OOH + HV = HO2. + HO.
B7A	1.81E-12	1.18E-12	-0.25	0.00	HO. + -OOH = HO.
B7B	3.71E-12	1.79E-12	-0.44	0.00	HO. + -OOH = RO2-R. + RO2.
C1	(Phot. Set = HCHONEWR)				HCHO + HV = 2 HO2. + CO
C2	(Phot. Set = HCHONEWM)				HCHO + HV = H2 + CO
C3	9.76E-12	1.13E-12	-1.29	2.00	HCHO + HO. = HO2. + CO + H2O
C4	7.79E-14	9.70E-15	-1.24	0.00	HCHO + HO2. = HOCOO.
C4A	1.77E+02	2.40E+12	13.91	0.00	HOCOO. = HO2. + HCHO
C4B	(Same k as for RO2.)				HOCOO. + NO = -C + NO2 + HO2.
C9	6.38E-16	2.80E-12	5.00	0.00	HCHO + NO3 = HNO3 + HO2. + CO
C10	1.57E-11	5.55E-12	-0.62	0.00	CCHO + HO. = CCO-O2. + H2O + RCO3.
C11A	(Phot. Set = CCHOR)				CCHO + HV = CO + HO2. + HCHO + RO2-R. + RO2.
C12	2.84E-15	1.40E-12	3.70	0.00	CCHO + NO3 = HNO3 + CCO-O2. + RCO3.
C25	1.97E-11	8.50E-12	-0.50	0.00	RCHO + HO. = C2CO-O2. + RCO3.
C26	(Phot. Set = RCHO)				RCHO + HV = CCHO + RO2-R. + RO2. + CO + HO2.
C27	2.84E-15	1.40E-12	3.70	0.00	NO3 + RCHO = HNO3 + C2CO-O2. + RCO3.
C38	2.23E-13	4.81E-13	0.46	2.00	ACET + HO. = R2O2. + HCHO + CCO-O2. + RCO3. + RO2.

Table A-2 (continued)

Rxn. Label	Kinetic Parameters [a] k(300)	A	Ea	B	Reactions [b]
C39	(Phot. Set = ACET-93C)				ACET + HV = CCO-O2. + HCHO + RO2-R. + RCO3. + RO2.
C44	1.16E-12	2.92E-13	-0.82	2.00	MEK + HO. = H2O + 0.5 "CCHO + HCHO + CCO-O2. + C2CO-O2." + RCO3. + 1.5 "R2O2. + RO2."
C57	(Phot. Set = KETONE)				MEK + HV + #0.1 = CCO-O2. + CCHO + RO2-R. + RCO3. + RO2.
C95	2.07E-12	2.19E-11	1.41	0.00	RNO3 + HO. = NO2 + 0.155 MEK + 1.05 RCHO + 0.48 CCHO + 0.16 HCHO + 0.11 -C + 1.39 "R2O2. + RO2."
C58A	(Phot. Set = GLYOXAL1)				GLY + HV = 0.8 HO2. + 0.45 HCHO + 1.55 CO
C58B	(Phot. Set = GLYOXAL2)				GLY + HV + #0.029 = 0.13 HCHO + 1.87 CO
C59	1.14E-11 (No T Dependence)				GLY + HO. = 0.6 HO2. + 1.2 CO + 0.4 "HCOCO-O2. + RCO3."
C60	(Same k as for CCHO)				GLY + NO3 = HNO3 + 0.6 HO2. + 1.2 CO + 0.4 "HCOCO-O2. + RCO3."
C68A	(Phot. Set = MEGLYOX1)				MGLY + HV = HO2. + CO + CCO-O2. + RCO3.
C68B	(Phot. Set = MEGLYOX2)				MGLY + HV + 0.107 = HO2. + CO + CCO-O2. + RCO3.
C69	1.72E-11 (No T Dependence)				MGLY + HO. = CO + CCO-O2. + RCO3.
C70	(Same k as for CCHO)				MGLY + NO3 = HNO3 + CO + CCO-O2. + RCO3.
G7	1.14E-11 (No T Dependence)				HO. + AFG1 = HCOCO-O2. + RCO3.
G8	(Phot. Set = ACROLEIN)				AFG1 + HV + #0.029 = HO2. + HCOCO-O2. + RCO3.
U2OH	1.72E-11 (No T Dependence)				HO. + AFG2 = C2CO-O2. + RCO3.
U2HV	(Phot. Set = ACROLEIN)				AFG2 + HV = HO2. + CO + CCO-O2. + RCO3.
G46	2.63E-11 (No T Dependence)				HO. + PHEN = 0.15 RO2-NP. + 0.85 RO2-R. + 0.2 GLY + 4.7 -C + RO2.
G51	3.60E-12 (No T Dependence)				NO3 + PHEN = HNO3 + BZ-O.
G52	4.20E-11 (No T Dependence)				HO. + CRES = 0.15 RO2-NP. + 0.85 RO2-R. + 0.2 MGLY + 5.5 -C + RO2.
G57	2.10E-11 (No T Dependence)				NO3 + CRES = HNO3 + BZ-O. + -C
G30	1.29E-11 (No T Dependence)				BALD + HO. = BZ-CO-O2. + RCO3.
G31	(Phot. Set = BZCHO)				BALD + HV + #0.05 = 7 -C
G32	2.61E-15	1.40E-12	3.75	0.00	BALD + NO3 = HNO3 + BZ-CO-O2.
G58	3.60E-12 (No T Dependence)				NPHE + NO3 = HNO3 + BZ(NO2)-O.
G59	(Same k as for BZ-O.)				BZ(NO2)-O. + NO2 = 2 -N + 6 -C
G60	(Same k as for RO2.)				BZ(NO2)-O. + HO2. = NPHE
G61	(Same k as for BZ-O.)				BZ(NO2)-O. = NPHE
C13	(Same k as for RCO3.)				CCO-O2. + NO = CO2 + NO2 + HCHO + RO2-R. + RO2.
C14	(Same k as for RCO3.)				CCO-O2. + NO2 = PAN
C15	(Same k as for RCO3.)				CCO-O2. + HO2. = -OOH + CO2 + HCHO
C16	(Same k as for RCO3.)				CCO-O2. + RO2. = RO2. + 0.5 HO2. + CO2 + HCHO
C17	(Same k as for RCO3.)				CCO-O2. + RCO3. = RCO3. + HO2. + CO2 + HCHO
C18	6.50E-04 (Falloff Kinetics)				PAN = CCO-O2. + NO2 + RCO3.
	k0 =	4.90E-03	23.97	0.00	
	kINF =	4.00E+16	27.08	0.00	
		F= 0.30	n= 1.00		
C28	(Same k as for RCO3.)				C2CO-O2. + NO = CCHO + RO2-R. + CO2 + NO2 + RO2.
C29	8.40E-12 (No T Dependence)				C2CO-O2. + NO2 = PPN
C30	(Same k as for RCO3.)				C2CO-O2. + HO2. = -OOH + CCHO + CO2
C31	(Same k as for RCO3.)				C2CO-O2. + RO2. = RO2. + 0.5 HO2. + CCHO + CO2
C32	(Same k as for RCO3.)				C2CO-O2. + RCO3. = RCO3. + HO2. + CCHO + CO2
C33	6.78E-04	1.60E+17	27.97	0.00	PPN = C2CO-O2. + NO2 + RCO3.
C62	(Same k as for RCO3.)				HCOCO-O2. + NO = NO2 + CO2 + CO + HO2.
C63	(Same k as for RCO3.)				HCOCO-O2. + NO2 = GPAN
C65	(Same k as for RCO3.)				HCOCO-O2. + HO2. = -OOH + CO2 + CO
C66	(Same k as for RCO3.)				HCOCO-O2. + RO2. = RO2. + 0.5 HO2. + CO2 + CO
C67	(Same k as for RCO3.)				HCOCO-O2. + RCO3. = RCO3. + HO2. + CO2 + CO
C64	(Same k as for PAN)				GPAN = HCOCO-O2. + NO2 + RCO3.
G33	(Same k as for RCO3.)				BZ-CO-O2. + NO = BZ-O. + CO2 + NO2 + R2O2. + RO2.
G43	3.53E-11	1.30E-11	-0.60	0.00	BZ-O. + NO2 = NPHE
G44	(Same k as for RO2.)				BZ-O. + HO2. = PHEN
G45	1.00E-03 (No T Dependence)				BZ-O. = PHEN
G34	8.40E-12 (No T Dependence)				BZ-CO-O2. + NO2 = PBZN
G36	(Same k as for RCO3.)				BZ-CO-O2. + HO2. = -OOH + CO2 + PHEN
G37	(Same k as for RCO3.)				BZ-CO-O2. + RO2. = RO2. + 0.5 HO2. + CO2 + PHEN

Table A-2 (continued)

Rxn. Label	Kinetic Parameters [a] k(300)	A	Ea	B	Reactions [b]
G38	(Same k as for RCO3.)				BZ-CO-O2. + RCO3. = RCO3. + HO2. + CO2 + PHEN
G35	2.17E-04	1.60E+15	25.90	0.00	PBZN = BZ-CO-O2. + NO2 + RCO3.
IPOH	3.36E-11	(No T Dependence)			ISOPROD + HO. = 0.293 CO + 0.252 CCHO + 0.126 HCHO + 0.041 GLY + 0.021 RCHO + 0.168 MGLY + 0.314 MEK + 0.503 RO2-R. + 0.21 CCO-O2. + 0.288 C2CO-O2. + 0.21 R2O2. + 0.713 RO2. + 0.498 RCO3. + -0.112 -C
IPO3	7.11E-18	(No T Dependence)			ISOPROD + O3 = 0.02 CCHO + 0.04 HCHO + 0.01 GLY + 0.84 MGLY + 0.09 MEK + 0.66 (HCHO2) + 0.09 (HCOCHO2) + 0.18 (HOCCHO2) + 0.06 (C2(O2)CHO) + 0.01 (C2(O2)COH) + -0.39 -C
IPHV	(Phot. Set = ACROLEIN)				ISOPROD + HV + 0.0036 = 0.333 CO + 0.067 CCHO + 0.9 HCHO + 0.033 MEK + 0.333 HO2. + 0.7 RO2-R. + 0.267 CCO-O2. + 0.7 C2CO-O2. + 0.7 RO2. + 0.967 RCO3. + -0.133 -C
IPN3	1.00E-15	(No T Dependence)			ISOPROD + NO3 = 0.643 CO + 0.282 HCHO + 0.85 RNO3 + 0.357 RCHO + 0.925 HO2. + 0.075 C2CO-O2. + 0.075 R2O2. + 0.925 RO2. + 0.075 RCO3. + 0.075 HNO3 + -2.471 -C
Hydrocarbon Species Represented Explicitly					
	2.56E-12	1.36E-12	-0.38	2.00	N-C4 + HO. = 0.076 RO2-N. + 0.924 RO2-R. + 0.397 R2O2. + 0.001 HCHO + 0.571 CCHO + 0.14 RCHO + 0.533 MEK + -0.076 -C + 1.397 RO2.
	5.63E-12	1.35E-11	0.52	0.00	N-C6 + HO. = 0.185 RO2-N. + 0.815 RO2-R. + 0.738 R2O2. + 0.02 CCHO + 0.105 RCHO + 1.134 MEK + 0.186 -C + 1.738 RO2.
	8.76E-12	3.15E-11	0.76	0.00	N-C8 + HO. = 0.333 RO2-N. + 0.667 RO2-R. + 0.706 R2O2. + 0.002 RCHO + 1.333 MEK + 0.998 -C + 1.706 RO2.
	8.43E-12	1.96E-12	-0.87	0.00	ETHENE + HO. = RO2-R. + RO2. + 1.56 HCHO + 0.22 CCHO
	1.68E-18	9.14E-15	5.13	0.00	ETHENE + O3 = HCHO + (HCHO2)
	2.18E-16	4.39E-13	4.53	2.00	ETHENE + NO3 = R2O2. + RO2. + 2 HCHO + NO2
	7.42E-13	1.04E-11	1.57	0.00	ETHENE + O = RO2-R. + HO2. + RO2. + HCHO + CO
	2.60E-11	4.85E-12	-1.00	0.00	PROPENE + HO. = RO2-R. + RO2. + HCHO + CCHO
	1.05E-17	5.51E-15	3.73	0.00	PROPENE + O3 = 0.6 HCHO + 0.4 CCHO + 0.4 (HCHO2) + 0.6 (CCHO2)
	9.74E-15	4.59E-13	2.30	0.00	PROPENE + NO3 = R2O2. + RO2. + HCHO + CCHO + NO2
	4.01E-12	1.18E-11	0.64	0.00	PROPENE + O = 0.4 HO2. + 0.5 RCHO + 0.5 MEK + -0.5 -C
	6.30E-11	1.01E-11	-1.09	0.00	T-2-BUTE + HO. = RO2-R. + RO2. + 2 CCHO
	1.95E-16	6.64E-15	2.10	0.00	T-2-BUTE + O3 = CCHO + (CCHO2)
	3.92E-13	1.10E-13	-0.76	2.00	T-2-BUTE + NO3 = R2O2. + RO2. + 2 CCHO + NO2
	2.34E-11	2.26E-11	-0.02	0.00	T-2-BUTE + O = 0.4 HO2. + 0.5 RCHO + 0.5 MEK + 0.5 -C
	9.88E-11	2.54E-11	-0.81	0.00	ISOP + HO. = 0.088 RO2-N. + 0.912 RO2-R. + 0.629 HCHO + 0.912 ISOPROD + 0.079 R2O2. + 1.079 RO2. + 0.283 -C
	1.34E-17	7.86E-15	3.80	0.00	ISOP + O3 = 0.4 HCHO + 0.6 ISOPROD + 0.55 (HCHO2) + 0.2 (C:CC(C)O2) + 0.2 (C:C(C)CHO2) + 0.05 -C
	3.60E-11	(No T Dependence)			ISOP + O = 0.75 "ISOPROD + -C "+ 0.25 "C2CO-O2. + RCO3. + 2 HCHO + RO2-R. + RO2."
	6.81E-13	3.03E-12	0.89	0.00	ISOP + NO3 = 0.8 "RCHO + RNO3 + RO2-R." + 0.2 "ISOPROD + R2O2. + NO2" + RO2. + -2.2 -C
	1.50E-19	(No T Dependence)			ISOP + NO2 = 0.8 "RCHO + RNO3 + RO2-R." + 0.2 "ISOPROD + R2O2. + NO" + RO2. + -2.2 -C
	5.31E-11	1.21E-11	-0.88	0.00	APIN + HO. = RO2-R. + RCHO + RO2. + 7 -C
	1.00E-16	9.90E-16	1.37	0.00	APIN + O3 = 0.05 HCHO + 0.2 CCHO + 0.5 RCHO + 0.61 MEK + 0.075 CO + 0.05 CCO-O2. + 0.05 C2CO-O2. + 0.1 RCO3. + 0.105 HO2. + 0.16 HO. + 0.135 RO2-R. + 0.15 R2O2. + 0.285 RO2. + 5.285 -C
	6.10E-12	1.19E-12	-0.97	0.00	APIN + NO3 = NO2 + R2O2. + RCHO + RO2. + 7 -C
	3.00E-11	(No T Dependence)			APIN + O = 0.4 HO2. + 0.5 MEK + 0.5 RCHO + 6.5 -C
	6.57E-11	(No T Dependence)			UNKN + HO. = RO2-R. + RO2. + 0.5 HCHO + RCHO + 6.5 -C
	5.85E-17	(No T Dependence)			UNKN + O3 = 0.135 RO2-R. + 0.135 HO2. + 0.075 R2O2. + 0.21 RO2. + 0.025 CCO-O2. + 0.025 C2CO-O2. + 0.05 RCO3. + 0.275 HCHO + 0.175 CCHO + 0.5 RCHO + 0.41 MEK + 0.185 CO + 5.925 -C + 0.11 HO.
	4.30E-12	(No T Dependence)			UNKN + NO3 = R2O2. + RO2. + 0.5 HCHO + RCHO + 6.5 -C + NO2

Table A-2 (continued)

Rxn. Label	Kinetic Parameters [a] k(300)	A	Ea	B	Reactions [b]
	2.90E-11	(No T Dependence)			UNKN + O = 0.4 HO2. + 0.5 RCHO + 0.5 MEK + 6.5 -C
	5.91E-12	1.81E-12	-0.70	0.00	TOLUENE + HO. = 0.085 BALD + 0.26 CRES + 0.118 GLY + 0.847 MGLY + 0.276 AFG2 + 0.74 RO2-R. + 0.26 HO2. + 0.981 -C + 0.74 RO2.
	2.36E-11	(No T Dependence)			M-XYLENE + HO. = 0.04 BALD + 0.18 CRES + 0.108 GLY + 1.554 MGLY + 0.505 AFG2 + 0.82 RO2-R. + 0.18 HO2. + 0.068 -C + 0.82 RO2.
Lumped Species used in EKMA Simulations [c]					
A1OH	3.46E-12	2.56E-12	-0.18	0.00	ALK1 + HO. = 0.911 RO2-R. + 0.074 RO2-N. + 0.005 RO2-XN. + 0.011 HO2. + 0.575 R2O2. + 1.564 RO2. + 0.065 HCHO + 0.339 CCHO + 0.196 RCHO + 0.322 ACET + 0.448 MEK + 0.024 CO + 0.025 GLY + 0.051 -C
A2OH	9.14E-12	5.12E-12	-0.35	0.00	ALK2 + HO. = 0.749 RO2-R. + 0.249 RO2-N. + 0.002 RO2-XN. + 0.891 R2O2. + 1.891 RO2. + 0.029 HCHO + 0.048 CCHO + 0.288 RCHO + 0.028 ACET + 1.105 MEK + 0.043 CO + 0.018 CO2 + 1.268 -C
B1OH	5.87E-12	(No T Dependence)			ARO1 + HO. = 0.742 RO2-R. + 0.258 HO2. + 0.742 RO2. + 0.015 PHEN + 0.244 CRES + 0.08 BALD + 0.124 GLY + 0.681 MGLY + 0.11 AFG1 + 0.244 AFG2 + 1.857 -C
B2OH	3.22E-11	1.20E-11	-0.59	0.00	ARO2 + HO. = 0.82 RO2-R. + 0.18 HO2. + 0.82 RO2. + 0.18 CRES + 0.036 BALD + 0.068 GLY + 1.02 MGLY + 0.532 AFG2 + 2.588 -C
O2OH	3.17E-11	2.22E-12	-1.59	0.00	OLE2 + HO. = 0.858 RO2-R. + 0.142 RO2-N. + RO2. + 0.858 HCHO + 0.252 CCHO + 0.606 RCHO + 1.267 -C
O2O3	1.08E-17	1.42E-15	2.91	0.00	OLE2 + O3 = 0.6 HCHO + 0.635 RCHO + 0.981 -C + 0.4 (HCHO2) + 0.529 (CCHO2) + 0.071 (RCHO2)
O2N3	1.16E-14	1.99E-13	1.69	0.00	OLE2 + NO3 = R2O2. + RO2. + HCHO + 0.294 CCHO + 0.706 RCHO + 1.451 -C + NO2
O2OA	4.11E-12	4.51E-12	0.06	0.00	OLE2 + O = 0.4 HO2. + 0.5 RCHO + 0.5 MEK + 1.657 -C
O3OH	6.23E-11	4.54E-12	-1.56	0.00	OLE3 + HO. = 0.861 RO2-R. + 0.139 RO2-N. + RO2. + 0.24 HCHO + 0.661 CCHO + 0.506 RCHO + 0.113 ACET + 0.086 MEK + 0.057 BALD + 0.848 -C
O3O3	1.70E-16	1.77E-15	1.40	0.00	OLE3 + O3 = 0.203 HCHO + 0.358 CCHO + 0.309 RCHO + 0.061 MEK + 0.027 BALD + 0.976 -C + 0.076 (HCHO2) + 0.409 (CCHO2) + 0.279 (RCHO2) + 0.158 (C(C)CO2 + 0.039 (C(R)CO2 + 0.04 (BZCHO2)
O3N3	1.07E-12	3.19E-13	-0.72	0.00	OLE3 + NO3 = R2O2. + RO2. + 0.278 HCHO + 0.767 CCHO + 0.588 RCHO + 0.131 ACET + 0.1 MEK + 0.066 BALD + 0.871 -C + NO2
O3OA	2.52E-11	8.66E-12	-0.64	0.00	OLE3 + O = 0.4 HO2. + 0.5 RCHO + 0.5 MEK + 2.205 -C
Dibasic Esters [d]					
	1.50E-12	(No T Dependence)			DBE-4 + HO. = 0.12 RO2-N. + 0.88 RO2-R. + 0.62 R2O2. + 0.88 MEK + 0.88 CO + -C + 1.62 RO2. **(Model "A")**
	1.50E-12	(No T Dependence)			DBE-4 + HO. = 0.14 RO2-N. + 0.86 RO2-R. + 0.6 R2O2. + 0.6 HCHO + 0.6 RCHO + 0.26 MEK + 0.26 CO + 0.6 CO2 + -C + 1.6 RO2. **(Model "B")**
	1.50E-12	(No T Dependence)			DBE-4 + HO. = 0.28 RO2-N. + 0.72 RO2-R. + 0.22 MEK + 0.22 CO + 1.5 -C + 0.5 BACL + RO2. **(Model "C")**
	1.50E-12	(No T Dependence)			DBE-4 + HO. = 0.1 RO2-N. + 0.9 RO2-R. + 0.9 MEK + 0.27 CO + 1.63 -C + RO2. **(Model "D")**
	3.50E-12	(No T Dependence)			DBE-5 + HO. = 0.25 RO2-N. + 0.75 RO2-R. + 0.46 R2O2. + 0.23 RCHO + 0.75 MEK + 0.56 CO + 1.5 -C + 1.46 RO2.
	8.80E-12	(No T Dependence)			DBE-6 + HO. = 0.33 RO2-N. + 0.67 RO2-R. + 0.49 R2O2. + 0.82 RCHO + 0.25 MEK + 0.06 CO + 2.63 -C + 0.05 BACL + 1.49 RO2.

Table A-2 (continued)

Rxn. Label	Kinetic Parameters [a] k(300)	A	Ea	B	Reactions [b]
Reactions used to Represent Chamber-Dependent Processes [e]					
O3W	(varied)	(No T Dependence)			O3 =
N25I	(varied)	(No T Dependence)			N2O5 = 2 NOX-WALL
N25S	(varied)	(No T Dependence)			N2O5 + H2O = 2 NOX-WALL
NO2W	(varied)	(No T Dependence)			NO2 = (yHONO) HONO + (1-yHONO) NOX-WALL
XSHC	(varied)	(No T Dependence)			HO. = HO2.
RSI	(Phot. Set = NO2)				HV + #RS/K1 = HO.
ONO2	(Phot. Set = NO2)				HV + #E-NO2/K1 = NO2 + #-1 NOX-WALL

[a] Except as noted, the expression for the rate constant is $k = A\, e^{Ea/RT}\, (T/300)^B$. Rate constants and A factor are in cm, molecule, sec. units. Units of Ea is kcal $mole^{-1}$. "Phot Set" means this is a photolysis reaction, with the absorption coefficients and quantum yields given in Table A-3. In addition, if "#(number)" or "#(parameter)" is given as a reactant, then the value of that number or parameter is multiplied by the result in the "rate constant expression" columns to obtain the rate constant used. Furthermore, "#RCONnn" as a reactant means that the rate constant for the reaction is obtained by multiplying the rate constant given by that for reaction "nn". Thus, the rate constant given is actually an equilibrium constant.

[b] The format of the reaction listing is the same as that used in the documentation of the detailed mechanism (Carter 1990).

[c] The rate constants and product yield parameters are based on the mixture of species in the base ROG mixture which are being represented.

[d] See text for discussion of the four alternative DBE-4 mechanisms. Only Models A and D are consistent with the chamber data, with Model A being considered to be more chemically reasonable.

[e] See Table A-4 for the values of the parameters used for the specific chambers modeled in this study.

Table A-3. Absorption cross sections and quantum yields for photolysis reactions.

WL (nm)	Abs (cm^2)	QY	WL (nm)	Abs (cm^2)	QY	WL (nm)	Abs (cm^2)	QY	WL (nm)	Abs (cm^2)	QY	WL (nm)	Abs (cm^2)	QY
Photolysis File = NO2														
250.0	2.83E-20	1.000	255.0	1.45E-20	1.000	260.0	1.90E-20	1.000	265.0	2.05E-20	1.000	270.0	3.13E-20	1.000
275.0	4.02E-20	1.000	280.0	5.54E-20	1.000	285.0	6.99E-20	1.000	290.0	8.18E-20	0.999	295.0	9.67E-20	0.998
300.0	1.17E-19	0.997	305.0	1.66E-19	0.996	310.0	1.76E-19	0.995	315.0	2.25E-19	0.994	320.0	2.54E-19	0.993
325.0	2.79E-19	0.992	330.0	2.99E-19	0.991	335.0	3.45E-19	0.990	340.0	3.88E-19	0.989	345.0	4.07E-19	0.988
350.0	4.10E-19	0.987	355.0	5.13E-19	0.986	360.0	4.51E-19	0.984	365.0	5.78E-19	0.983	370.0	5.42E-19	0.981
375.0	5.35E-19	0.979	380.0	5.99E-19	0.975	381.0	5.98E-19	0.974	382.0	5.97E-19	0.973	383.0	5.96E-19	0.972
384.0	5.95E-19	0.971	385.0	5.94E-19	0.969	386.0	5.95E-19	0.967	387.0	5.96E-19	0.966	388.0	5.98E-19	0.964
389.0	5.99E-19	0.962	390.0	6.00E-19	0.960	391.0	5.98E-19	0.959	392.0	5.96E-19	0.957	393.0	5.93E-19	0.953
394.0	5.91E-19	0.950	395.0	5.89E-19	0.942	396.0	6.06E-19	0.922	397.0	6.24E-19	0.870	398.0	6.41E-19	0.820
399.0	6.59E-19	0.760	400.0	6.76E-19	0.695	401.0	6.67E-19	0.635	402.0	6.58E-19	0.560	403.0	6.50E-19	0.485
404.0	6.41E-19	0.425	405.0	6.32E-19	0.350	406.0	6.21E-19	0.290	407.0	6.10E-19	0.225	408.0	5.99E-19	0.185
409.0	5.88E-19	0.153	410.0	5.77E-19	0.130	411.0	5.88E-19	0.110	412.0	5.98E-19	0.094	413.0	6.09E-19	0.083
414.0	6.19E-19	0.070	415.0	6.30E-19	0.059	416.0	6.29E-19	0.048	417.0	6.27E-19	0.039	418.0	6.26E-19	0.030
419.0	6.24E-19	0.023	420.0	6.23E-19	0.018	421.0	6.18E-19	0.012	422.0	6.14E-19	0.008	423.0	6.09E-19	0.004
424.0	6.05E-19	0.000	425.0	6.00E-19	0.000									
Photolysis File = NO3NO														
585.0	2.77E-18	0.000	590.0	5.14E-18	0.250	595.0	4.08E-18	0.400	600.0	2.83E-18	0.250	605.0	3.45E-18	0.200
610.0	1.48E-18	0.200	615.0	1.96E-18	0.100	620.0	3.58E-18	0.100	625.0	9.25E-18	0.050	630.0	5.66E-18	0.050
635.0	1.45E-18	0.030	640.0	1.11E-18	0.000									
Photolysis File = NO3NO2														
400.0	0.00E+00	1.000	405.0	3.00E-20	1.000	410.0	4.00E-20	1.000	415.0	5.00E-20	1.000	420.0	8.00E-20	1.000
425.0	1.00E-19	1.000	430.0	1.30E-19	1.000	435.0	1.80E-19	1.000	440.0	1.90E-19	1.000	445.0	2.20E-19	1.000
450.0	2.80E-19	1.000	455.0	3.30E-19	1.000	460.0	3.70E-19	1.000	465.0	4.30E-19	1.000	470.0	5.10E-19	1.000
475.0	6.00E-19	1.000	480.0	6.40E-19	1.000	485.0	6.90E-19	1.000	490.0	8.80E-19	1.000	495.0	9.50E-19	1.000
500.0	1.01E-18	1.000	505.0	1.10E-18	1.000	510.0	1.32E-18	1.000	515.0	1.40E-18	1.000	520.0	1.45E-18	1.000
525.0	1.48E-18	1.000	530.0	1.94E-18	1.000	535.0	2.04E-18	1.000	540.0	1.81E-18	1.000	545.0	1.81E-18	1.000
550.0	2.36E-18	1.000	555.0	2.68E-18	1.000	560.0	3.07E-18	1.000	565.0	2.53E-18	1.000	570.0	2.54E-18	1.000
575.0	2.74E-18	1.000	580.0	3.05E-18	1.000	585.0	2.77E-18	1.000	590.0	5.14E-18	0.750	595.0	4.08E-18	0.600
600.0	2.83E-18	0.550	605.0	3.45E-18	0.400	610.0	1.45E-18	0.300	615.0	1.96E-18	0.250	620.0	3.58E-18	0.200
625.0	9.25E-18	0.150	630.0	5.66E-18	0.050	635.0	1.45E-18	0.000						
Photolysis File = O3O3P														
280.0	3.97E-18	0.100	281.0	3.60E-18	0.100	282.0	3.24E-18	0.100	283.0	3.01E-18	0.100	284.0	2.73E-18	0.100
285.0	2.44E-18	0.100	286.0	2.21E-18	0.100	287.0	2.01E-18	0.100	288.0	1.76E-18	0.100	289.0	1.58E-18	0.100
290.0	1.41E-18	0.100	291.0	1.26E-18	0.100	292.0	1.10E-18	0.100	293.0	9.89E-19	0.100	294.0	8.59E-19	0.100
295.0	7.70E-19	0.100	296.0	6.67E-19	0.100	297.0	5.84E-19	0.100	298.0	5.07E-19	0.100	299.0	4.52E-19	0.100
300.0	3.92E-19	0.100	301.0	3.42E-19	0.100	302.0	3.06E-19	0.100	303.0	2.60E-19	0.100	304.0	2.37E-19	0.100
305.0	2.01E-19	0.112	306.0	1.79E-19	0.149	307.0	1.56E-19	0.197	308.0	1.38E-19	0.259	309.0	1.25E-19	0.339
310.0	1.02E-19	0.437	311.0	9.17E-20	0.546	312.0	7.88E-20	0.652	313.0	6.77E-20	0.743	314.0	6.35E-20	0.816
315.0	5.10E-20	0.872	316.0	4.61E-20	0.916	317.0	4.17E-20	0.949	318.0	3.72E-20	0.976	319.0	2.69E-20	0.997
320.0	3.23E-20	1.000	330.0	6.70E-21	1.000	340.0	1.70E-21	1.000	350.0	4.00E-22	1.000	355.0	0.00E+00	1.000
400.0	0.00E+00	1.000	450.0	1.60E-22	1.000	500.0	1.34E-21	1.000	550.0	3.32E-21	1.000	600.0	5.06E-21	1.000
650.0	2.45E-21	1.000	700.0	8.70E-22	1.000	750.0	3.20E-22	1.000	800.0	1.60E-22	1.000	900.0	0.00E+00	1.000
Photolysis File = O3O1D														
280.0	3.97E-18	0.900	281.0	3.60E-18	0.900	282.0	3.24E-18	0.900	283.0	3.01E-18	0.900	284.0	2.73E-18	0.900
285.0	2.44E-18	0.900	286.0	2.21E-18	0.900	287.0	2.01E-18	0.900	288.0	1.76E-18	0.900	289.0	1.58E-18	0.900
290.0	1.41E-18	0.900	291.0	1.26E-18	0.900	292.0	1.10E-18	0.900	293.0	9.89E-19	0.900	294.0	8.59E-19	0.900
295.0	7.70E-19	0.900	296.0	6.67E-19	0.900	297.0	5.84E-19	0.900	298.0	5.07E-19	0.900	299.0	4.52E-19	0.900
300.0	3.92E-19	0.900	301.0	3.42E-19	0.900	302.0	3.06E-19	0.900	303.0	2.60E-19	0.900	304.0	2.37E-19	0.900
305.0	2.01E-19	0.888	306.0	1.79E-19	0.851	307.0	1.56E-19	0.803	308.0	1.38E-19	0.741	309.0	1.25E-19	0.661
310.0	1.02E-19	0.563	311.0	9.17E-20	0.454	312.0	7.88E-20	0.348	313.0	6.77E-20	0.257	314.0	6.35E-20	0.184
315.0	5.10E-20	0.128	316.0	4.61E-20	0.084	317.0	4.17E-20	0.051	318.0	3.72E-20	0.024	319.0	2.69E-20	0.003
320.0	3.23E-20	0.000												
Photolysis File = HONO														
311.0	0.00E+00	1.000	312.0	2.00E-21	1.000	313.0	4.20E-21	1.000	314.0	4.60E-21	1.000	315.0	4.20E-21	1.000
316.0	3.00E-21	1.000	317.0	4.60E-21	1.000	318.0	3.60E-20	1.000	319.0	6.10E-20	1.000	320.0	2.10E-20	1.000
321.0	4.27E-20	1.000	322.0	4.01E-20	1.000	323.0	3.93E-20	1.000	324.0	4.01E-20	1.000	325.0	4.04E-20	1.000
326.0	3.13E-20	1.000	327.0	4.12E-20	1.000	328.0	7.55E-20	1.000	329.0	6.64E-20	1.000	330.0	7.29E-20	1.000
331.0	8.70E-20	1.000	332.0	1.38E-19	1.000	333.0	5.91E-20	1.000	334.0	5.91E-20	1.000	335.0	6.45E-20	1.000
336.0	5.91E-20	1.000	337.0	4.58E-20	1.000	338.0	1.91E-19	1.000	339.0	1.63E-19	1.000	340.0	1.05E-19	1.000
341.0	8.70E-20	1.000	342.0	3.35E-19	1.000	343.0	2.01E-19	1.000	344.0	1.02E-19	1.000	345.0	8.54E-20	1.000
346.0	8.32E-20	1.000	347.0	8.20E-20	1.000	348.0	7.49E-20	1.000	349.0	7.13E-20	1.000	350.0	6.83E-20	1.000
351.0	1.74E-19	1.000	352.0	1.14E-19	1.000	353.0	3.71E-19	1.000	354.0	4.96E-19	1.000	355.0	2.46E-19	1.000
356.0	1.19E-19	1.000	357.0	9.35E-20	1.000	358.0	7.78E-20	1.000	359.0	7.29E-20	1.000	360.0	6.83E-20	1.000
361.0	6.90E-20	1.000	362.0	7.32E-20	1.000	363.0	9.00E-20	1.000	364.0	1.21E-19	1.000	365.0	1.33E-19	1.000
366.0	2.13E-19	1.000	367.0	3.52E-19	1.000	368.0	4.50E-19	1.000	369.0	2.93E-19	1.000	370.0	1.19E-19	1.000
371.0	9.46E-20	1.000	372.0	8.85E-20	1.000	373.0	7.44E-20	1.000	374.0	4.77E-20	1.000	375.0	2.70E-20	1.000
376.0	1.90E-20	1.000	377.0	1.50E-20	1.000	378.0	1.90E-20	1.000	379.0	5.80E-20	1.000	380.0	7.78E-20	1.000
381.0	1.14E-19	1.000	382.0	1.40E-19	1.000	383.0	1.72E-19	1.000	384.0	1.99E-19	1.000	385.0	1.90E-19	1.000
386.0	1.19E-19	1.000	387.0	5.65E-20	1.000	388.0	3.20E-20	1.000	389.0	1.90E-20	1.000	390.0	1.20E-20	1.000
391.0	5.00E-21	1.000	392.0	0.00E+00	1.000									
Photolysis File = H2O2														
250.0	8.30E-20	1.000	255.0	6.70E-20	1.000	260.0	5.20E-20	1.000	265.0	4.20E-20	1.000	270.0	3.20E-20	1.000
275.0	2.50E-20	1.000	280.0	2.00E-20	1.000	285.0	1.50E-20	1.000	290.0	1.13E-20	1.000	295.0	8.70E-21	1.000
300.0	6.60E-21	1.000	305.0	4.90E-21	1.000	310.0	3.70E-21	1.000	315.0	2.80E-21	1.000	320.0	2.00E-21	1.000
325.0	1.50E-21	1.000	330.0	1.20E-21	1.000	335.0	9.00E-22	1.000	340.0	7.00E-22	1.000	345.0	5.00E-22	1.000
350.0	3.00E-22	1.000	355.0	0.00E+00	1.000									

Table A-3. (continued)

WL (nm)	Abs (cm^2)	QY	WL (nm)	Abs (cm^2)	QY	WL (nm)	Abs (cm^2)	QY	WL (nm)	Abs (cm^2)	QY	WL (nm)	Abs (cm^2)	QY
Photolysis File = CO2H														
210.0	3.75E-19	1.000	220.0	2.20E-19	1.000	230.0	1.38E-19	1.000	240.0	8.80E-20	1.000	250.0	5.80E-20	1.000
260.0	3.80E-20	1.000	270.0	2.50E-20	1.000	280.0	1.50E-20	1.000	290.0	9.00E-21	1.000	300.0	5.80E-21	1.000
310.0	3.40E-21	1.000	320.0	1.90E-21	1.000	330.0	1.10E-21	1.000	340.0	6.00E-22	1.000	350.0	4.00E-22	1.000
360.0	0.00E+00	1.000												
Photolysis File = HCHONEWR														
280.0	2.49E-20	0.590	280.5	1.42E-20	0.596	281.0	1.51E-20	0.602	281.5	1.32E-20	0.608	282.0	9.73E-21	0.614
282.5	6.76E-21	0.620	283.0	5.82E-21	0.626	283.5	9.10E-21	0.632	284.0	3.71E-20	0.638	284.5	4.81E-20	0.644
285.0	3.95E-20	0.650	285.5	2.87E-20	0.656	286.0	2.24E-20	0.662	286.5	1.74E-20	0.668	287.0	1.13E-20	0.674
287.5	1.10E-20	0.680	288.0	2.62E-20	0.686	288.5	4.00E-20	0.692	289.0	3.55E-20	0.698	289.5	2.12E-20	0.704
290.0	1.07E-20	0.710	290.5	1.35E-20	0.713	291.0	1.99E-20	0.717	291.5	1.56E-20	0.721	292.0	8.65E-21	0.724
292.5	5.90E-21	0.727	293.0	1.11E-20	0.731	293.5	6.26E-20	0.735	294.0	7.40E-20	0.738	294.5	5.36E-20	0.741
295.0	4.17E-20	0.745	295.5	3.51E-20	0.749	296.0	2.70E-20	0.752	296.5	1.75E-20	0.755	297.0	1.16E-20	0.759
297.5	1.51E-20	0.763	298.0	3.69E-20	0.766	298.5	4.40E-20	0.769	299.0	3.44E-20	0.773	299.5	2.02E-20	0.776
300.0	1.06E-20	0.780	300.4	7.01E-21	0.780	300.6	8.63E-21	0.779	300.8	1.47E-20	0.779	301.0	2.01E-20	0.779
301.2	2.17E-20	0.779	301.4	1.96E-20	0.779	301.6	1.54E-20	0.778	301.8	1.26E-20	0.778	302.0	1.03E-20	0.778
302.2	8.53E-21	0.778	302.4	7.13E-21	0.778	302.6	6.61E-21	0.777	302.8	1.44E-20	0.777	303.0	3.18E-20	0.777
303.2	3.81E-20	0.777	303.4	5.57E-20	0.777	303.6	6.91E-20	0.776	303.8	6.58E-20	0.776	304.0	6.96E-20	0.776
304.2	5.79E-20	0.776	304.4	5.24E-20	0.776	304.6	4.30E-20	0.775	304.8	3.28E-20	0.775	305.0	3.60E-20	0.775
305.2	5.12E-20	0.775	305.4	4.77E-20	0.775	305.6	4.43E-20	0.774	305.8	4.60E-20	0.774	306.0	4.01E-20	0.774
306.2	3.28E-20	0.774	306.4	2.66E-20	0.774	306.6	2.42E-20	0.773	306.8	1.95E-20	0.773	307.0	1.58E-20	0.773
307.2	1.37E-20	0.773	307.4	1.19E-20	0.773	307.6	1.01E-20	0.772	307.8	9.01E-21	0.772	308.0	8.84E-21	0.772
308.2	2.08E-20	0.772	308.4	2.39E-20	0.772	308.6	3.08E-20	0.771	308.8	3.39E-20	0.771	309.0	3.18E-20	0.771
309.2	3.06E-20	0.771	309.4	2.84E-20	0.771	309.6	2.46E-20	0.770	309.8	1.95E-20	0.770	310.0	1.57E-20	0.770
310.2	1.26E-20	0.767	310.4	9.26E-21	0.764	310.6	7.71E-21	0.761	310.8	6.05E-21	0.758	311.0	5.13E-21	0.755
311.2	4.82E-21	0.752	311.4	4.54E-21	0.749	311.6	6.81E-21	0.746	311.8	1.04E-20	0.743	312.0	1.43E-20	0.740
312.2	1.47E-20	0.737	312.4	1.35E-20	0.734	312.6	1.13E-20	0.731	312.8	9.86E-21	0.728	313.0	7.82E-21	0.725
313.2	6.48E-21	0.722	313.4	1.07E-20	0.719	313.6	2.39E-20	0.716	313.8	3.80E-20	0.713	314.0	5.76E-20	0.710
314.2	6.14E-20	0.707	314.4	7.45E-20	0.704	314.6	5.78E-20	0.701	314.8	5.59E-20	0.698	315.0	4.91E-20	0.695
315.2	4.37E-20	0.692	315.4	3.92E-20	0.689	315.6	2.89E-20	0.686	315.8	2.82E-20	0.683	316.0	2.10E-20	0.680
316.2	1.66E-20	0.677	316.4	2.05E-20	0.674	316.6	4.38E-20	0.671	316.8	5.86E-20	0.668	317.0	6.28E-20	0.665
317.2	5.07E-20	0.662	317.4	4.33E-20	0.659	317.6	4.17E-20	0.656	317.8	3.11E-20	0.653	318.0	2.64E-20	0.650
318.2	2.24E-20	0.647	318.4	1.70E-20	0.644	318.6	1.24E-20	0.641	318.8	1.11E-20	0.638	319.0	7.70E-21	0.635
319.2	6.36E-21	0.632	319.4	5.36E-21	0.629	319.6	4.79E-21	0.626	319.8	6.48E-21	0.623	320.0	1.48E-20	0.620
320.2	1.47E-20	0.614	320.4	1.36E-20	0.608	320.6	1.69E-20	0.601	320.8	1.32E-20	0.595	321.0	1.49E-20	0.589
321.2	1.17E-20	0.583	321.4	1.15E-20	0.577	321.6	9.64E-21	0.570	321.8	7.26E-21	0.564	322.0	5.94E-21	0.558
322.2	4.13E-21	0.552	322.4	3.36E-21	0.546	322.6	2.39E-21	0.539	322.8	2.01E-21	0.533	323.0	1.76E-21	0.527
323.2	2.82E-21	0.521	323.4	4.65E-21	0.515	323.6	7.00E-21	0.508	323.8	7.80E-21	0.502	324.0	7.87E-21	0.496
324.2	6.59E-21	0.490	324.4	5.60E-21	0.484	324.6	4.66E-21	0.477	324.8	4.21E-21	0.471	325.0	7.77E-21	0.465
325.2	2.15E-20	0.459	325.4	3.75E-20	0.453	325.6	4.10E-20	0.446	325.8	6.47E-20	0.440	326.0	7.59E-20	0.434
326.2	6.51E-20	0.428	326.4	5.53E-20	0.422	326.6	5.76E-20	0.415	326.8	4.43E-20	0.409	327.0	3.44E-20	0.403
327.2	3.22E-20	0.397	327.4	2.13E-20	0.391	327.6	1.91E-20	0.384	327.8	1.42E-20	0.378	328.0	9.15E-21	0.372
328.2	6.79E-21	0.366	328.4	4.99E-21	0.360	328.6	4.77E-21	0.353	328.8	1.75E-20	0.347	329.0	3.27E-20	0.341
329.2	3.99E-20	0.335	329.4	5.13E-20	0.329	329.6	4.00E-20	0.322	329.8	3.61E-20	0.316	330.0	3.38E-20	0.310
330.2	3.08E-20	0.304	330.4	2.16E-20	0.298	330.6	2.09E-20	0.291	330.8	1.41E-20	0.285	331.0	9.95E-21	0.279
331.2	7.76E-21	0.273	331.4	6.16E-21	0.267	331.6	4.06E-21	0.260	331.8	3.03E-21	0.254	332.0	2.41E-21	0.248
332.2	1.74E-21	0.242	332.4	1.33E-21	0.236	332.6	2.70E-21	0.229	332.8	1.65E-21	0.223	333.0	1.17E-21	0.217
333.2	9.84E-22	0.211	333.4	8.52E-22	0.205	333.6	6.32E-22	0.198	333.8	5.21E-22	0.192	334.0	1.46E-21	0.186
334.2	1.80E-21	0.180	334.4	1.43E-21	0.174	334.6	1.03E-21	0.167	334.8	7.19E-22	0.161	335.0	4.84E-22	0.155
335.2	2.73E-22	0.149	335.4	1.34E-22	0.143	335.6	-1.62E-22	0.136	335.8	1.25E-22	0.130	336.0	4.47E-22	0.124
336.2	1.23E-21	0.118	336.4	2.02E-21	0.112	336.6	3.00E-21	0.105	336.8	2.40E-21	0.099	337.0	3.07E-21	0.093
337.2	2.29E-21	0.087	337.4	2.46E-21	0.081	337.6	2.92E-21	0.074	337.8	8.10E-21	0.068	338.0	1.82E-20	0.062
338.2	3.10E-20	0.056	338.4	3.24E-20	0.050	338.6	4.79E-20	0.043	338.8	5.25E-20	0.037	339.0	5.85E-20	0.031
339.2	4.33E-20	0.025	339.4	4.20E-20	0.019	339.6	3.99E-20	0.012	339.8	3.11E-20	0.006	340.0	2.72E-20	0.000
Photolysis File = HCHONEWM														
280.0	2.49E-20	0.350	280.5	1.42E-20	0.346	281.0	1.51E-20	0.341	281.5	1.32E-20	0.336	282.0	9.73E-21	0.332
282.5	6.76E-21	0.327	283.0	5.82E-21	0.323	283.5	9.10E-21	0.319	284.0	3.71E-20	0.314	284.5	4.81E-20	0.309
285.0	3.95E-20	0.305	285.5	2.87E-20	0.301	286.0	2.24E-20	0.296	286.5	1.74E-20	0.291	287.0	1.13E-20	0.287
287.5	1.10E-20	0.282	288.0	2.62E-20	0.278	288.5	4.00E-20	0.273	289.0	3.55E-20	0.269	289.5	2.12E-20	0.264
290.0	1.07E-20	0.260	290.5	1.35E-20	0.258	291.0	1.99E-20	0.256	291.5	1.56E-20	0.254	292.0	8.65E-21	0.252
292.5	5.90E-21	0.250	293.0	1.11E-20	0.248	293.5	6.26E-20	0.246	294.0	7.40E-20	0.244	294.5	5.36E-20	0.242
295.0	4.17E-20	0.240	295.5	3.51E-20	0.238	296.0	2.70E-20	0.236	296.5	1.75E-20	0.234	297.0	1.16E-20	0.232
297.5	1.51E-20	0.230	298.0	3.69E-20	0.228	298.5	4.40E-20	0.226	299.0	3.44E-20	0.224	299.5	2.02E-20	0.222
300.0	1.06E-20	0.220	300.4	7.01E-21	0.220	300.6	8.63E-21	0.221	300.8	1.47E-20	0.221	301.0	2.01E-20	0.221
301.2	2.17E-20	0.221	301.4	1.96E-20	0.221	301.6	1.54E-20	0.222	301.8	1.26E-20	0.222	302.0	1.03E-20	0.222
302.2	8.53E-21	0.222	302.4	7.13E-21	0.222	302.6	6.61E-21	0.223	302.8	1.44E-20	0.223	303.0	3.18E-20	0.223
303.2	3.81E-20	0.223	303.4	5.57E-20	0.223	303.6	6.91E-20	0.224	303.8	6.58E-20	0.224	304.0	6.96E-20	0.224
304.2	5.79E-20	0.224	304.4	5.24E-20	0.224	304.6	4.30E-20	0.225	304.8	3.28E-20	0.225	305.0	3.60E-20	0.225
305.2	5.12E-20	0.225	305.4	4.77E-20	0.225	305.6	4.43E-20	0.226	305.8	4.60E-20	0.226	306.0	4.01E-20	0.226
306.2	3.28E-20	0.226	306.4	2.66E-20	0.226	306.6	2.42E-20	0.227	306.8	1.95E-20	0.227	307.0	1.58E-20	0.227
307.2	1.37E-20	0.227	307.4	1.19E-20	0.227	307.6	1.01E-20	0.228	307.8	9.01E-21	0.228	308.0	8.84E-21	0.228
308.2	2.08E-20	0.228	308.4	2.39E-20	0.228	308.6	3.08E-20	0.229	308.8	3.39E-20	0.229	309.0	3.18E-20	0.229
309.2	3.06E-20	0.229	309.4	2.84E-20	0.229	309.6	2.46E-20	0.230	309.8	1.95E-20	0.230	310.0	1.57E-20	0.230
310.2	1.26E-20	0.233	310.4	9.26E-21	0.236	310.6	7.71E-21	0.239	310.8	6.05E-21	0.242	311.0	5.13E-21	0.245
311.2	4.82E-21	0.248	311.4	4.54E-21	0.251	311.6	6.81E-21	0.254	311.8	1.04E-20	0.257	312.0	1.43E-20	0.260
312.2	1.47E-20	0.263	312.4	1.35E-20	0.266	312.6	1.13E-20	0.269	312.8	9.86E-21	0.272	313.0	7.82E-21	0.275
313.2	6.48E-21	0.278	313.4	1.07E-20	0.281	313.6	2.39E-20	0.284	313.8	3.80E-20	0.287	314.0	5.76E-20	0.290
314.2	6.14E-20	0.293	314.4	7.45E-20	0.296	314.6	5.78E-20	0.299	314.8	5.59E-20	0.302	315.0	4.91E-20	0.305
315.2	4.37E-20	0.308	315.4	3.92E-20	0.311	315.6	2.89E-20	0.314	315.8	2.82E-20	0.317	316.0	2.10E-20	0.320
316.2	1.66E-20	0.323	316.4	2.05E-20	0.326	316.6	4.38E-20	0.329	316.8	5.86E-20	0.332	317.0	6.28E-20	0.335
317.2	5.07E-20	0.338	317.4	4.33E-20	0.341	317.6	4.17E-20	0.344	317.8	3.11E-20	0.347	318.0	2.64E-20	0.350
318.2	2.24E-20	0.353	318.4	1.70E-20	0.356	318.6	1.24E-20	0.359	318.8	1.11E-20	0.362	319.0	7.70E-21	0.365

Table A-3. (continued)

WL (nm)	Abs (cm^2)	QY	WL (nm)	Abs (cm^2)	QY	WL (nm)	Abs (cm^2)	QY	WL (nm)	Abs (cm^2)	QY	WL (nm)	Abs (cm^2)	QY
319.2	6.36E-21	0.368	319.4	5.36E-21	0.371	319.6	4.79E-21	0.374	319.8	6.48E-21	0.377	320.0	1.48E-20	0.380
320.2	1.47E-20	0.386	320.4	1.36E-20	0.392	320.6	1.69E-20	0.399	320.8	1.32E-20	0.405	321.0	1.49E-20	0.411
321.2	1.17E-20	0.417	321.4	1.15E-20	0.423	321.6	9.64E-21	0.430	321.8	7.26E-21	0.436	322.0	5.94E-21	0.442
322.2	4.13E-21	0.448	322.4	3.36E-21	0.454	322.6	2.39E-21	0.461	322.8	2.01E-21	0.467	323.0	1.76E-21	0.473
323.2	2.82E-21	0.479	323.4	4.65E-21	0.485	323.6	7.00E-21	0.492	323.8	7.80E-21	0.498	324.0	7.87E-21	0.504
324.2	6.59E-21	0.510	324.4	5.60E-21	0.516	324.6	4.66E-21	0.523	324.8	4.21E-21	0.529	325.0	7.77E-21	0.535
325.2	2.15E-20	0.541	325.4	3.75E-20	0.547	325.6	4.10E-20	0.554	325.8	6.47E-20	0.560	326.0	7.59E-20	0.566
326.2	6.51E-20	0.572	326.4	5.53E-20	0.578	326.6	5.76E-20	0.585	326.8	4.43E-20	0.591	327.0	3.44E-20	0.597
327.2	3.22E-20	0.603	327.4	2.13E-20	0.609	327.6	1.91E-20	0.616	327.8	1.42E-20	0.622	328.0	9.15E-21	0.628
328.2	6.79E-21	0.634	328.4	4.99E-21	0.640	328.6	4.77E-21	0.647	328.8	1.75E-20	0.653	329.0	3.27E-20	0.659
329.2	3.99E-20	0.665	329.4	5.13E-20	0.671	329.6	4.00E-20	0.678	329.8	3.61E-20	0.684	330.0	3.38E-20	0.690
330.2	3.08E-20	0.694	330.4	2.16E-20	0.699	330.6	2.09E-20	0.703	330.8	1.41E-20	0.708	331.0	9.95E-21	0.712
331.2	7.76E-21	0.717	331.4	6.16E-21	0.721	331.6	4.06E-21	0.726	331.8	3.03E-21	0.730	332.0	2.41E-21	0.735
332.2	1.74E-21	0.739	332.4	1.33E-21	0.744	332.6	2.70E-21	0.748	332.8	1.65E-21	0.753	333.0	1.17E-21	0.757
333.2	9.84E-22	0.762	333.4	8.52E-22	0.766	333.6	6.32E-22	0.771	333.8	5.21E-22	0.775	334.0	1.46E-21	0.780
334.2	1.80E-21	0.784	334.4	1.43E-21	0.789	334.6	1.03E-21	0.793	334.8	7.19E-22	0.798	335.0	4.84E-22	0.802
335.2	2.73E-22	0.798	335.4	1.34E-22	0.794	335.6	0.00E+00	0.790	335.8	1.25E-22	0.786	336.0	4.47E-22	0.782
336.2	1.23E-21	0.778	336.4	2.02E-21	0.773	336.6	3.00E-21	0.769	336.8	2.40E-21	0.764	337.0	3.07E-21	0.759
337.2	2.29E-21	0.754	337.4	2.46E-21	0.749	337.6	2.92E-21	0.745	337.8	8.10E-21	0.740	338.0	1.82E-20	0.734
338.2	3.10E-20	0.729	338.4	3.24E-20	0.724	338.6	4.79E-20	0.719	338.8	5.25E-20	0.714	339.0	5.85E-20	0.709
339.2	4.33E-20	0.703	339.4	4.20E-20	0.698	339.6	3.99E-20	0.693	339.8	3.11E-20	0.687	340.0	2.72E-20	0.682
340.2	1.99E-20	0.676	340.4	1.76E-20	0.671	340.6	1.39E-20	0.666	340.8	1.01E-20	0.660	341.0	6.57E-21	0.655
341.2	4.83E-21	0.649	341.4	3.47E-21	0.643	341.6	2.23E-21	0.638	341.8	1.55E-21	0.632	342.0	3.70E-21	0.627
342.2	4.64E-21	0.621	342.4	1.08E-20	0.616	342.6	1.14E-20	0.610	342.8	1.79E-20	0.604	343.0	2.33E-20	0.599
343.2	1.72E-20	0.593	343.4	1.55E-20	0.588	343.6	1.46E-20	0.582	343.8	1.38E-20	0.576	344.0	1.00E-20	0.571
344.2	8.26E-21	0.565	344.4	6.32E-21	0.559	344.6	4.28E-21	0.554	344.8	3.22E-21	0.548	345.0	2.54E-21	0.542
345.2	1.60E-21	0.537	345.4	1.15E-21	0.531	345.6	8.90E-22	0.525	345.8	6.50E-22	0.520	346.0	5.09E-22	0.514
346.2	5.15E-22	0.508	346.4	3.45E-22	0.503	346.6	3.18E-22	0.497	346.8	3.56E-22	0.491	347.0	3.24E-22	0.485
347.2	3.34E-22	0.480	347.4	2.88E-22	0.474	347.6	2.84E-22	0.468	347.8	9.37E-22	0.463	348.0	9.70E-22	0.457
348.2	7.60E-22	0.451	348.4	6.24E-22	0.446	348.6	4.99E-22	0.440	348.8	4.08E-22	0.434	349.0	3.39E-22	0.428
349.2	1.64E-22	0.423	349.4	1.49E-22	0.417	349.6	8.30E-23	0.411	349.8	2.52E-23	0.406	350.0	2.57E-23	0.400
350.2	0.00E+00	0.394	350.4	5.16E-23	0.389	350.6	0.00E+00	0.383	350.8	2.16E-23	0.377	351.0	7.07E-23	0.371
351.2	3.45E-23	0.366	351.4	1.97E-22	0.360	351.6	4.80E-22	0.354	351.8	3.13E-21	0.349	352.0	6.41E-21	0.343
352.2	8.38E-21	0.337	352.4	1.55E-20	0.331	352.6	1.86E-20	0.326	352.8	1.94E-20	0.320	353.0	2.78E-20	0.314
353.2	1.96E-20	0.309	353.4	1.67E-20	0.303	353.6	1.75E-20	0.297	353.8	1.63E-20	0.291	354.0	1.36E-20	0.286
354.2	1.07E-20	0.280	354.4	9.82E-21	0.274	354.6	8.66E-21	0.269	354.8	6.44E-21	0.263	355.0	4.84E-21	0.257
355.2	3.49E-21	0.251	355.4	2.41E-21	0.246	355.6	1.74E-21	0.240	355.8	1.11E-21	0.234	356.0	7.37E-22	0.229
356.2	4.17E-22	0.223	356.4	1.95E-22	0.217	356.6	1.50E-22	0.211	356.8	8.14E-23	0.206	357.0	0.00E+00	0.200
Photolysis File = CCHOR														
260.0	2.00E-20	0.310	270.0	3.40E-20	0.390	280.0	4.50E-20	0.580	290.0	4.90E-20	0.530	295.0	4.50E-20	0.480
300.0	4.30E-20	0.430	305.0	3.40E-20	0.370	315.0	2.10E-20	0.170	320.0	1.80E-20	0.100	325.0	1.10E-20	0.040
330.0	6.90E-21	0.000												
Photolysis File = RCHO														
280.0	5.26E-20	0.960	290.0	5.77E-20	0.910	300.0	5.05E-20	0.860	310.0	3.68E-20	0.600	320.0	1.66E-20	0.360
330.0	6.49E-21	0.200	340.0	1.44E-21	0.080	345.0	0.00E+00	0.020						
Photolysis File = ACET-93C														
250.0	2.37E-20	0.760	260.0	3.66E-20	0.800	270.0	4.63E-20	0.640	280.0	5.05E-20	0.550	290.0	4.21E-20	0.300
300.0	2.78E-20	0.150	310.0	1.44E-20	0.050	320.0	4.80E-21	0.026	330.0	8.00E-22	0.017	340.0	1.00E-22	0.000
350.0	3.00E-23	0.000	360.0	0.00E+00	0.000									
Photolysis File = KETONE														
210.0	1.10E-21	1.000	220.0	1.20E-21	1.000	230.0	4.60E-21	1.000	240.0	1.30E-20	1.000	250.0	2.68E-20	1.000
260.0	4.21E-20	1.000	270.0	5.54E-20	1.000	280.0	5.92E-20	1.000	290.0	5.16E-20	1.000	300.0	3.44E-20	1.000
310.0	1.53E-20	1.000	320.0	4.60E-21	1.000	330.0	1.10E-21	1.000	340.0	0.00E+00	1.000			
Photolysis File = GLYOXAL1														
230.0	2.87E-21	1.000	235.0	2.87E-21	1.000	240.0	4.30E-21	1.000	245.0	5.73E-21	1.000	250.0	8.60E-21	1.000
255.0	1.15E-20	1.000	260.0	1.43E-20	1.000	265.0	1.86E-20	1.000	270.0	2.29E-20	1.000	275.0	2.58E-20	1.000
280.0	2.87E-20	1.000	285.0	3.30E-20	1.000	290.0	3.15E-20	1.000	295.0	3.30E-20	1.000	300.0	3.58E-20	1.000
305.0	2.72E-20	1.000	310.0	2.72E-20	1.000	312.5	2.87E-20	1.000	315.0	2.29E-20	1.000	320.0	1.43E-20	1.000
325.0	1.15E-20	1.000	327.5	1.43E-20	1.000	330.0	1.15E-20	1.000	335.0	2.87E-21	1.000	340.0	0.00E+00	1.000
Photolysis File = GLYOXAL2														
355.0	0.00E+00	1.000	360.0	2.29E-21	1.000	365.0	2.87E-21	1.000	370.0	8.03E-21	1.000	375.0	1.00E-20	1.000
380.0	1.72E-20	1.000	382.0	1.58E-20	1.000	384.0	1.49E-20	1.000	386.0	1.49E-20	1.000	388.0	2.87E-20	1.000
390.0	3.15E-20	1.000	391.0	3.24E-20	1.000	392.0	3.04E-20	1.000	393.0	2.23E-20	1.000	394.0	2.63E-20	1.000
395.0	3.04E-20	1.000	396.0	2.63E-20	1.000	397.0	2.43E-20	1.000	398.0	3.24E-20	1.000	399.0	3.04E-20	1.000
400.0	2.84E-20	1.000	401.0	3.24E-20	1.000	402.0	4.46E-20	1.000	403.0	5.27E-20	1.000	404.0	4.26E-20	1.000
405.0	3.04E-20	1.000	406.0	3.04E-20	1.000	407.0	2.84E-20	1.000	408.0	2.43E-20	1.000	409.0	2.84E-20	1.000
410.0	6.08E-20	1.000	411.0	5.07E-20	1.000	411.5	6.08E-20	1.000	412.0	4.86E-20	1.000	413.0	8.31E-20	1.000
413.5	6.48E-20	1.000	414.0	7.50E-20	1.000	414.5	8.11E-20	1.000	415.0	8.11E-20	1.000	415.5	6.89E-20	1.000
416.0	4.26E-20	1.000	417.0	4.86E-20	1.000	418.0	5.88E-20	1.000	419.0	6.69E-20	1.000	420.0	3.85E-20	1.000
421.0	5.67E-20	1.000	421.5	4.46E-20	1.000	422.0	5.27E-20	1.000	422.5	1.05E-19	1.000	423.0	8.51E-20	1.000
424.0	6.08E-20	1.000	425.0	7.29E-20	1.000	426.0	1.18E-19	1.000	426.5	1.30E-19	1.000	427.0	1.07E-19	1.000
428.0	1.66E-19	1.000	429.0	4.05E-20	1.000	430.0	5.07E-20	1.000	431.0	4.86E-20	1.000	432.0	4.05E-20	1.000
433.0	3.65E-20	1.000	434.0	4.05E-20	1.000	434.5	6.08E-20	1.000	435.0	5.07E-20	1.000	436.0	8.11E-20	1.000
436.5	1.13E-19	1.000	437.0	5.27E-20	1.000	438.0	1.01E-19	1.000	438.5	1.38E-19	1.000	439.0	7.70E-20	1.000
440.0	2.47E-19	1.000	441.0	8.11E-20	1.000	442.0	6.08E-20	1.000	443.0	7.50E-20	1.000	444.0	9.32E-20	1.000
445.0	1.13E-19	1.000	446.0	5.27E-20	1.000	447.0	2.43E-20	1.000	448.0	2.84E-20	1.000	449.0	3.85E-20	1.000
450.0	6.08E-20	1.000	451.0	1.09E-19	1.000	451.5	9.32E-20	1.000	452.0	1.22E-19	1.000	453.0	2.39E-19	1.000
454.0	1.70E-19	1.000	455.0	3.40E-19	1.000	455.5	4.05E-19	1.000	456.0	1.01E-19	1.000	457.0	1.62E-20	1.000

Table A-3. (continued)

WL (nm)	Abs (cm^2)	QY	WL (nm)	Abs (cm^2)	QY	WL (nm)	Abs (cm^2)	QY	WL (nm)	Abs (cm^2)	QY	WL (nm)	Abs (cm^2)	QY
458.0	1.22E-20	1.000	458.5	1.42E-20	1.000	459.0	4.05E-21	1.000	460.0	4.05E-21	1.000	460.5	6.08E-21	1.000
461.0	2.03E-21	1.000	462.0	0.00E+00	1.000									
Photolysis File = MEGLYOX1														
220.0	2.10E-21	1.000	225.0	2.10E-21	1.000	230.0	4.21E-21	1.000	235.0	7.57E-21	1.000	240.0	9.25E-21	1.000
245.0	8.41E-21	1.000	250.0	9.25E-21	1.000	255.0	9.25E-21	1.000	260.0	9.67E-21	1.000	265.0	1.05E-20	1.000
270.0	1.26E-20	1.000	275.0	1.43E-20	1.000	280.0	1.51E-20	1.000	285.0	1.43E-20	1.000	290.0	1.47E-20	1.000
295.0	1.18E-20	1.000	300.0	1.14E-20	1.000	305.0	9.25E-21	1.000	310.0	6.31E-21	1.000	315.0	5.47E-21	1.000
320.0	3.36E-21	1.000	325.0	1.68E-21	1.000	330.0	8.41E-22	1.000	335.0	0.00E+00	1.000			
Photolysis File = MEGLYOX2														
350.0	0.00E+00	1.000	354.0	4.21E-22	1.000	358.0	1.26E-21	1.000	360.0	2.10E-21	1.000	362.0	2.10E-21	1.000
364.0	2.94E-21	1.000	366.0	3.36E-21	1.000	368.0	4.21E-21	1.000	370.0	5.47E-21	1.000	372.0	5.89E-21	1.000
374.0	7.57E-21	1.000	376.0	7.99E-21	1.000	378.0	8.83E-21	1.000	380.0	1.01E-20	1.000	382.0	1.09E-20	1.000
384.0	1.35E-20	1.000	386.0	1.51E-20	1.000	388.0	1.72E-20	1.000	390.0	2.06E-20	1.000	392.0	2.10E-20	1.000
394.0	2.31E-20	1.000	396.0	2.48E-20	1.000	398.0	2.61E-20	1.000	400.0	2.78E-20	1.000	402.0	2.99E-20	1.000
404.0	3.20E-20	1.000	406.0	3.79E-20	1.000	408.0	3.95E-20	1.000	410.0	4.33E-20	1.000	412.0	4.71E-20	1.000
414.0	4.79E-20	1.000	416.0	4.88E-20	1.000	418.0	5.05E-20	1.000	420.0	5.21E-20	1.000	422.0	5.30E-20	1.000
424.0	5.17E-20	1.000	426.0	5.30E-20	1.000	428.0	5.21E-20	1.000	430.0	5.55E-20	1.000	432.0	5.13E-20	1.000
434.0	5.68E-20	1.000	436.0	6.22E-20	1.000	438.0	6.06E-20	1.000	440.0	5.47E-20	1.000	441.0	6.14E-20	1.000
442.0	5.47E-20	1.000	443.0	5.55E-20	1.000	443.5	6.81E-20	1.000	444.0	5.97E-20	1.000	445.0	5.13E-20	1.000
446.0	4.88E-20	1.000	447.0	5.72E-20	1.000	448.0	5.47E-20	1.000	449.0	6.56E-20	1.000	450.0	5.05E-20	1.000
451.0	3.03E-20	1.000	452.0	4.29E-20	1.000	453.0	2.78E-20	1.000	454.0	2.27E-20	1.000	456.0	1.77E-20	1.000
458.0	8.41E-21	1.000	460.0	4.21E-21	1.000	464.0	1.68E-21	1.000	468.0	0.00E+00	1.000			
Photolysis File = BZCHO														
299.0	1.78E-19	1.000	304.0	7.40E-20	1.000	306.0	6.91E-20	1.000	309.0	6.41E-20	1.000	313.0	6.91E-20	1.000
314.0	6.91E-20	1.000	318.0	6.41E-20	1.000	325.0	8.39E-20	1.000	332.0	7.65E-20	1.000	338.0	8.88E-20	1.000
342.0	8.88E-20	1.000	346.0	7.89E-20	1.000	349.0	7.89E-20	1.000	354.0	9.13E-20	1.000	355.0	8.14E-20	1.000
364.0	5.67E-20	1.000	368.0	6.66E-20	1.000	369.0	8.39E-20	1.000	370.0	8.39E-20	1.000	372.0	3.45E-20	1.000
374.0	3.21E-20	1.000	376.0	2.47E-20	1.000	377.0	2.47E-20	1.000	380.0	3.58E-20	1.000	382.0	9.90E-21	1.000
386.0	0.00E+00	1.000												
Photolysis File = ACROLEIN														
250.0	1.80E-21	1.000	252.0	2.05E-21	1.000	253.0	2.20E-21	1.000	254.0	2.32E-21	1.000	255.0	2.45E-21	1.000
256.0	2.56E-21	1.000	257.0	2.65E-21	1.000	258.0	2.74E-21	1.000	259.0	2.83E-21	1.000	260.0	2.98E-21	1.000
261.0	3.24E-21	1.000	262.0	3.47E-21	1.000	263.0	3.58E-21	1.000	264.0	3.93E-21	1.000	265.0	4.67E-21	1.000
266.0	5.10E-21	1.000	267.0	5.38E-21	1.000	268.0	5.73E-21	1.000	269.0	6.13E-21	1.000	270.0	6.64E-21	1.000
271.0	7.20E-21	1.000	272.0	7.77E-21	1.000	273.0	8.37E-21	1.000	274.0	8.94E-21	1.000	275.0	9.55E-21	1.000
276.0	1.04E-20	1.000	277.0	1.12E-20	1.000	278.0	1.19E-20	1.000	279.0	1.27E-20	1.000	280.0	1.27E-20	1.000
281.0	1.26E-20	1.000	282.0	1.26E-20	1.000	283.0	1.28E-20	1.000	284.0	1.33E-20	1.000	285.0	1.38E-20	1.000
286.0	1.44E-20	1.000	287.0	1.50E-20	1.000	288.0	1.57E-20	1.000	289.0	1.63E-20	1.000	290.0	1.71E-20	1.000
291.0	1.78E-20	1.000	292.0	1.86E-20	1.000	293.0	1.95E-20	1.000	294.0	2.05E-20	1.000	295.0	2.15E-20	1.000
296.0	2.26E-20	1.000	297.0	2.37E-20	1.000	298.0	2.48E-20	1.000	299.0	2.60E-20	1.000	300.0	2.73E-20	1.000
301.0	2.85E-20	1.000	302.0	2.99E-20	1.000	303.0	3.13E-20	1.000	304.0	3.27E-20	1.000	305.0	3.39E-20	1.000
306.0	3.51E-20	1.000	307.0	3.63E-20	1.000	308.0	3.77E-20	1.000	309.0	3.91E-20	1.000	310.0	4.07E-20	1.000
311.0	4.25E-20	1.000	312.0	4.39E-20	1.000	313.0	4.44E-20	1.000	314.0	4.50E-20	1.000	315.0	4.59E-20	1.000
316.0	4.75E-20	1.000	317.0	4.90E-20	1.000	318.0	5.05E-20	1.000	319.0	5.19E-20	1.000	320.0	5.31E-20	1.000
321.0	5.43E-20	1.000	322.0	5.52E-20	1.000	323.0	5.60E-20	1.000	324.0	5.67E-20	1.000	325.0	5.67E-20	1.000
326.0	5.62E-20	1.000	327.0	5.63E-20	1.000	328.0	5.71E-20	1.000	329.0	5.76E-20	1.000	330.0	5.80E-20	1.000
331.0	5.95E-20	1.000	332.0	6.23E-20	1.000	333.0	6.39E-20	1.000	334.0	6.38E-20	1.000	335.0	6.24E-20	1.000
336.0	6.01E-20	1.000	337.0	5.79E-20	1.000	338.0	5.63E-20	1.000	339.0	5.56E-20	1.000	340.0	5.52E-20	1.000
341.0	5.54E-20	1.000	342.0	5.53E-20	1.000	343.0	5.47E-20	1.000	344.0	5.41E-20	1.000	345.0	5.40E-20	1.000
346.0	5.48E-20	1.000	347.0	5.90E-20	1.000	348.0	6.08E-20	1.000	349.0	6.00E-20	1.000	350.0	5.53E-20	1.000
351.0	5.03E-20	1.000	352.0	4.50E-20	1.000	353.0	4.03E-20	1.000	354.0	3.75E-20	1.000	355.0	3.55E-20	1.000
356.0	3.45E-20	1.000	357.0	3.46E-20	1.000	358.0	3.49E-20	1.000	359.0	3.41E-20	1.000	360.0	3.23E-20	1.000
361.0	2.95E-20	1.000	362.0	2.81E-20	1.000	363.0	2.91E-20	1.000	364.0	3.25E-20	1.000	365.0	3.54E-20	1.000
366.0	3.30E-20	1.000	367.0	2.78E-20	1.000	368.0	2.15E-20	1.000	369.0	1.59E-20	1.000	370.0	1.19E-20	1.000
371.0	8.99E-21	1.000	372.0	7.22E-21	1.000	373.0	5.86E-21	1.000	374.0	4.69E-21	1.000	375.0	3.72E-21	1.000
376.0	3.57E-21	1.000	377.0	3.55E-21	1.000	378.0	2.83E-21	1.000	379.0	1.69E-21	1.000	380.0	8.29E-24	1.000
381.0	0.00E+00	1.000												

Table A-4. Values of chamber-dependent parameters used in the model simulations of the environmental chamber experiments for this study.

Parm.	Value(s)	Discussion
k(O3W)	8.5×10^{-4} min^{-1}	k(O3W) is rate constant for unimolecular wall loss of O_3. The value used runs is based on the results of runs CTC053 and CTC106, which are reasonably consistent with each other.
k(N25I) k(N25S)	2.8×10^{-3} min^{-1}, 1.5×10^{-6} - k_g ppm^{-1} min^{-1}	k(N25I) is unimolecular decay of N_2O_5 to the walls. K(N25S) is the rate constant for bimolecular reaction with H_2O, forming 2 HNO3. The value used is based on the N_2O_5 decay rate measurements in a similar chamber reported by Tuazon et al. (1983). The same rate constants are used for all Teflon bag chambers (Carter et al., 1995b).
k(NO2W) yHONO	1.6×10^{-4} min^{-1} 0.2	k(NO2W) is the rate constant for a unimolecular decay of NO_2 to the walls, forming HONO with a yield of yHOHO. The values used are based on dark NO_2 decay and HONO formation measured in a similar chamber by Pitts et al. (1984). This is assumed to be the same in all Teflon bag chambers (Carter et al. 1995b).
k(XSHC)	250 min^{-1}	k(XSHC) is the rate constant for a unimolecular conversion of HO to HO_2, which is used to represent the effect of background VOC reactants. It is estimated by modeling pure air irradiations carried out in this reactor. This is an important parameter affecting model predictions except for pure air or NO_x-air runs.
RS/K1	0.07 ppb	The continuous chamber radical source is represented as a light-dependent flux of OH radicals, whose rate is given by the NO_2 photolysis rate (k_1) multiplied by the parameter RS/K1. This parameter is derived from model simulations of n-butane - NO_x and CO - NO_x experiments as discussed by Carter et al. (1995b,c). The values used are based on averages which fit the n-butane - NO_x experiments as discussed by Carter et al. (1997).
E-NO2/K1	0.04 ppb	The rate of NO_2 offgasing from the chamber walls is obtained by multiplying the parameter E-NO2/K1 by the NO_2 photolysis rate. Model simulations of acetaldehyde - air runs are used to derive this parameter. For the CTC, the value used is based on the results of CTC019.
HONO-F	0.0	HONO-F is the fraction of initially present NO_2 which is assumed to be converted to HONO prior to the start of the run. When the light-induced radical source is represented by a continuous OH flux, best fits to most n-butane - NO_x experiments are obtained if this is assumed to be negligible.